A CRYSTALLOGRAPHIC AND MECHANISTIC STUDY OF Mn Triad COMPLEXES AS MODEL RADIOPHARMACEUTICALS

by

MOKOLOKOLO PETRUS PENNIE

A dissertation submitted to fulfil the requirements for the degree of

MAGISTER SCIENTIAE

in the

DEPARTMENT OF CHEMISTRY

FACULTY OF NATURAL AND AGRICULTURAL SCIENCES

at the

UNIVERSITY OF THE FREE STATE

SUPERVISOR: PROF. HENDRIK VISSER

CO-SUPERVISOR: DR. ALICE BRINK

FEBRUARY 2015

ACKNOWLEDGEMENTS

TABLE OF CONTENTS

ABSTRACT

Keywords: Manganese, tricarbonyl complex, salicylidene Schiff base, substitution kinetics

A series of *fac*-manganese(I) tricarbonyl complexes were synthesized and analysed to better understand the chemical properties of the group 7 radiopharmaceutical model complex. Five new complexes containing N,O', N,N',O and O,O' donating functionalities were successfully synthesized. The Schiff base ligands, SalH-*m*Tol = 2-(*m*-tolyliminomethyl)phenol, SalH-cyHex = 2-(Cyclohexyliminomethyl)phenol and 5Me-SalH-Hist = 2-(2-imidazol-4-yl)ethyliminomethyl-5-methylphenol are derived from a salicylidene backbone. The O,O' are the β-diketone ligands (acetylacetone= AcacH and trifluoroacetylacetone = TfacacH). The ligands were strategically selected to ensure systematic variation in electronic and steric effects. The synthesis of complexes *fac*-[Mn(Sal-*m*Tol)(CO)$_3$]$_2$, *fac*-[Mn(Sal-CyHex)(CO)$_3$]$_2$, *fac*-[Mn(4-Me-Sal-Hist)(CO)$_2$], *fac*-[Mn(Acac)(CO)$_3$(OHCH$_3$)] and *fac*-[Mn(Tfacac)(CO)$_3$(OHCH$_3$)] is reported and all the complexes were characterised by IR, NMR, UV-Vis and single crystal X-Ray diffraction to better understand the solid and solution state.

All complexes afford an octahedral environment around the metal centre with the chelating ligands and three carbonyl ligands in *facial* arrangement. The octahedron is satisfied by a bridging oxygen atom in the dimeric complexes *fac*-[Mn(Sal-*m*Tol)(CO)$_3$]$_2$ and *fac*-[Mn(Sal-CyHex)(CO)$_3$]$_2$, and a methanol molecule in complexes *fac*-[Mn(Acac)(CO)$_3$(OHCH$_3$)] and *fac*-[Mn(Tfacac)(CO)$_3$(OHCH$_3$)]

Substitution kinetics of the coordinated methanol molecule in complexes *fac*-[Mn(Acac)(CO)$_3$(OHCH$_3$)] and *fac*-[Mn(Tfacac)(CO)$_3$(OHCH$_3$)] by a neutral imidazole ligand was evaluated. The negative values obtained for the activation entropy parameter, $\Delta S^{\neq}$ [-88(1) J K^{-1} mol^{-1} and -18(6) J K^{-1} mol^{-1}], in both complexes is suggestive of an associative type mechanism. As anticipated, the overall rate of

Abstract

methanol substitution in complex *fac*-[Mn(Acac)(CO)$_3$](OHCH$_3$)] is faster than in *fac*-[Mn(Tfacac)(CO)$_3$(OHCH$_3$)] as indicated by the overall larger k_1 and K_1, due to the presence of electron withdrawing fluorine atoms on the ligand backbone.

OPSOMMING

Sleutelwoord: Mangaan, trikarboniel kompleks, salisilideen Schiff basis, substitusie kinetika

`n Reeks *fas*-mangaan(I) trikarboniel komplekse is vervaardig en geanaliseer ten einde die chemiese eienskappe van die groep 7 radiofarmaseutiese model kompleks beter te verstaan. Vyf nuwe komplekse bevattende $N,O^{'}$, $N,N^{'},O$ en $O,O^{'}$ skenkende funksionaliteite is suksesvol gesintetiseer. Die Schiff basis ligande, SalH-*m*Tol = 2-(*m*-tolieliminometiel)fenol, SalH-cyHex = 2-(Sikloheksieliminometiel)fenol en 5Me-SalH-Hist = 2-(2-imidazol-4-iel)etieliminometiel-5-metielfenol, is derivate van `n salisilideen ruggraat. Die $O,O^{'}$ is die β-diketoon ligande (asetielasetoon = AcacH en trifluoroasetielasetoon = TfasacH). Die ligande is strategies gekies om sistematiese variasie in elektroniese en steriese effekte te verseker. Die sinteses van die komplekse *fas*-[Mn(Sal-*m*Tol)(CO)$_3$]$_2$, *fas*-[Mn(Sal-CyHex)(CO)$_3$]$_2$, *fas*-[Mn(4-Me-Sal-Hist)(CO)$_2$], *fas*-[Mn(Acac)(CO)$_3$(OHCH$_3$)] en *fas*-[Mn(Tfasac)(CO)$_3$(OHCH$_3$)] is gerapporteer en alle komplekse is deur IR, KMR, UV-Vis en enkelkristal X-Straal diffraksie gekarakteriseer ten einde die vaste- en vloeistoftoestande beter te verstaan.

Alle komplekse vertoon `n oktahedriese omgewing rondom die metaalkern met die chelerende ligande en drie karboniel ligande in *fasiale* rangskikking. Die oktahedron word versadig deur `n brugvormende suurstofatoom in die dimeriese komplekse *fas*-[Mn(Sal-*m*Tol)(CO)$_3$]$_2$ en *fas*-[Mn(Sal-CyHex)(CO)$_3$]$_2$, en `n metanol molekuul in komplekse *fas*-[Mn(Acac)(CO)$_3$(OHCH$_3$)] en *fas*-[Mn(Tfasac)(CO)$_3$(OHCH$_3$)] .

Substitusiekinetika van die gekoördineerde metanol molekuul in die komplekse *fas*-[Mn(Acac)(CO)$_3$(OHCH$_3$)] en *fas*-[Mn(Tfasac)(CO)$_3$(OHCH$_3$)] met `n neutrale imidasool ligand is geëvalueer. Die negatiewe waardes wat vir die aktiveringsentropieparameter, $\Delta S^{\neq}$ [-88(1) J K$^{-1}$ mol$^{-1}$ en -18(6) J K$^{-1}$ mol$^{-1}$], in beide komplekse verkry is, is aanduidend van `n assosiatiewe tipe meganisme. Na verwagting is die algehele tempo

Opsomming

van metanol substitusie in die kompleks *fas*-[Mn(Acac)(CO)$_3$(OHCH$_3$)] vinniger as in *fas*-[Mn(Tfasac)(CO)$_3$(OHCH$_3$)], soos aangedui deur die algeheel groter waardes vir k_1 en K_1, weens die aanwesigheid van elektron-onttrekkende fluooratome op die ligand-ruggraat.

ABBREVIATIONS

2,4-Quin	quinoline-2,4-dicarboxylic acid
Å	angstrom
BBB	blood brain barrier
BFC	bifunctional chelate
Bipy	2,2'-bipyridyl
Br^-	bromide ions
DMSA	dimercaptosuccinic acid
fac	*facial*
Flav	3-hydroxyflavone
FT-IR	fourier transform infra-red
HOMO	highest occupied molecular orbital
IR	infra-red
L-L'-bid	bidentate ligand
LUMO	lowest occupied molecular orbital
MAG_3	mercaptoacetylglycylglycylglycine
MEMRI	manganese enhanced magnetic resonance imaging
MIBI	2-methoxy-2-methylpropylisocyanide
Mn-SOD	manganese superoxide dismutase
MRI	magnetic resonance imaging
NMR	nuclear magnetic resonance spectroscopy
PET	positron emission tomography
Phen	1,10-phenanthroline
Pico	pyridine-2-carboxylic acid
Py	pyridine
SPECT	single photon emission computed tomography
$t_{1/2}$	half-life
Trop	tropolone
TU	thiourea
UV/vis	ultraviolet/visible spectroscopy

Abbreviations

α	alpha
β^-	beta
γ	gamma
β^+	positron
σ	sigma
π	pi
v_{CO}	C=O stretching frequency
keV	kilo electron volts
MeV	mega electron volts
$\Delta H^\dagger$	enthalpy activation energy
$\Delta S^\dagger$	entropy activation energy
$\Delta V^\dagger$	volume of activation
k_{obs}	observed *pseudo* first-order rate constant
k_1	first-order rate constant for forward reaction
k_{-1}	rate constant for reverse reaction
K_1	equilibrium constant
°	degrees

1 GENERAL BACKGROUND AND AIM

1.1 Metals in medicine

Hydrogen, oxygen, carbon and nitrogen make up to 96 % of all the elements present in the human body.[1] The remaining percentage is made up by metals. These metals can essentially be divided in two main groups: bulk metals (sodium, calcium, potassium, magnesium) and trace elements (iron, zinc, copper, manganese, nickel, molybdenum, chromium). The bulk metals are present in relatively larger quantities compared to the trace metals. The two groups of metals play an important role in the total functioning of the body and are indispensable to humans. Calcium plays a major role in skeletal and bone functioning. Its functions include aiding muscle contractions and nerve impulse transmission. Sodium is important for muscles contractions and serves as an electrolyte for conducting nerve impulses. Iron is an important component in the transportation of oxygen in the body.

The use of metals for medicinal purposes can be traced back to ancient times.[2] The natural use of metals in biological systems probed the incorporation of metal ions in medicines. The idea gave birth to medicinal inorganic chemistry. Medicinal inorganic chemistry fundamentally implicates the employment of a metal ion in a biological system. The particular chemical reactivity of metals, tuneable physical and chemical properties, and structural variations of their compounds lends them a great advantage when compared to traditional organic drugs.

---

[1] E.J. Frieden, *Chem. Ed.*, 1985, 62, 917.
[2] P.J. Sadler, *Adv. Inorg. Chem.,* 1991, *36*, 1.

The minute availability of metal ions in the human body should not be equated to the strength of their functionality. These metal ions play a major role in the total functioning of the body. Although large quantities are detrimental, in the same way a deficiency of these metal ions can also induce negative effects. The level of availability of metal ions in the environment or diet clearly influences the organism reaction towards the specific metal ion. Millions of people worldwide are subjected to various diseases caused by deficiency of some important micro nutrients. Similarly, when food is ample, organisms might be exposed to irregular quantity that exceeds their requirement which consequently results in toxic effects. The occurrence of metal ions deficiency include inborn and genetically determined enzyme defects leading to a dysfunction caused by either or a combination of factors such as the absorption, transportation, storage or excretion of the metal ion. High concentrations of metal ions can affect the biological activity in living organism resulting to impairments or deformity in some cases.

1.2 A brief outline of the Mn-Triad in medicine

The manganese triad comprises of manganese, technetium and rhenium. The three metals play an important role in medicinal application for diagnosis and treatment of various diseases. Manganese carbonyl complexes are used to treat various diseases through the release of controlled amounts of CO to target tissues and organs. Compound Mn-SOD (super oxide dismutase) catalyses the conversion of harmful superoxide radicals into oxygen and hydrogen peroxide. Manganese is also used as an imaging technique for diagnostic medicine.[3,4] Rhenium and technetium have played an immense role in the development of radiopharmaceuticals. Radiopharmaceuticals are drugs consisting of a radionuclide and a target biomolecule or organic ligand that defines the location of the drug. These drugs are used for diagnosis or therapy of various diseases such as cancer. Diagnostic radiopharmaceuticals are labelled with gamma emitting radioisotopes for positron emitting tomography (PET) or for single photon emission computed tomography (SPECT). Both PET and SPECT are imaging

---

[3] D. Salvemini, D. P.Riley and S. Cuzzocrea, *Nat. Rev. Drug Disc.*, 2002, 1, 367
[4] D. P. Riley, *Chem. Rev.*, 1999, 99, 2573.

modalities in clinical use. A more in-depth discussion of these functionalities will be described in the ensuing chapter.

1.3 Aim of Study

The quantities of literature available points out unequivocally, the importance of technetium and to some extend rhenium, towards the development of radiopharmaceuticals. Rhenium and technetium have overlapping chemical properties and this factor enables the modelling of technetium studies using rhenium which is easier to work with since it is naturally nonradioactive. The monovalent oxidation state of the fac-[M(CO_3)]$^+$ is chemically inert and this characteristic renders these types of complexes attractive to in $vivo$ application. An endeavour to search for suitable bi- and tridentate ligands has been embarked on. Most of the ligands investigated afford a facial octahedral environment around the metal centre and this provides efficient shielding from attack of other ligands.[5] The compact size of the fac-[M(CO)_3]$^+$ fragment is small enough to prevent attack from other ligands. The low oxidation state permits a wide range of ligands for the design of suitable complexes.

The main objective of the study was to investigate the coordinative and kinetic behaviour of fac-manganese(I) tricarbonyl complexes relative to technetium and rhenium analogues, in order to broaden the horizon on the growing interest in the use of fac-[M(CO)_3]$^+$ core towards the design of novel radiopharmaceutical for imaging and therapeutic purposes. To study the kinetic effect of bonded β-diketone ligands, on the somewhat inert manganese(I) tricarbonyl complex specifically towards the development of the [2+1] labelling approach. The β-diketone ligands have the ability to stabilise various complexes through mononegative O_2-chelation. These ligands can be synthetically modified to incorporate a target biomolecule at the alkyl carbon and also at the terminal carbons. Previous studies have demonstrated the effect of bonded ligands on the rate of methanol substitution in complexes of the type fac-[M(CO)_3(L,L'-Bid)(X)]^n

---

[5] R. Schibli, P. A. Schubiger, *Eur. J. Nucl Med., 2002*, 11, 1529.

(*L,L'*-Bid = neutral or monoanionic bidentate ligands with varied *L,L'* donor atoms, *N,N'* or *N,O'* and X = labile methanol molecule.[6,7]

These studies revealed that the rate of methanol substitution is to some degree, dependent on the nature of the coordinated bidentate ligand.

The main objectives explored during the course of this study are summarized below:

- Synthesis of new *fac*-manganese(I) tricarbonyl complexes with a variation of bidentate ligands containing O,O- and N,O-Bid donor functionalities

- Characterization of all the synthesized complexes in solid and solution state using X-ray crystallography, NMR, UV/Vis and Infrared spectroscopy.

- Kinetic investigation on the substitution of the coordinated methanol molecule in *fac*-[Mn(Acac)(CO)$_3$(OHCH$_3$)] and *fac*-[Mn(Tfacac)(CO)$_3$(HOCH$_3$)] in order to determine the intimate mechanism of substitution.

- Evaluate and compare the reactivity of the Mn-Triad to better understand chemical trends

A brief history on the discovery of manganese, rhenium and technetium and their relevance to medicine will be discussed in the next chapter. Followed by the synthetic and crystallographic evaluation of the manganese(I) tricarbonyl complexes investigated during the course of this study.

---

[6] M. Schutte, G. Kemp, H.G. Visser, A. Roodt, A., *Inorg. Chem.*, 2011,50,12486.

[7] T. N. Twala, M. Schutte-Smith, A. Roodt, H. G. Visser, *Dalton Trans*, 2015, DOI: 10.1039/C4DT03524K.

2 LITERATURE STUDY

2.1 Introduction

A great contrast exists between the group 7 transition metals in regards to history, reactivity, availability and abundance.[1] Rhenium and technetium have similar chemical properties and differ markedly from manganese. The history and discovery together with the relevant application of these metals in medicine will be briefly discussed.

2.2 Brief history of Manganese

Carl Wilhelm Scheele first recognised manganese while working with the mineral pyrolusite.[1] The element was later isolated by Johan Gottlieb Gahn in 1774 through the reduction of manganese oxide with oil and charcoal. Manganese is the 12th most prevalent element making up 0.106 % of the earth crust. It is the 3rd most abundant transition metal surpassed only by iron and titanium. It is a white-grey metal bearing resemblance to iron, although harder and more brittle. The metal has a melting point of 1246 ^{0}C, boiling point of 2061 ^{0}C and electronegativity of 1.55 on the Pauling scale. Manganese does not occur as a free metal in nature but mainly in oxide and carbonate deposits as a result of weathering of primary silicate deposits.[2]

Manganese has a wide geographical distribution within South Africa, Australia, Brazil, Indian and Gabon being the main suppliers. The chief source of manganese is the mineral pyrolusite which consists mainly of MnO_2. It is also found in other minerals such as huastmannite (Mn_3O_4), magnate $Mn(O)(OH)$ and rhodochrosite ($MnCO_3$). Table 2.1 shows some of the most common manganese containing minerals.[3] Material such as waste batteries, spent electrodes, steel scraps and spent

[1] S. E. Olsen, M. tangstad, T. Lindstad, *Production of Manganese Ferroalloys*, SINTEF and Tapir Academic Press, Trondheim, 2007.
[2] G. V. Scăeţeanu, L. Ilie, C. Călin, *J. Am. Chem. Sci.*, 2013, 3, 247.
[3] T. Kaneko, T. Matsuzaki, T. Kugimiya, K. Ide, M. Kumakura , A. Kasama , *J. ISIJ.*, 1993, 79, 941.

catalysts are a secondary source of manganese since they contain deposits of MnO_2.

Manganese ores readily dissolve in dilute acid to form Mn(II) salts. In cases where the ores are not soluble in acids, they are reductively roasted at 700 ^{0}C to produce manganese oxide (MnO), and manganese is removed with sulphuric acid. Impurities such as Fe, Ni, Al, Mo and Si are removed from solution by neutralisation and 99.97 % pure manganese is prepared by the electrolysis of the solution.[4,5,6]

Table 2.1: Selected manganese containing minerals.[3]

Mineral	Formula	Chemical name
Pyrolusite	MnO_2	Manganese (IV) dioxide
Rhodamite	$MnSiO_3$	Manganese silicate
Rhodochrosite	$MnCO_3$	Manganese (II) carbonate
Bixbyite	Mn_2O_3	Manganese sesquioxide
Braunite	$3Mn_2O_3.MnSiO_3$	Silicate mineral with both Mn(II) and Mn(III)
Hauerite	MnS_2	Manganese disulphide
Knebelite	$(MnFe)_2SiO_4$	Iron manganese silicate
Manganese blende	MnS	Manganese (II) monosulphide
Manganite	$Mn_2O_3 .H_2O$	Manganese oxide hydroxide

The element can be found in numerous oxidation states ranging from -3 to +7. In the lower oxidation states, +2, +3 and +4, manganese is classified as a hard Lewis acid and forms the most stable complexes with hard Lewis bases such as the oxyanion which may be carboxylate, phenolate, alkoxide or hydroxide. Manganese(II) is the most common oxidation state due its ability to form thermodynamically stable complexes in both acidic and basic solutions.

Manganese is essential in both human life (trace amounts) and industry. Its uses can be traced back to ancient times when it was used to paint caves and to decolorize

---

[4] V. C. H. Weinheim, *Ullmann's Encyclopedia of Industrial Chemistry*, 1990,16,1990.

[5] Kirk-Othmer, *Encyclopedia of Industrial Chemical Technology*, 3rd. Ed., John Wiley, New York, 1980.

[6] I. Omae, *Application of Organometallic Compound*, John Wiley and Sons, Chichester, 1998.

glass.[7] The manifold applications include, steel production, textile bleaching, dry cell batteries, animal feeds, medicine and catalysis.[1]

Manganese forms a number of alloys with other metals to strengthen and harden steel agents. Because of its high affinity for sulphur and oxygen, manganese is used as a deoxidising and desulfurizing agent in steel manufacturing. Sulphur is considered a poison in steel manufacturing due to its tendency to induce cracking and brittleness.

2.3 Discovery of Rhenium and Technetium

Rhenium was first discovered in 1925 by Noddack via its X-ray spectrum.[8] He later isolated it from molybdenum ores. Like manganese, rhenium does not occur as a free metal but found in minerals associated with other metals such as Mo, Pd, Cu, Pt or Zn. Rhenium is one of the rarest elements and forms about 0.0007% of the earth's crust. Although the organometallic chemistry of rhenium was held back by factors such as cost of the starting material, an explosive interest emerged in the past two or so decades due to the relevant properties in radiopharmaceutical application. The vastness of the oxidation states extending from -3 to +7, the strong bonding character that exists between rhenium and other elements stabilizing ordinary reactive species and the possibility to isolate normal unstable compounds are some of the aspects that brand the chemistry of rhenium attractive.[9]

Technetium was first isolated by Perrier and co-workers in 1937. It was separated from molybdenum by bombardment of the target with deuterons. Between the elements of the Mn-triad consisting of manganese, rhenium and technetium, the chemistry of Tc is possibly the least developed which may have been retarded by the lack of stable isotopes and possibly the related radioactivity.[10] Currently, there are over 20 known technetium isotopes ^{91}Tc-^{110}Tc, with ^{99m}Tc being the most important of the isotopes. ^{99m}Tc has a short-lived half-life of 6 h which is ideal for synthesis, dosage and administration of the drug for diagnostic or therapeutic purposes. The γ-ray emission energy of 141 KeV provides high resolution images.

[7] C. J. Jones, J. R Thornback, *Medicinal Applications of Coordination chemistry,* The Royal Society Chemistry, 2007.
[8] I. Noddack, W. Z. Noddack, *Phys. Chem.*, 1927, 125, 264.
[9] P. Charles P, *Science.*, 1993, 259, 1552.
[10] R. Alberto, *Eur. J. Inorg. Chem.*, 2009, 1, 21.

2.4 Rhenium and technetium in nuclear medicine

Radiopharmaceuticals are inorganic drugs containing a radioactive nucleus and are used routinely in nuclear medicine as diagnostic tools for imaging and treatment of various diseases, for example cancer.[11,12,13,14] Radiopharmaceutical drugs are made up of two intrinsic parts: a radionuclide that conducts the course of action through its decay process and a target biomolecule or organic ligand that defines the localization of the drug. A variety of rhenium and technetium based radiopharmaceuticals has come to the fore since the first experimental application of $^{99m}TcO^-_4$ for imaging of the thyroid gland based on the principle that the pertechnetate anion would behave similarly to iodide and is known to be absorbed by the thyroid gland. The prominent use of radiolabeled compounds for medicinal purpose was encouraged by the subsequent development of nuclear reactors and the large production of artificial radionuclides

The radionuclide ^{99m}Tc has been the workhorse in nuclear medicine and is being used in over 80% of all diagnostic nuclear radiopharmaceuticals.[15] The most important of the isotopes is ^{99m}Tc. ^{99m}Tc has a short-lived half-life of 6 h and emits low energy gamma rays (141 KeV). ^{99m}Tc is produced indirectly either by neutron irradiation of ^{98}Mo or as a fission product of ^{235}U. Figure 2.1 shows the decay series.

---

[11] D. Jain, *Semin. Nucl. Med.*, 29 1999, 221.
[12] S.S. Jurisson, J.D. Lydon, *Chem. Rev.*, 1999, 99, 2205.
[13] S. Liu, D.S. Edwards, *Top. Curr. Chem.*, 2002, 222, 259.
[14] S. Liu, *Chem. Soc. Rev.*, 2004, 33, 1.
[15] J. R. Dilworth, S. J. Parrott, *Chem. Soc. Rev.*, 1998, 27, 43.

Heavy Fission Product

I, Xe, Cs,
Ba, Ce

$n \longrightarrow$ U-235 $\longrightarrow$

Fission

Br, Kr,
Sr, Mo

Ligth Fission Product

Br, Kr,
Sr, Mo

Light Fission Product

$\longrightarrow$ Mo-99 $\longrightarrow$

$\beta^- + \gamma$

radioactive decay
$T_{1/2} = 2.75$ days

88 %

12 %

Tc-99m $\quad \gamma = 140$ KeV

radioactive decay
$T_{1/2} = 6$ hours

Tc-99 $\xrightarrow{\beta^-}$ Ru-99

radioactive
decay

$T_{1/2} = 2.1 \times 10^5$ years
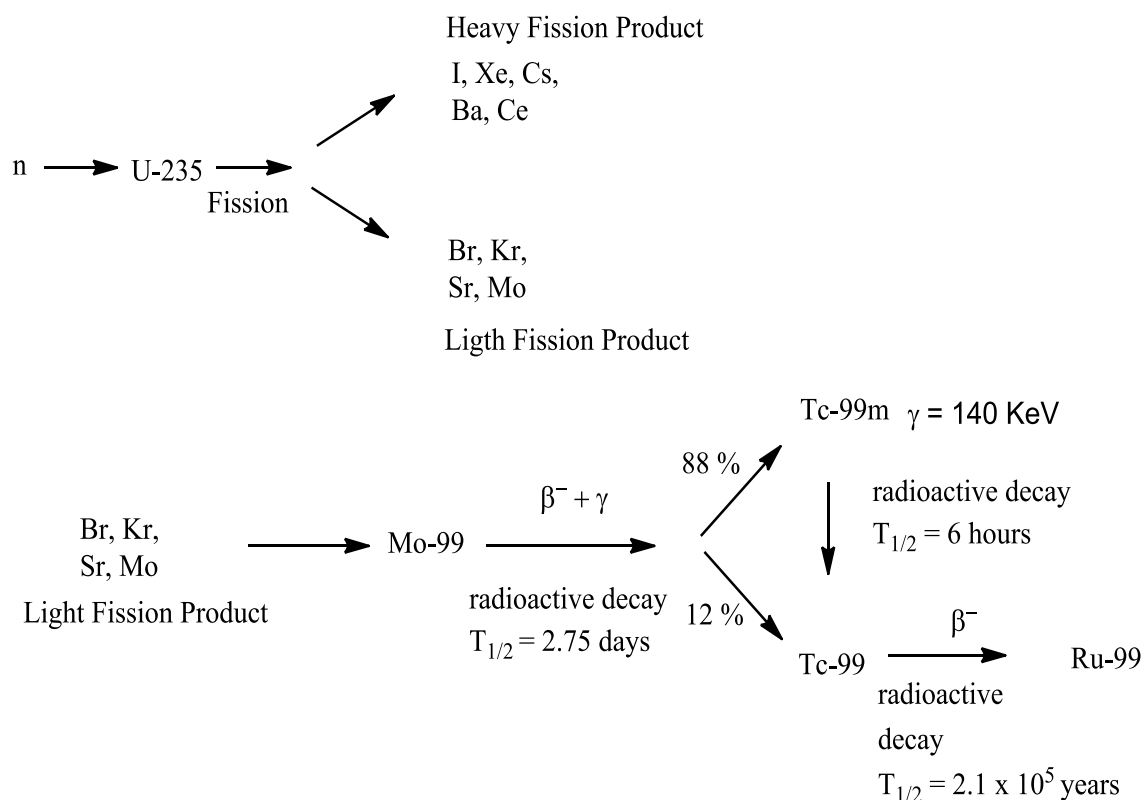
Figure 2.1: An illustration of the decay sequence and production of ^{99m}Tc.[41]

2.4.1 Drug designing

In an ideal state, a radiopharmaceutical agent would manoeuvre towards the target cells or tumor and interact exclusively with the desired cells; the unreacted agent would be excreted rapidly to lessen radioactivity in the body. Radiopharmaceuticals can be categorised into two classes namely: diagnosis and therapeutic radiopharmaceuticals. The main aspects in radiopharmaceutical design include; type of radionuclide, half-life, mode of decay, biological and chemical properties of the radionuclide, pharmacokinetics, cost and availability.

2.4.2 Therapeutic radiopharmaceuticals

Therapeutic radiopharmaceuticals entail the systematic introduction of high-energy doses of radiation to target areas, often cancerous tumors.[16] Auger electrons and β or α particle are in dominion due to their physical and nuclear properties. An ideal therapeutic should have:[17,18,19]

---

[16] S. Bhattacharyya, M. Dixit, *Dalton Trans.*, 2011, 40, 6112.
[17] H. M. Vriesendorp, S. M. Quadri, P.E. Borchardt , BioDrugs., 1998. 10, 275.

> ➤ High tumor uptake and fast clearance in order to minimise radiation exposure to normal tissue and organs

> ➤ High solution stability in order to overcome competition with other chelating ligands

> ➤ High tumor-to-background ratio

> ➤ Long tumor residence time to maximise efficiency of killing cancer cells

> ➤ Retain chemical and biological integrity during transportation

Radiation can be introduced externally (external beam radiation), internally through radioactive material placed in proximity to cancer cells (internal radiation therapy) and also through the introduction of a radioactive compound directly into the blood stream or via ingestion (systematic radiation).

The type of radiation therapy received by patients depends on factors such as:

> ➤ The size and type of tumor

> ➤ The location of the tumor

> ➤ The sensitivity of normal tissues around the infected area

> ➤ The general health and medical history of the patient

External beam radiation makes use of specialised machines to deliver high energy radiation to target areas. In brachytherapy (internal radiation), a sealed radioactive compound is physically implanted in the body to selectively irradiate the tumor with high levels of radiation.[20,21]

2.4.3 Diagnostic radiopharmaceuticals

Radiodiagnostic imaging is a non-invasive process that provides opportunity to assessing the disease or disease state by using single photon emission computed tomography (SPECT) and positron emission tomography (PET) which are both powerful diagnostic modalities in clinical use.[22] These imaging strategies have the capacity to provide an accurate evaluation of the chemical and biological interaction

[18] T.M. Illidge, S. Brock, *Curr. Pharm. Des.*, 2000, 6, 1399.

[19] S. Liu, D.S. Edwards, *Bioconjug. Chem.*, 2001, 12, 249.

[20] T. S. Lawrence , R. K. Ten Haken, A. Giaccia , *Cancer: Principles and Practice of Oncology*, 8th ed, Eds.: V. T. DeVita Jr., T. S. Lawrence, S. A. Rosenberg, Lippincott Williams and Wilkins, Philadelphia, 2008.

[21] R. R. Patel, D. W. Arthur, *Oncol. Clin. North. Am.*, 2006, 20, 97.

[22] D. Gaynora, D. M. Griffith, *Dalton Trans.*, 2012, 41, 13239.

of the radiopharmaceutical and the target organ or tissue. The process involves the introduction of a radiopharmaceutical agent into the body in sufficiently low concentration in order to deliberately: define/locate the morphology of the disease, monitor the effects of treatment though accumulation of the radiopharmaceutical in the organ or tissue.

2.4.4 Type of radionuclide

Pierre and Marie Curie, F. Soddy and E. Rutherford all played a tremendous role to the discovery of many radioactive isotopes since the detection of the natural radioactivity in potassium uranyl sulfate in 1896.[23] The deliberate work of these scientists hallmarked the notion that majority of elements found in nature with an atomic number greater than that of bismuth (83) are radioactive. There are over 3000 nuclides known thus far, of which 2700 are radioactive, and the rest are stable. A handful of the radioactive nuclides used in medicine are artificially produced in cyclotrons and neutron generators.[24] Table 2.2 shows some of the radioactive nuclides used in medical applications.

---

[23] G. B. Saha, *Fundamentals of Nuclear Pharmacy*, 5th Ed, Springer Science and Business Media, Inc., 233 Spring Street, New York, 2003.
[24] G. B Saha, *Physics and Radiobiology of nuclear medicine*, 3rd Ed, Springer Science and Business Media, Inc., 233 Springer street, New York, 2006.

Table 2.2: Selected isotopes used in diagnostic or therapeutic radiopharmaceuticals. [25,26,27,28,29,30]

Isotope	Half-Life(hours)	Energy	Decay mode	Source
Scintigraphic Imaging		**γ Gamma Energy (keV)**		
^{67}Ga	78.3	93 (10%), 185 (24%), 296 (22%)	EC	Cyclotron ^{68}Zn(p, 2n)-^{67}Ga
^{99m}Tc	6.02	141 (89%)	IT	^{99m}Mo-^{99m}Tc Generator
^{111}In	67.9	171 (88%), 247 (94%)	EC	Cyclotron ^{111}Cd(p, n)-^{111}I
PET Imaging	**Half-Life**	**β^+ Positron Energy (keV)**	**Decay mode**	**Source**
^{61}Cu	3.3	1220, 1150, 940, 560 $E\gamma = 283\ (13\%), 380\ (93\%)$ keV	β^+ (62%) EC (38%)	Cyclotron ^{61}Ni(p, n)-^{61}Cu
^{62}Cu	0.16	2910	β^+ (98%) EC (2%)	^{62}Zn-^{62}Cu Generator
^{64}Cu	12.7	656	β^+ (19%) EC (41%) β^+ (40%)	Cyclotron ^{64}Ni(p, n)-^{64}Cu
^{68}Ga	1.1	1880, 770	β^+ (90%) EC (10%)	^{68}Ge-^{68}Ga Generator
^{66}Ga	9.5	4150, 935	β^+ (56%)	Cyclotron ^{68}Zn(p, 2n)-^{67}Ga
^{89}Zr	78.5	897	β^+ (23%) EC (77%)	Cyclotron ^{63}Cu(α, nγ)-^{66}Ga
Therapeutic Applications	**Half-Life (hours)**	**β Beta Energy (MeV)**	**Maximum range (mm)**	**Source**
^{188}Re	17.0	2.12 (85%) $E\gamma = 155\ (15\%)$ keV	11.0	^{188}W-^{188}Re Generator
^{186}Re	88.8	1.07 (91%) $E\gamma = 137\ (9\%)$ keV	5.0	^{185}Re(n, γ)-^{186}Re Reactor
^{67}Cu	62.0	0.40 (45%), 0.48 (3%), 0.58 (20%) $E\gamma = 93\ (17\%), 185\ (48\%)$ keV	1.8	^{68}Zn(p, 2p)-^{67}Cu Accelerator
^{90}Y	63.84	2.28 (100%)	12.0	^{90}Sr-^{90}Y

[25] C. A. Boswell, M. W. Brechbiel, *Nuclear Medicine and Biology.*, 2007, 34, 757.

[26] S. Mather, *Eur. J. Nuclear Medicine.*, 2001, 28, 543.

[27] D. A. Weber, L. Eckerman, L. T. Dillman, J. C. Ryman, *MIRD: Radionuclide Data and Decay Schemes, Society of Nuclear Medicine*, New York, USA, 1989.

[28] C. A. Lipinski, F. Lombardo, B.W. Fominy, P.J Feeney, *Adv. Drug Del. Rev.*, 2001, 46, 3.

[29] R. B. Firestone, *Table of Isotopes*, Eds.; V,S Shirley, S. B. Baglin, S. Y. F Chu, J. Zipkin, Wiley, New York, USA, 1996.

[30] S. Liu, D.S Edwards, *Chem. Rev.*, 1999, 99, 2235.

		$E\gamma = -$		Generator
^{153}Sm	46.8	0.64 (30%0, 0.71 (50%), 0.81 (20%) $E\gamma = 103$ (28%) keV 1.85	3.0	^{152}Sm(n, γ)- ^{153}Sm Reactor
^{166}Ho	26.4	$E\gamma = 80.6$ (6.6%) keV, 1.38 (0.9%) MeV	8.0	Reactor

The choice of a radionuclide depends on the purpose to which the radionuclide is being used, that is, diagnostic or therapeutic purposes. The size, type and location of the tumour dictate which radionuclide should be employed depending on its physical and chemical properties. Diagnostic agents comprises of radionuclide that emit high energy particles that can penetrate the body and be detected externally. Therapeutic radionuclides differ from those used in diagnosis in that they are predominantly alpha or beta emitting particles that can cause ionization and in the process break down bonds resulting in intended ablation.[31]

2.4.5 Half-life

The half-life of a radionuclide is defined as the time required for half of the radiopharmaceutical to disappear from the biological system and is denoted by ($t_{1/2}$). This is an important aspect in radiopharmaceutical design since it determines the rate of radioactive decay. A radiopharmaceutical administered to a patient is eliminated through the body via mechanism such as urinary or facet excretion and perspiration. A radionuclide should have a relatively effective half-life which is sufficient enough to complete the study at hand, that is, preparation of the drug, transportation, administration and clearance.

2.4.6 Mode of decay

A single element can have a number of different isotopes. Isotope (elements with the same atomic number but different mass numbers) and nuclide are interchangeable terms. Some of the many isotopes may have an unstable configuration of protons and neutrons; as a result they will seek stability through the disintegration of the nucleus to a more stable configuration. The transformation can be through one or a

---

[31] C. S. Cutler, H. M. Hennkens, N. Sisay, S. Huclier-Markai, S. S. Jurisson, *Chem. Rev.* 2013, 113, 858.

combination of the radioactive decay processes: α decay, β⁻ decay, β⁺ decay, spontaneous fission, electron capture, and isomeric transition.[23]

β-particle emitters are extensively used in therapeutic application in clinical practise. When low energy particles are used, the radiation needs to be delivered directly to the primary target, nucleus, however direct delivery to the nucleus is not necessary when very high energy β-particles with longer tissue penetration range are used. High energy particles do however effect a crossfire to healthy non-targeted organs and tissues.[32,33,34]

α-particle emitters are generally heavy metals with shorter particle range rendering the radionuclides suitable for treatment of smaller tumors.[35,36] The particle energy spans around 40 μm to 100 μm.[37,38] The relative short energy range of α-emitters affords them the ability to produce high degree of activity while having tolerable effects on the non-targeted surrounding tissues.

Auger electron emitters have lower energy electrons relative to α and β particles. The emitted particles deposit their energy over subcellular dimensions producing highly localised energy density in direct vicinity of the decay site.[39,40] The clustered ionisation within the decay site has immense therapeutic potential thus making auger electron emitters ideal for direct targeting.

2.4.7 Methods of Labelling

Traditionally, radiopharmaceutical research was directed to the development of radiotracers and their biological distribution to major organs and tissues, for example, ⁹⁹ᵐTc-sestamibi and ⁹⁹ᵐTc-tetrofosmin are widely used as perfusion imaging agents.[41] The biodistribution of these traditional radiopharmaceuticals is defined solely by the chemical and physical properties of the compound. Due to

[32] W. A. Volkert, T. J. Hoffman, *Chem. Rev.*, 1999, 99, 2269.

[33] P. A. Schubiger, R. Alberto, A. Smith, *Bioconjug. Chem.*, 1996, 7, 164.

[34] R. W. Howell, D. V Rao, K. S. Sastry, *Med. Phys.* 1989, 16, 66.

[35] R. W. Howell, M. T. Azure, V. R. Narra, D. V. Rao, *Radiat. Res.*, 1997, 142, 290.

[36] J. L. Humm, *J. Nucl. Med.*, 1990, 31, 75.

[37] M. R. Zalutsky, D. D. Bigner, *Acta Oncol.*, 1996, 35, 373.

[38] R. W. Kozak, R. W. Atcher, C. A. Gansow, A. M. Friedman, J. J. Hines, T. A. Waldmann, *Proc. Natl. Acad. Sci.*, 1986, 83, 474.

[39] S. J. Adelstein, A. I. Kassis, *J. Radiat. Appl. Inst. B.*, 1987, 14,165.

[40] E. Pomplun, J. Booz, D. E. Charlton, *Radiat. Res.*, 1987, 111, 533.

[41] S. Liu, *Chem. Soc. Rev.*, 2004, 33, 445.

research developments in radiopharmaceuticals, there has been a paradigm shift to the use of radiolabeled receptor ligands as target specific radiopharmaceuticals for diagnosis and therapy. Target specific radiopharmaceuticals are a class of compounds whose biodistribution is defined by the biological interactions with the target organ or tissue.[30]

In the ensuing years, considerable amount of research has been directed to the design of radiometer labelled receptor-target agents where the receptor ligands are biomolecules such as monoclonal antibodies, peptides or smaller molecules such as folic acid.[42] Coordination chemistry plays a central role in the design and development of these radiolabelled receptor molecules. The process encompasses the chemical phase which deals with the synthesis of the ligand, development of radiolabelling method and techniques, assessment of purity and stability of the radioligand. The commonly used strategies in clinical use for radiolabelling are the (1) integrated, (2) bifunctional approach and (3) peptide approach.
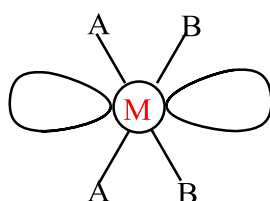
Integrated approach
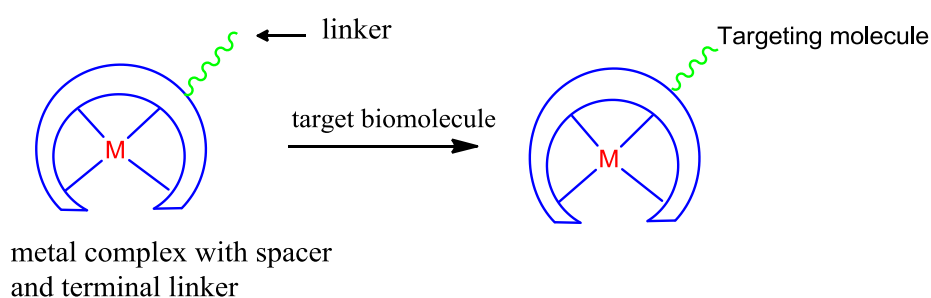
Bifunctional approach

Figure 2.2: **Representation of the integrated and bifunctional approaches used for radiolabelling.[41]**

---

[42] C. J. Anderson, M. J. Welch, *Chem. Rev.* 1999, *99,* 2219.

2.4.7.1 Integrated approach

The integrated approach entails the replacement of a fragment on a high-affinity receptor ligand with a radionuclide chelate whilst effecting minimal changes in size, conformation and binding affinity of the receptor.[43] The radionuclide is incorporated into the molecule primarily through the formation of covalent or coordinative covalent bonds, example ^{99m}Tc-DTPA. The major challenge is to find ways of binding the radioactive precursor without influencing the chemical and biological properties of the biomolecule.

2.4.7.2 Bifunctional approach

The bifunctional approach involves the employment of high binding affinity receptor as a target molecule. The approach can essentially be divided into the following components, receptor ligand as a **(1)** target biomolecule, **(2)** pharmacokinetic modifying linker, **(3)** bifunctional chelating agent and the **(4)** radionuclide.

The biomolecule serves as a carrier of the radionuclide to the target receptor site. A bifunctional chelate is positioned between the radionuclide and the biomolecule either directly or through a linker. The biologically active molecule can typically be a small peptide molecule or a monoclonal antibody designed for binding to particular receptors overexpressed on tumor cells.[44] The chelating agent is often placed in such a way that there is no interaction with the receptor providing a good chance of retaining the receptor binding affinity and specificity consequently increasing the selective uptake of the radiopharmaceutical. The radionuclide should not detach from the ligand after administration in order to map out the distribution and monitor the effects of the radionuclide. The linker serves as a platform for modifying pharmacokinetics such as uptake and clearance of the radiopharmaceutical. The linker can be a simple hydrocarbon chain, a peptide sequence or poly (ethylene glycol). The targeting abilities of the biomolecule can be influenced by factors such as the size, charge, charge, lipophilicity and the length of the linker. All these factors have an overarching effect on the target-to-background (T/B) ratios.[45]

---

[43] R. K. Hom, J. A. Katzenellenbogen, *Nucl. Med. Biol.,* 1997, *24*, 485.
[44] D. J. Yang, E. E. KIM, T. Inoue, *Ann. Nucl. Med.*, 2006, 20, 1.
[45] P. M. Smith-Jones, B. Stolz, R. Alberto, H. Knecht, C. Bruns, *Nucl. Med. Biol.,* 1997, *24*, 761.

A balance of several factors should be considered when it comes to the development of novel bifunctional chelators (BFC).[46] These factors include:

(i)   The BFC should form thermodynamic stable and kinetic inert complexes to inhibit possible ligand interactions or exchange and also possible loss of the radionuclide

(ii)   There should be rapid complexation kinetics at low temperature and concentration at relevant pH levels

(iii) The BFC should selectively bind to the specific radiometal and biomolecule

(iv)   Tuneable chemical and electronic properties in order to adjust the pharmacokinetic properties

(v)   Reasonable easy preparation and cost-efficiency

The coordination chemistry of several bifunctional coupling systems with relevant technetium core has been extensively studied.[47,48] Tetradentate chelators with NS or NO not only form kinetically stable complexes with the $[Tc=O]^{3+}$ core under physiological conditions, but also provide shielding of the metal centre from possible reactivity.

TcO(N$_2$S$_2$) CPB-DADT

TcO(N$_2$S$_2$) CBO-DADT
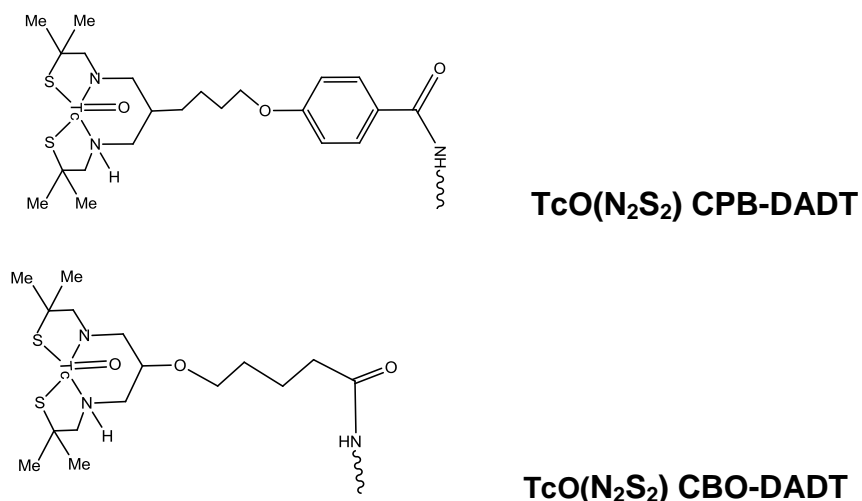
Figure 2.3: N$_2$S$_2$ Diaminedithiol (DATS), bifunctional chelating agents.

---

[46] M. D. Bartholomä, *Inorg. Chim. Acta.*, 2012, 389 , 36.

[47] A. Duatti, L. Uccelli, *Trends. Inorg. Chem.* 1996, 4, 27.

[48] A. Boschia, A. Duatti, *Topics. Curr. Chem.*, 2005, 252, 85.

The rich coordination chemistry of $[^{99m}Tc(CO)_3]^+$ core is being actively pursued with various mono-, bi and tridentate and a combination thereof for the development of novel bifunctional chelators. Tridentate ligands are proving to be the most versatile. The tridentate chelators form stable complexes with effective clearance from the blood and important organs.[49]

Bidentate ligands are more versatile when combined with mono ligands in the so-called [2+1] approach. The water ligand in fac-$[M(CO)_3(H_2O)(L)]^+$ (L = bidentate ligand), is loosely coordinated and can be replaced with a monodentate ligand. The [2+1] approach with the fac-$[M(CO)_3]^+$ core can be used for mimicking structures of biologically relevant molecules.[50] The biomolecule can be attached to either the monodentate or the bidentate ligand for labelling and the reserve ligand serving as variable for tuning of physiochemical properties of the biomolecule. Generally the mixed ligand concept forms a single exclusive complex due to the high kinetic stability. The [2+1] approach is currently under intense studies to solve problems associated with this labelling method such as insufficient in $vivo$ stability which is possibly facilitated by the loosely coordinated monodentate ligand entertaining some cross-activity in physiological conditions.
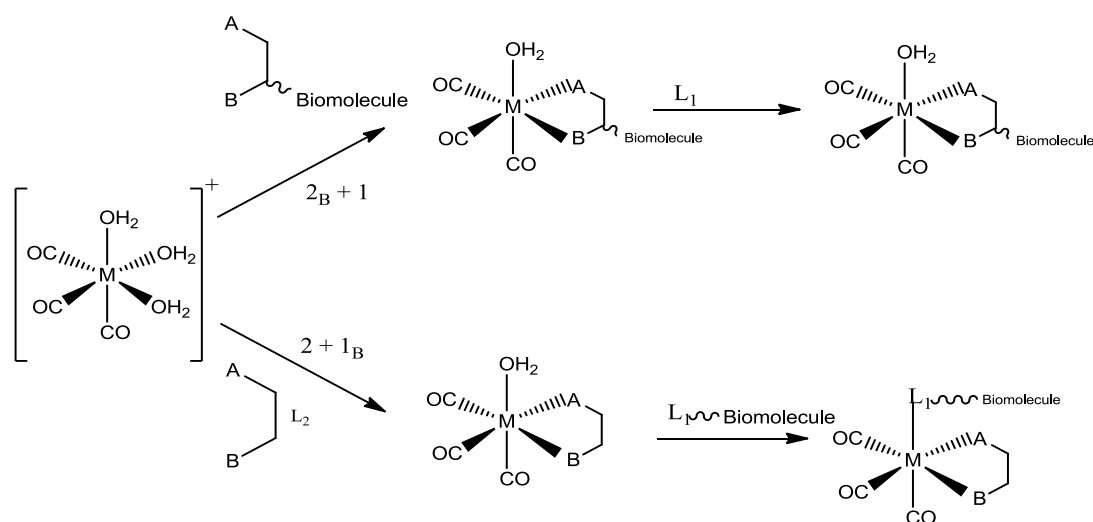
Figure 2.4:   An illustration of the [2+1] mixed ligand approach, A_1, B_1 = different donating atoms; L = monodentate ligand.[51]

[49] A. Egli , R. Alberto, L. Tannahill, R. Schibli, A. U, Schaffland, R. Waibel , D. Tourwe, L. Jeannin, K. Iterbeke, P. A. Schubiger, *J Nucl Med.,* 1999, 40, 1913.
[50] R. Alberto, R. Schibli, U. Abram, B. Johannsen, H-J. Pietzsch, P. A. Schubiger, *J. Am. Chem. Soc.,* 1999,121, 6076.
[51] R. Alberto, *Top. Curr. Chem.*, 2005, 252, 1.

2.5 Manganese in Medicine

A fundamental understanding of the coordination chemistry or organometallic chemistry of the group 7 transition metals (manganese, rhenium and technetium) has provided opportunity to incorporate these metals in the development of fields such as catalysis and medicine for human life sustenance and development. The development of an element's chemistry is essentially governed by its relevance in application for the bettering of the human conditions, with specific reference to medicine. Rhenium and technetium are spearheading the radiopharmaceutical development due to their ideal nuclear properties mentioned earlier, whilst manganese is used in other therapy and diagnosis methods which will be briefly discussed below.

2.5.1 Manganese carbonyl releasing molecules

Carbon monoxide (CO), like Nitric oxide (NO) and hydrogen sulphide (H_2S), is produced from the degradation of haem by activity of haem oxygenase enzymes in mammalian cells. Carbon monoxide is notoriously known for its disturbance on the flow of oxygen in the blood stream. For many years people became accustomed to the idea of the gas being nothing but a toxicant and a pollutant. This molecule has the ability to bind tightly to haemoglobin (shuttle for carrying oxygen in the blood) and replacing the oxygen needed to sustain life. The idea of CO gas being more than just a toxicant increased over the years with mounting evidence on the importance of CO in biological systems. [52,53,54] The early observations made on the activity of CO in biological system triggered enthusiasm in the development of CO releasing molecules (CORMs).[55,56,57] Storage and delivery of the gas presented the greatest limitations owing to the unfavourable effects projected by the impedance on oxygen transport and delivery by the CO gas. It was postulated that, storing the gas in a stable chemical form would enable controlled targeting and delivery to specific

---

[52] J. Rutter, M. Reick, S. L. McKnight , *Annu. Rev. Biochem.*, 2002, 71, 307.

[53] A. Grilli, M. A. De Lutiis, A. Patruno, L. Speranza, F. Gizzi, A. A. Taccardi, P. Di Napoli, R. De Caterina, P. Conti, M. Felaco, *Ann Clin Lab Sci.*, 2003, 33, 208.

[54] J. E. Clark, P. Naughton, S. Shurey, C. J. Green, T. R. Johnson, B. E. Mann, R. Foresti, R. Motterlini, *Circ. Res.*, 2003, 93, e2.

[55] R. D Rimmer, A. E. Pierri, P. C. Ford, *Coord. Chem. Rev.*, 2012, 256, 1509.

[56] R. Motterlini, J. E. Clark, R. Foresti, P. Sarathchandra, B. E. Mann, C. J Green, *Curr . Pharm. Des.*, 2003, 30, 2525.

[57] R. Motterlini, J. E. Clark, R. Foresti, P. Sarathchandra, B. E. Mann, C. J. Green, *Circ. Res.*, 2002, 90, e17.

organs and tissues consequently minimising exposure to none-targeted areas.[58] A quest to search for suitable "carriers" of CO gas was embarked on. Transition metals were the first resort owing to their high affinity towards CO ligands.

The versatile nature of transition metal-carbonyl complexes made it even more attractive to study their CO-releasing properties. The search encapsulates biocompatible ligands that are capable to facilitate CO delivery to target site maximising the efficiency of the desired biological effects such as cytoprotection during inflammation and promotion of wound healing process.[59,60,61]

Compound dimanganese dicarbonyl (CORM-1) together with tricabonyldichloro ruthenium(II)-dimer (CORM-2) is part of the earliest reported literature on the possible biological application of light mediated CO releasing molecules for therapeutic purpose. The investigation was performed using a myoglobin assay in which a cell culture containing deoxy-Mb in phosphorous buffer was placed in a tube (permitting direct irradiation) containing an aliquot of $Mn_2(CO)_{10}$ in DMSO. The study disclosed evidence that $Mn_2(CO)_{10}$ did not release CO when left in the dark, however upon exposure to cold light source, conversion of deoxy-Mb to MbCO was observed which was indicative of the CO release. The encouraging data prompted the search for suitable metal carbonyls that could release CO in aqueous solution. Numerous factors need to be considered when designing CO releasing molecules. Some of these intricate properties to make account of include; stability in physiological temperatures, stability in physiological temperatures, toxicity, target and delivery, method of activation, rates of CO loss in physiological conditions.[62]

These complexes are tailored to liberate controlled amounts of CO in biological systems and have been proven to hold therapeutic effects in several disease states. Numerous strategies of CO initiation are under investigation and these include; enzyme activation (ET-CORMs), ligand exchange in solution and photoactivation (Photo-CORM).[63,64] Photoactivated compounds entail a dark-stable drug which

---

[58] C. A. Piantadosi, *Antioxid. Redox. Signal.*, 2002, 4, 259.

[59] L. E. Otterbein, Antioxid. *Redox Signal.*, 2002, 4, 309.

[60] H. P. Kim, S.W. Ryter, A. M. K. Choi, *Ann. Rev. Pharmacol. Toxicol.* 2006, 46, 411.

[61] A. F. N. Tavares, M. Teixeira, C. C. Romao, J. D. Seixas, L. S. Nobre, L. M. Saraiva, J. *Biol. Chem.* 2011, 286, 26708.

[62] R. D. Rimmer, A. E. Pierri, P. C. Ford, *Coord. Chem. Rev.*, 2012, 256, 1509.

[63] W-Q. Zhang, A. J. Atkin, I. J. S Fairlamb, A.C. Whitwood, J. M. Lynam, *Organomet.*, 2011, 30, 4643.

release CO gas upon irradiation.[65] Compounds CORM-3 and CORM-A1 are the first identified water soluble releasing molecules. This implies great pharmaceutical benefits since water solubility is one of the main features in the design and development of novel therapeutic compounds.

CORM-1: $Mn_2(CO)_{10}$

CORM-2: $[Ru(CO)_3Cl_2]_2$

CORM-3: $Ru(CO)_3Cl$-glycinate

CORM-A1: $(Na_2)[H_3BCO_2]$
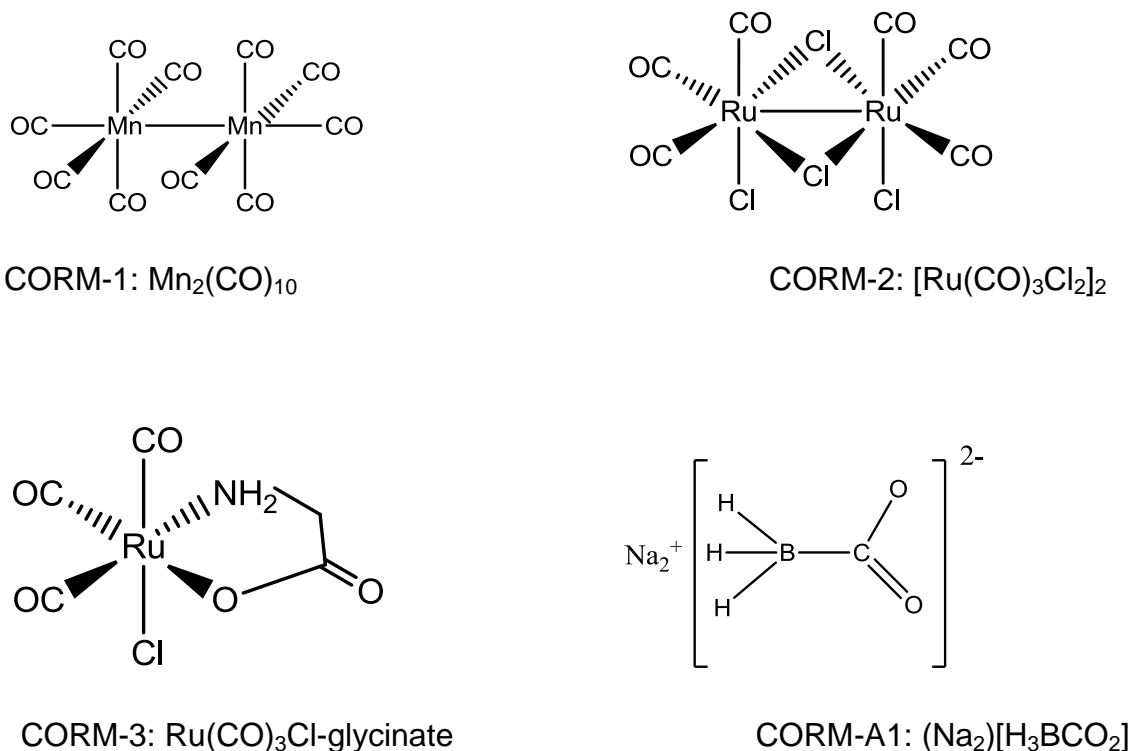
Figure 2.5: Chemical structures of selected CORMs.[66,56,67]

2.5.2 Manganese Superoxide Dismutase

All mammals consume oxygen for life sustenance, although not all the oxygen consumed is used for cellular respiration, a fraction of the total oxygen consumed converts into highly reactive superoxide anion radicals. Super-oxide dismutase (SOD) is an enzyme that catalyses the dismutase of superoxide radicals into oxygen and hydrogen peroxide.[68] The inability of the body to adequately control the

---

[64] *A. J. Atkin, I. J. S. Fairlamb, J. S. Ward, J. M. Lynam, J. Organomet.,* 2012, 31, 5894.

[65] P. Rudolf, F Kanal, J. Knorr, C. Nagel, J. Niesel, T. Brixner, U. Schatzschneider, P. Nuernberger, *J. Phys. Chem. Lett.*, 2013, 4, 596.

[66] R. Motterlini, J. E. Clark, R. Foresti, P. Sarathchandra, B. E. Mann, C. J. Green, *J. Vasc. Res.* 2001, 38, 25.

[67] M. J. Clarke, *Coord. Chem. Rev.,* 2002, 232, 69.

[68] Olga Iranzo., *Bioorg. Chem.*, 2011, 39, 73.

concentrations of the undesired chemical by-products, superoxide anion, is detrimental to the body and might aggravate some disease such as cardiovascular diseases, cancer, hypertension, inflammation and diabetes.[69] Under normal circumstances, the body can survive from oxidative stress using the endogenous Mn-SOD found in the cells, however serious discrepancies occur as soon as there is an overproduction of the radical anion compromising the body's ability to cope with the influx. Several Mn-SOD mimics are under intensive development with the potential of pharmaceutical treatment of inflammation and tissue injury.[70,71]

$$2O_2^{\cdot-} + 2H_2 \longrightarrow H_2O_2 + O_2$$
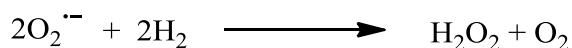
Scheme 2.1: Illustration of the conversion of the superoxide anion.

2.5.3 Magnetic Resonance Imaging

Magnetic resonance imaging (MRI) is a technique used to provide detailed images of organs or tissues in the body. The technique utilises a strong magnetic field and radio waves to create a computerised image. The use of manganese compounds as contrast agents has expanded over the years probably due to a better understanding of the chemistry toxicity profile of the metal.[72] The divalent ion of manganese (Mn^{2+}) has proven to be a particular useful contrast agent for brain imaging and has given birth to manganese enhanced magnetic resonance imaging (MEMRI) owing to its contrast enhancing properties. Mn^{2+} is analogues to Ca^{2+} thus can enter excitable cells though voltage-gated calcium channels which provides a window to look for activity in active brain cells. A controlled systematic administration of Mn^{2+} will negate neuronal pathways to map out activity in specific regions in the brain.[73,74] Mn^{2+} is paramagnetic and thus shortens the spin relaxation time of water by accumulating at these regions and as a consequence facilitates high resolution magnetic resonance imaging.[75,76,77]

[69] I. N. Zelko, T. J. Mariani, R. J. Folz, *Free. Radic. Biolo. Med.*, 2002, 33, 337.

[70] D. Salvemini, D. P.Riley and S. Cuzzocrea, *Nat. Rev. Drug Disc.*, 2002, 1, 367.

[71] D. P. Riley, *Chem. Rev.*, 1999, 99, 2573.

[72] J. Crossgrove, W. Zheng, *NMR. Biomed.*, 2004, 17, 544.

[73] R. G. Pautler, A. C. Silva, A. P.Koretsky A, *Magn. Reson Med.* 1998, 40, 740.

[74] I. Tindemans, T. Boumans, M. Verhoye, A. Van der Linden, *NMR. Biomed.*, 2006, 19, 18.

[75] D. A. Cory, D. J. Schwartzentruber, B. H.Mock, *Magn. Reson. Imaging.*, 1987, 5, 65.

[76] M. H. Mendonça-Dias, E. Gaggelli, P. C. Lauterbur, *Semin. Nucl. Med.*, 983, 13, 364.

2.6 Technetium imaging agents

The great efforts directed to the coordination chemistry of ^{99m}technetium led to the successful development of several first generation ^{99m}Tc based radiotracers for heart, brain, kidney and liver imaging, example ^{99m}Tc(MIBI)$_6$]$^+$ (MIBI = 2-methoxy-2-methylpropylisonitrile).[41] The sophistication of the modulators, positron emission tomography (PET) and single photon emission tomography (SPECT) used for non-invasive imaging studies coupled with the development of target specific radiopharmaceuticals has steered to a new dimension of second and third generation imaging agents. These radiopharmaceuticals are branded according to their relative synthetic approach and the biodistribution and will be briefly discussed below.

2.6.1 First generation Radiopharmaceuticals

The majority of commercially available technetium radiopharmaceuticals for imaging belong to the first generation radiopharmaceuticals and will be briefly discussed below. The successful application of first generation radiopharmaceuticals is highly dependent on the physiochemical properties such as size, charge, lipophilicity of the complex which are believed to be the determining factors in the biodistribution of the radiopharmaceutical in target organs and tissues.

Brain imaging: The efficiency of a brain imaging radiopharmaceutical depends on its ability to cross over the blood-brain barrier.[78] Once these tracers have diffused through the barrier, they are retained in the brain following a metabolic conversion into non-diffusible form.

Heart imaging: Heart imaging radiopharmaceuticals monitor and evaluate regional blood flow abnormalities in coronary artery diseases.[79,80] The design of these ^{99m}Tc complexes was prompted by the postulation made by Deutsch *et al* that unipositively charged lipophilic complexes would localize in the heart muscles.[81]

---

[77] A. C. Silva, J. H. Lee, I. Aoki, A. P. Koretsky, *Biomed.*, 2004, 17, 532.
[78] D. D. Dishino, M. J. Welch, M. R. Kilbourne, M. E. Raichle, *J. Nucl. Med.*, 1983, 24, 1030
[79] A. D. Nunn, *Semin. Nucl. Med*, 1990, 20, 111.
[80] L. H. Opie, B. Hesse. *Eur. J.Nucl.* Med., 1997, 24, 1183.
[81] Deutsch E, Bushong KA. Glavan RC, *Science.*,1981, 214, 85.

Renal Imaging: Renal imaging radiopharmaceuticals are used for the evaluation of renal plasma flow function and morphology. These can be divided into two classes, the first class comprises of radiotracers that are quickly washed out from the kidneys and can be used to evaluate the kidney functions and urinary drainage, the second class includes radiotracers that are retained in the kidneys for evaluation.[82]

Skeletal imaging: The primary purpose of using ^{99m}Tc compounds in bone imaging is to identify if there has been metastasis in the bone.[83] The development of bone seeking radiopharmaceuticals is centred on analogues of calcium, hydroxyl groups and phosphates due to the propensity of these elements to localise in bones.

2.6.2 Second generation imaging

Second generation technetium based imaging radiopharmaceuticals are designed to specifically bind to a particular receptor. These radiopharmaceuticals are generally prepared via the bifunctional and integrated strategies. The ligands bind covalently to the radioactive precursor which is attached to a biomolecule. Peptides, proteins are amongst the possible target molecules.

Inflammation and the central nervous system: Radiopharmaceuticals that bind the central nervous system receptors provide insightful knowledge regarding the pathophysiology of a number of neurological and psychiatric disorders such as Alzheimer's disease, Parkinson's disease and epilepsy.[84,85]

Monoclonal antibodies: These antibodies can be used to locate the disease, determine the diseases state and monitor the progress of therapy.[86] Monoclonal antibodies are in principle carriers of the radionuclide tracer to the target area provided there is no interference with the coordination on the antibody to the receptor site. Labelling of only fragments of the antibodies is favourable over the whole antibody due to effective biodistribution kinetics imposed by the size.

---

[82] M.F Reiser, H.-U. Kauczor, H.Hricak, M. Knauth, *Radiological imaging of the kidney*, Springer-Verlang, Berlin, Heidelberg, 2014

[83] J. R. Dilworth, S. J. Parrott, *Chem. Soc. Rev.*, 1998, 27, 43.
[84] D. J. Brooks, *Drug Disc. Today.*, 2005, 2, 317.
[85] B. K. Madras, G. M. MIller, A. J. Fischman, *Biol. Psychiatry.*, 2005, 57,1397.
[86] D. J. Hnatowich, G. Mardirossan, M. Ruscowski, M. Fargarasi, F. Firziand P. Winnard, *J. Nucl. Med. Chem.*, 1993, 34, 172.

Hypoxia imaging: A cell is deemed hypoxic when there is an imbalance between the metabolic demands of the affected parts and the supply of oxygen to the cells. These radiopharmaceuticals are mainly based on nitroimidazole derivatives as the basic targeting fragment for imaging hypoxia.[87]

2.7 Aqueous chemistry of *fac*-[M(CO)$_3$(H$_2$O)]$^+$, M = ^{99m}Tc, Re

Traditionally, the development of technetium radiopharmaceuticals was focused on higher oxidation state cores including [TcO]$^{3+}$ and [TcN]$^{2+}$, low oxidation state technetium played only a subordinate role probably due to the lack of suitable starting material.[88] However a paradigm shift occurred since the development of a feasible synthetic path of stable organometallic technetium(I) and rhenium(I) complexes by Alberto *et al*. The complex is synthesized from the direct reduction of ^{99m}TcO$_4^-$ under mild conditions in aqueous medium. The aqua complex has an octahedral configuration with three tightly bound CO ligands facially coordinated to the metal centre and the three labile water ligands completing the octahedral geometry.[89,90]
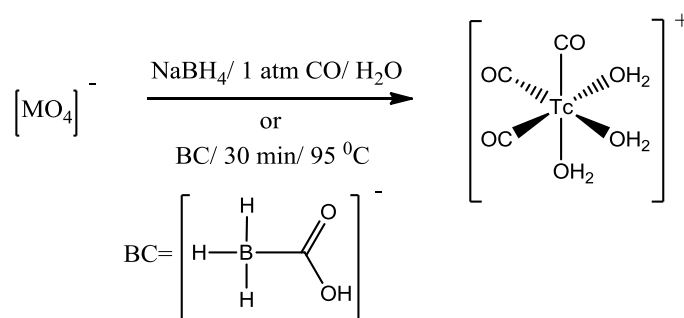
Figure 2.6: The synthesis of the *fac*-[^{99m}Tc(CO)$_3$(H$_2$O)$_3$]$^+$ labelling precursor.

As described earlier, second generation target specific radiopharmaceuticals are essentially the combination of radioactive nuclide, biomolecule and receptor ligands that require metal complexes that provide highest possible stability whilst avoiding

---

[87] X. Zhang, T. Melo, J. R. Ballinger, A. M. Rauth, *Int. J. Radiat. Oncol. Biol. Phys.*, 1998, 42, 737.

[88] W. Xiangyun, W. Yi, L. Xinqi, C. Taiwei, H. Shaowen, W. Xionghui , L. Boli, *Phys. Chem. Chem. Phys.*, 2003, 5, 456.

[89] R. Alberto, J.K. Pak, D. van Staveren, S. Mundwiler, P. Benny, *Biopolymer*s., 2004, 76, 324.

[90] S. Mundwiler, R. Waibel, B. Springler, S. Kunze, R. Alberto, *Nucl. Med. Biol.*, 2005, 32, 473.

interference between the metal centre and the binding site of the biomolecule.[91] The primary attractions of the fac-$[^{99m}Tc(CO)_3(H_2O)_3]^+$ as a precursor in radiopharmaceutical labelling, are the reduced size and the kinetic stability of the complex.[92] The kinetic inertness of the aqua complex implies *in vivo* stability, the compact size of the core prevents attack from foreign ligands or re-oxidation which may result to decomposition. The low oxidation state allows a broader spectrum of donor and accepter ligands which is a great advantage in the designing of complexes whose properties can be tuned to accommodate that of the biomolecule.

A great advantage of using the aqua precursor for radiolabelling molecules relies on the effortless compromising of the water ligands by a variety of functional groups containing oxygen, nitrogen and sulphur atoms which can mimic biological binding sites. A series of mono-, bis- and tridentate ligand systems containing N-heterocycles such as pyridines, pyrazoles, imidazoles, amines, amides, carboxylic acids, phosphines, thiols and thio-ethers have been successfully coordinated to fac-$[M(CO)_3]^+$ core, where M= Re, ^{99m}Tc. A majority of the ligands in these studies can be modified allowing fine tuning of physical and chemical properties of the final complex, example, charge, size and lipophilicity. The design of suitable chelates is dependent on the coordination requirements of a specific radiometal and the overall stability of the complex.[93] The high affinity of technetium to sulphur atom makes sulphur containing ligands such as thiols, thio-ethers especially macrocyclic thio-ethers, attractive in the development of bifunctional chelation.

There exist a tug of war between the use of bi- or tridentate functionalities, but if one bases their argument on thermodynamic considerations, the tridentate chelators have the upper hand since they provide favourable pharmacokinetic properties such as efficient clearance. A study was conducted with a series of bi- and tridentate ligand system containing amines and carboxylic acid functionalities to evaluate the potential formation of *in vitro* and *in vivo* stable fac-$[^{99m}Tc(CO)_3]^+$ complexes.[94] The complexes containing tridentate functionalities showed efficient clearance from all organs and tissues, whilst those containing bidentate ligands had high retention in

---

[91] R. Alberto. *Eur. J. Inorg. Chem.,* 2009, 2009, 21.

[92] R. Schibli, P. A. Schubiger, *Eur. J. Nucl Med., 2002*, 11, 1529.

[93] M. J. Heeg, S. S. Jurisson, *Acc. Chem. Res.* 1999, 32, 1053.

[94] R. Schibli, R. La Bella, R. Alberto, E. Garcia-Garayoa, K. Ortner, U. Abram, P. A. Schubiger, *Bioconjug. Chem.,* 2000, *11,* 345.

the liver and kidneys. This behaviour was attributed to the lower thermodynamic stability of the bidentate containing complexes and possibly the reactivity on the vacant coordination site.
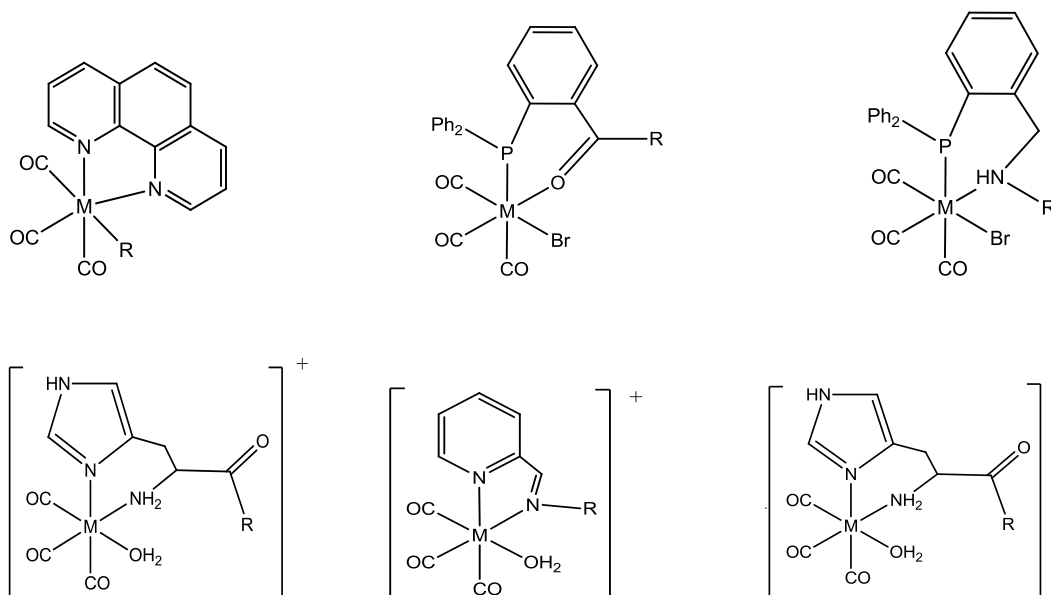
Figure 2.7: Selected examples of bidentate chelates.

2.7.1 Substitution kinetics of *fac*-[M(CO)$_3$(H$_2$O)$_3$]$^+$, M = Mn, ^{99m}Tc, Re

The potential use of *fac*-[M(CO)$_3$]$^+$ (M=Tc, Re) core has garnered much interest due to its promising effects in the development of new organometallic precursors for labelling of biomolecules in diagnostic and therapeutic medicine. The three water ligands attached to the highly inert *fac*-[M(CO)$_3$]$^+$ core are labile and can be readily substituted by a variety of mono-, bi- and tridentate ligands. Understanding the kinetic and coordinating properties of the complexes is an important aspect in the design and application of the radiopharmaceuticals as it provides valuable insight regarding preparation, uptake and clearance of the radiopharmaceutical.[95,96] It is thus imperative to study the fundamental reactivity of the precursor in aqueous medium, that is, the rates of water exchange, reactivity of the CO ligands and the

[95] L. Maria, A. Paulo, I.C. Santos, I. Santos, P. Kurz, B. Spingler, R. Alberto, *J. Am. Chem. Soc.*, 2006, 128, 14590.
[96] M. Moreno-Manãs, J. Marquet, A. Vallribera, Tetrahedron., 1996, 52, 337.

effect of the entering ligands on the rates of reaction in order to develop more suitable labelling strategies and incorporate suitable biomolecules into the system.[97]

The substitution kinetic behaviour of fac-[Re(CO)$_3$(H$_2$O)$_3$]$^+$ was first described by Salignac et al. An array of charged and uncharged nucleophiles such as (CH$_3$CN, Br$^-$, DMS, phen, TFA, TU) were used in effort to probe into the water exchange mechanism of the fac-[Re(CO)$_3$(H$_2$O)$_3$]$^+$ complex. The three water ligands in fac-[M(CO)$_3$(H$_2$O)$_3$]$^+$ are readily replaced by a variety of unidentate and bidentate ligands forming stable compounds. Three distinctive processes of the water substitution were identified for CH$_3$CN and DMS corresponding to the formation of mono, bi- and trisolvanto complexes. The formation of the new species was verified by ^{1}H NMR at 2.389, 2.379, 2.346 ppm and 2.436, 2.492 and 2.520 ppm corresponding to the formation of mono-, di- and triacetonitrile and tri-DMS complexes respectively. The dependence of the reaction mechanism on the entering ligand was demonstrated. An interchange (I_d/I_a) mechanism was proposed for rhenium going from N-donor ligands to softer S-donor ligands. A decrease in rate of formation was observed with an increase in degree of substitution corresponding to mono-, bi- and tri-DMS complex, $k_{f,1}$ = 1.51 x 10^{-3}, $k_{f,2}$ = 0.53 x 10^{-3} and $k_{f,3}$ = 0.10 x 10^{-3} M s^{-1}. A similar trend was observed in the water substitution of fac-[Tc(CO)$_3$(H$_2$O)$_3$]$^+$ with monodentate ligands such as imidazole and thioethers in saline. The DMS complexes show higher stability compared to the acetonitrile with stability constants of k_1 = 18.3 ± 0.1 M^{-1} and 3.0 ± 0.1 M^{-1} respectively. The effect was credited to the high affinity character of rhenium towards sulphur. The rate of substitution with DMS is twice as fast compared to CH$_3$CN substitution.

The water substitution rate is reasonably fast for the first two water ligands but ultimately slows down on the substitution of the third incoming ligand. It was proposed that after the substitution of the first two monoligand, the cationic metal centre attracts a negative charge for charge balancing reasons. This effect generates an equilibrium between the Cl$^-$ anion is with water consequently slowing down the rate of substitution of the third incoming ligand.[98,99] The overall rates of substitution are to some extend dependent on the nature of the entering ligands.

---

[97] N. Aebischer, R. Schibli, R. Alberto, A. E. Merbach., *Angew. Chem. Int. Ed.* 2000, 39, 254.

[98] R. Waibel, R. Alberto, J. Willuda, R. Finnern, R. Schibli, A. Stichelberger, A.Egli, U. Abram,

A dissociative mechanism was tentatively assigned for the water exchange with O and N donating atoms. The assignment is verified by the slightly positive activation parameter, $\Delta S^{\ddagger} = +14 \pm 10$ J K^{-1} mol^{-1}. An associative mechanism was assigned to the more reactive S-donor ligands. The Softer S-donor ligands are able to discriminate between the water and entering ligands better than the hard N-donor ligands, this feature rationalised the mechanism interchange from S-donor ligands, to the N-donor ligands.

$$fac\text{-}[M(CO)_3(H_2O)_3]^+ + L \quad \underset{k_{-1}}{\overset{k_1, K_1}{\rightleftharpoons}} \quad fac\text{-}[M(CO)_3(L)(H_2O)_2]^+ + H_2O$$

$$fac\text{-}[M(CO)_3(L)(H2O)_2]^+ + L \quad \underset{k_{-2}}{\overset{k_2, K_2}{\rightleftharpoons}} \quad fac\text{-}[M(CO)_3(L)_2(H_2O)]^+ + H_2O$$

$$fac\text{-}[M(CO)_3(L)_2(H_2O)]^+ + L \quad \overset{k_3, K_3}{\rightleftharpoons} \quad fac\text{-}[M(CO)_3(L)_3]^+ + H_2O$$
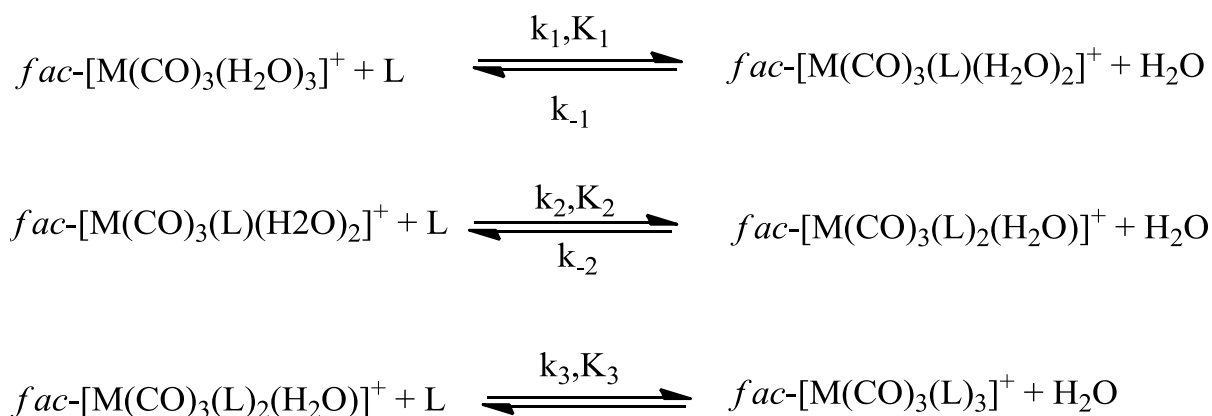
Scheme 2.2: Representation of stepwise water exchange in *fac*-[Re(CO)$_3$(H$_2$O)$_3$]$^+$.

An investigative study was performed on the effects of entering bidentate ligands on the metal centre with the notion of gaining insight in the potential use of the complex *fac*-[M(CO)$_3$(L,L'-Bid)(H$_2$O)]^n, n = 0, 1, in radiopharmaceuticals using the [2+1] mixed ligand approach defined in the preceding section. The water substitution of *fac*-[Re(CO)$_3$(H$_2$O)$_3$]$^+$ was investigated with a range of neutral or monoionic bidentate ligands with varied L,L' donor atoms, *N,N', N,O-,* and *O,O'*: bipy, phen.[100]

The rates of formation, $k_1(10^3$ M^{-1} s^{-1}), for N,N-bidentate complexes, *fac*-[Re(CO)$_3$(bipy)(MeOH)]$^+$ and *fac*-[Re(CO)$_3$(phen)(MeOH)]$^+$ were found to be, k_1(Br) [42, 50] and k_1(py) [0.096, 0.064] respectively. The rates of formation for the N,O'-bidentate complexes, *fac*-[Re(CO)$_3$(2.4-dPicoH)(MeOH)]$^+$ and *fac*-[Re(CO)$_3$(Pico)(MeOH)]$^+$ were found to be k_1(Br) [15.7; 11.8] and k_1(py) [1.641; 1.6] respectively and the O,O'-bidentate complex *fac*-[Re(CO)$_3$(2.4-dQuinH)(MeOH)]$^+$ and

J-P. Mach, A. Plüeckthun, P. A. Schubiger, *Nature Biotechnol.*, 1999, 17, 897.

[99] S. Seifert, J-U. Künstler, A. Gupta, H. Funke, T. Reich, H-J. Pietzsch, R. Alberto R, B. Johannsen, *Inorg. Chim. Acta.*, 2001, 322, 79.

[100] M. Schutte, G. Kemp, H. G. Visser, A. Roodt, *Inorg. Chem.*, 2011, 50, 12486.

fac-[Re(CO)$_3$(Quin)(MeOH)]$^+$ were found to be k_1(Br) [3.31; 3.9] respectively. From the data, it is clear that the rates of formation for the monoanionic entering ligands is orders of magnitude faster than the rates obtained for the neutral pyridine type ligands. This points out at the high affinity of positively charged complexes towards negatively charged entering ligands. The kinetic investigations demonstrated the effect of the electron withdrawing species on the overall methanol substitution reaction. A pronounced increase of electron density around the metal ion endorses an increase in the rates of entering ligands. This was demonstrated by the faster methanol substitution rate in *fac*-[Re(CO)$_3$(Flav)(MeOH)]$^+$ compared to *fac*-[Re(CO)$_3$(TropBr$_3$)(MeOH)]$^+$ with DMAP as the entering ligand. The fluorine atoms on attached to the ligand decrease the electron density around the metal ion, strengthening the metal-methanol bond. The strengthening of the coordinated methanol bond leads to a slower substitution rate. Similar behaviour was observed in acetylacetone ligands and its fluorinated forms. The rate of methanol substitution decreased with an increase in degree of fluorine substitution in the ligand backbone.[101] One can conclude that, the rate of the methanol substitution is in direct correlation with the degree of substitution on the acetylacetone backbone and also on the nature of the bidentate ligand and its donating functionalities.

A similar correlation was obtained from analogues of *fac*-manganese(I) tricarbonyl complexes, *fac*-[Mn(CO)$_3$(Bipy)(CH$_3$OH)]$^+$ and f*ac*-[Mn(CO)$_3$(Phen)(CH$_3$OH)]$^+$. The rate of methanol substitution was investigated with a variety of monoligands Br$^-$, pyridine and thiourea. Equally to rhenium(I) complexes, the rate of substitution with Br$^-$ was orders of magnitudes faster compared to the neutral entering ligands. The reaction with bromine k_1(Br$^-$) [0.31; 0.50] is two times faster compared to pyridine k_1(Py) [2.93 x 10^{-3}; 2.39 x 10^{-3}], three times faster compared to thiourea [9.53 x 10^{-2}; 7.4 x 10^{-2}] and six times faster compared to pyridine [9.53 x 10^{-2}; 7.4 x 10^{-2}] for complexes, *fac*-[Mn(CO)$_3$(Bipy)(CH$_3$OH)]$^+$ and *fac*-[Mn(CO)$_3$(Phen)(CH$_3$OH)]$^+$ respectively. As anticipated, rate of the methanol substitution reaction in *fac*-[M(CO)$_3$(L,L'-Bid)(CH$_3$OH)]^n (M = Mn, Re), with Br$^-$ and Py is an order of magnitude slower in rhenium(I) compared to manganese(I). A contrasting behaviour was observed on the complexes of the type *fac*-[Mn(CO)$_3$(N,O-Bid)(CH$_3$OH)]^n. The order

---

[101] A. Manicum, M. Schutte-Smitt, G. Kemp, H. G. Visser, *Polyhedron.*, 2015, 85, 190.

of reactivity was reversed with the reaction with thiourea being 10 orders of magnitude faster than the reaction with pyridine, k_1(TU) > k_1(Py) > k_1(Br⁻) for *fac-[*Mn(CO)$_3$(Pico)(CH$_3$OH)]. The switch in reactivity might be attributed to the overall positive charge on the complex in the two cases. The metal complexes are positively charged when N,N'= Bid ligands are used and neutral in N,O' ligands respect. This outcome highlights the higher affinity of positively charged metal complexes to charged halide ligands.

An underlying factor outlined by the methanol substitution reactions between manganese and rhenium metals is the decrease in substitution rate going from manganese to rhenium. This behaviour corroborates with the water self-exchange rate constants k_{ex} determined to be 23 s⁻¹ for Mn, 0.49 s⁻¹ for Tc and 0.054 s⁻¹ for Re.[102,103] The water exchange rate decrease when going down the group 7 group and decrease across the row, the trend can be attributed to the charge increase of the isoelectric complexes. It was demonstrated that the reactivity depends heavily on the nature of the metal centre and has a small dependence on the nature of the entering ligand. Backbonding increases when moving down the group subsequently enhancing the electrophilicity of the metal. As a result the ligands are bound more tightly to the metal centre. The slow self-exchange rate of rhenium and technetium might justify the necessity to apply heat when labelling molecules with either rhenium or technetium for efficient reaction rates.

[102] P. V. Grundler, L. Helm, R. Alberto, A. E. Merbach, *Inorg. Chem.* 2006, *45*, 10378.
[103] B. Salignac, P. V. Grundler, S. Cayemittes, U. Frey, R. Scopelliti, A. E. Merbach, R. Hedinger, K. Hegetschweiler, R. Alberto, U. Prinz, G. Raabe, U. Kolle, S. Hall, *Inorg. Chem.* 2003, *42*, 3516.

3 BASIC THEORY OF IR, NMR, UV/VIS AND X-RAY DIFFRACTION

3.1 Introduction

Spectroscopy defines the interaction of light with matter through three distinctive processes, that is, transmission, scattering and absorption. Numerous techniques have been developed for the quantitative and qualitative determination of both inorganic and organic molecules. All the complexes synthesised in this study were characterised using these techniques. This chapter presents a brief outline on the fundamental principles of the techniques.

3.2 Infrared spectroscopy

Infrared refers to the part of the electromagnetic spectrum between the visible and microwave region. Infrared Spectroscopy is one of the most used spectroscopy based methods. The popularity of the method is perpetuated by factors such as cost efficiency, rapidness and easy handling. The method offers opportunity for quantitative and qualitative identification of compounds and functional groups in gaseous, liquid, solid and other states of mater. This technique is based on the principle that within any molecule, atoms vibrate with defined frequencies characteristic of the functional groups and bonds involved. A spectrum is obtained by passing infrared radiation through a sample and determining what fraction of incident radiation is absorbed at a specific energy corresponding to the frequency of vibration of the subjected molecular sample. The IR region can be divided into three regions, the near, mid, and far IR. The mid-IR region is of much relevance in practical use and spans around 4000-400 cm^{-1}.

The interaction of infrared radiation with matter is described from the changes in molecular dipoles associated with vibrations and rotations. An electric dipole moment of a molecule changes as the molecule expands and contracts. The stretching

(bonds) and bending (angle) movements are collectively referred to as vibrations. The stretch can be in-phase (symmetrical stretching) or out-of-phase (asymmetric stretching)
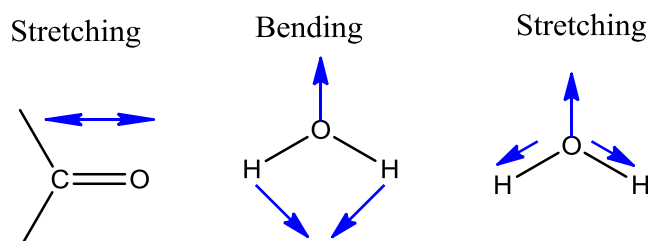
Figure 3.1: Stretching and bending vibration modes.

Symmetric Steching   Asymmetric Stretching
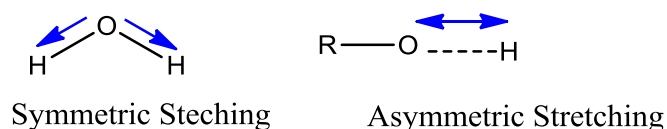
Figure 3.2: Symmetric and asymmetric Stretching mode.

Only molecules producing dipole moment change are IR active. The carbonyl group is permanently polarized because of the difference in electronegativity between carbon and oxygen atom. The large dipole moment created accounts for the use of carbonyl groups to characterised complexes.

Metal-CO bonding interactions comprises of a CO to metal sigma donation and a metal to CO π back-donation. CO ligands have the ability to stabilise electron rich low valent metals by acting as a strong π acceptor. The metal carbonyl displays two distinctive binding modes, that is, terminal and bridging modes. Infrared spectroscopy can distinguish between these two binding modes of metal carbonyl fragments through their vibrating frequency region. The terminal CO stretching frequency spans around 2100-2000 cm^{-1} while the bridging ones show v(CO) stretching band around 1720-1850 cm $^{-1}$. The amount of electron density back-donated to the CO group influences the vibrating frequency of the carbonyl bands. An increase of electron density around the metal centre results in an increase in back-donation to the CO ligands. This channel of electron density between the metal and the carbonyl ligands has an overarching effect on the metal-carbonyl bond.
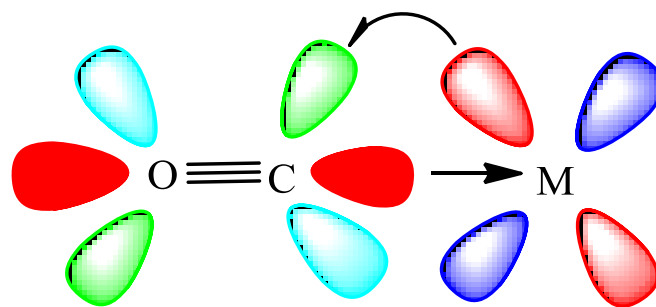
Figure 3.3: Representation of electron backbonding between metal-carbonyls.[1]

3.3 Ultraviolet and Visible (Uv-Vis) Spectroscopy

Ultraviolet and visible (UV-Vis) absorption spectroscopy technique is used to quantify the light absorbed and scattered by a sample.[2] The absorption measurements can be concentrated at a single point or over an extended spectral range. The technique uses electromagnetic radiation between 190 nm to 800 nm and is subdivided into ultraviolet(UV, 190-400 nm) and visible (Vis, 400-800 nm). The spectroscopy method is a useful characterization of the absorption, transmission and the reflectivity of a variety of important materials such as pigments and other compounds from plants.

The concentration of material in solution can be determined by measuring the absorption at a specific wavelength or range and then applying Beer-Lambert law. Beers law states that the absorbance (A) is directly proportional to the path length, *b*, and concentration, *c*, of the absorbing species. $A = \varepsilon bc$, where ε is a proportionality constant called the absorptivity. The absorption of UV or visible radiation corresponds to the excitation of outer electrons. When an atom or molecule absorbs energy, electrons are promoted from their ground state to an excited state. Changes in electronic energy levels within a molecule arise due to transfer of electrons. Three main electronic transitions can be considered: single bonding, σ, double or triple bonding, μ, and non-bonding (*n*, lone pair electrons) orbitals. Upon the absorption of energy by the molecule, an electron is promoted from the highest occupied molecular orbital (HOMO) to the lowest unoccupied molecular orbital (LUMO). The

---

[1] S. L. Upstone, *Ultraviolet/Visible Light Absorption Spectrophotometry in Clinical Chemistry, Encyclopedia of Analytical Chemistry,* Ed,: R. A. Meyers, John Wiley & Sons Ltd, Chichester, 2000, 1699

[2] D. L. Pavia, G. M. Lampman, G. S. Kriz, *Introduction to Spectroscopy*, 3rd Ed., USA, Thompson Learning, Inc., 2001.

wavelength at which molecules absorbs energy is dependent on how strongly the valance electrons are bound to the atom.
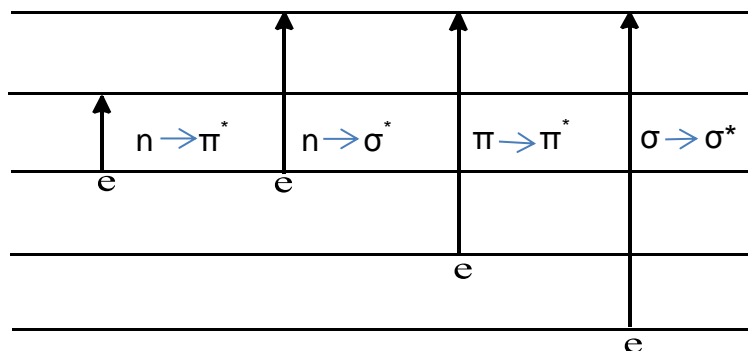
Figure 3.4: A representation of the electron transition.

3.4 Nuclear Magnetic Resonance Spectroscopy

Nuclear magnetic resonance spectroscopy is an indispensable tool used for structural analysis of biomolecules, natural compounds, tissue extracts and also in medicine for imaging of the human tissues and organs. The evaluation of molecular structure through measurements of the interaction of an oscillating radiofrequency electromagnetic field with a collection of nuclei subjected to a strong magnetic field. The technique is based on the quantum property of nuclei called spin I, described as an intrinsic angular momentum of quantum particles that can assume integer or half-integer values (0, 1/52, 1, 3/2,…9/2). The magnetic quantum numbers are related to the nuclear spin quantum numbers, I, by equation: $m = (2I +1)$. NMR spectroscopy can essentially be applied to all none zero nuclei spin. The most important nuclei for organic and biochemists are ^{1}H, ^{13}C, ^{15}N and ^{31}P, which all have I = ½.

In the absence of a strong external magnetic field, the nuclear spin are arranged randomly, however when the sample is subjected to a strong external magnetic field, the magnetic moment of the protons interact with the magnetic field and the nuclei adopts a specific orientation either with or against the field of the magnet.[3] Some of the nuclei will align parallel to the magnetic field and some antiparallel. The energy of

---

[3] H. Friebolin, *Basic One- and Two-Dimensional NMR Spectroscopy*, 2nd Ed., VCH Publishers, New York, 1993

the nuclei spins that are antiparallel to the magnetic field is higher than the energy of the parallel nuclei.
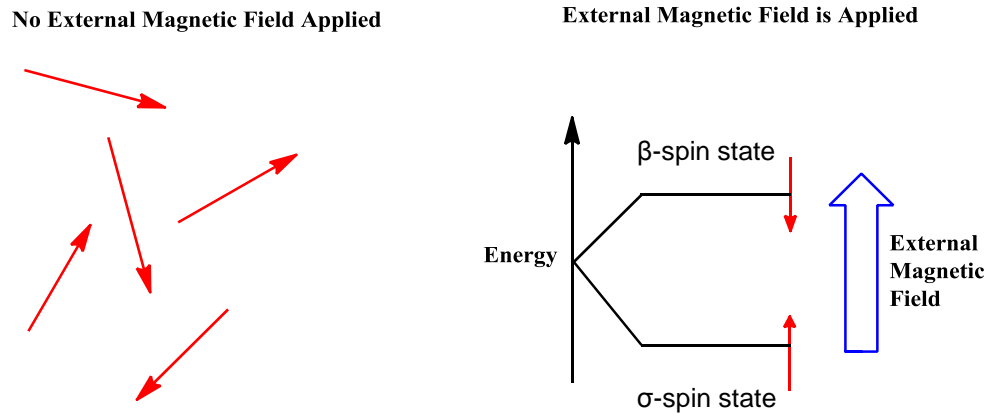
Figure 3.5: Ordering of nuclei in effect to the magnetic field.

Since a proton or carbon has two different magnetic quantum numbers, it has two different energy states in the presence of a static magnetic field. The spin quantum numbers of an electron are +1/2 and -1/2. These numbers indicate that an electron can have only one or two possible spin orientation. The orientations are normally represented by arrows pointing either upwards or downwards.
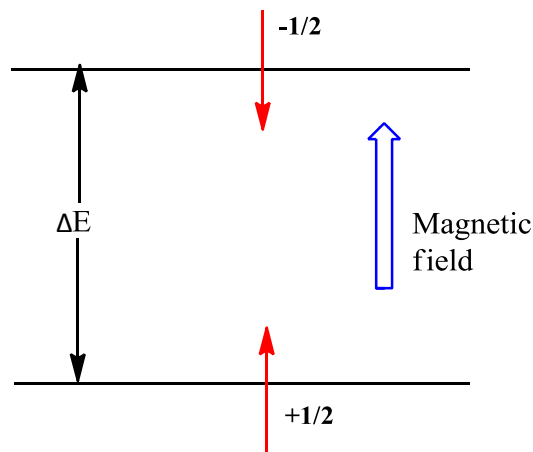
Figure 3.6: Energy occupation of nuclei in a magnetic field.

ΔE is the energy difference between the spin states. This energy difference is directly proportional to the strength of the applied magnetic field.

When a magnetic field is applied, the nucleus moves about its own axis of spin with angular frequency *w*. The frequency is directly proportional to the strength of the

applied magnetic field, the stronger the field, the higher the rate of rotation/ precession. Since the nucleus has a charge, the rotation generates an oscillating electric field of the same frequency. When the frequency of the oscillating electric field component of the incoming radiation matches the frequency of the electric field generated by the rotating nucleus, the two fields can couple, and energy can be transferred from incoming radiation to the nucleus, thus causing a spin change. This condition is called resonance. Relaxation is when the nuclei returns to their natural state. An electromagnetic signal whose frequency is depended on the energy difference is released. The signal frequency is picked and plotted as a function of intensity.

3.5 Single crystal X-ray diffraction

X-ray diffraction is a powerful tool used to determine the structure of crystalline material. The method reveals the structure of molecules through the determination of how they diffract X-ray radiation when arranged in a crystal lattice. Crystals are a build-up of individual molecules of a substance in one or few orientations resulting in a regular arrangement of atoms in three dimensions. This arrangement of atoms can be represented by a repeat unit called the unit cell. The unit cell is defined as the smallest repeating unit of atoms that can describe the crystal.[4]

Crystal data is obtained by placing a crystal in the path of a narrow beam of an x-ray source and x-ray detector. The total scattering intensities from a molecule is the sum of all the waves scattered by the individual atoms packed in a crystal lattice in one or few orientations transformed into discrete diffraction spot wherein constructive and destructive interference between waves amplify and diminish the resultant wave respectively.

---

[4] R. A. Engh., *Encyclopedic Reference of Genomics and Proteomics in Molecular Medicine* 2006, 2026.

3.5.1 Bragg's law and X-ray diffraction

The basic workings of X-ray diffraction can be explained by means of the Braggs law of diffraction. Bragg's law assumption to diffraction is to regard crystals as an array of layers or planes with an equal interplanar distance.[5] Some of the X-rays are reflected off a plane with the angle of reflection equal to the angle of incidence, but the rest are transmitted to be subsequently reflected by succeeding planes. X-rays from adjacent planes are normally reflected out of phase due to different path lengths. The phase difference is rectified by the Braggs law given by equation 3.1
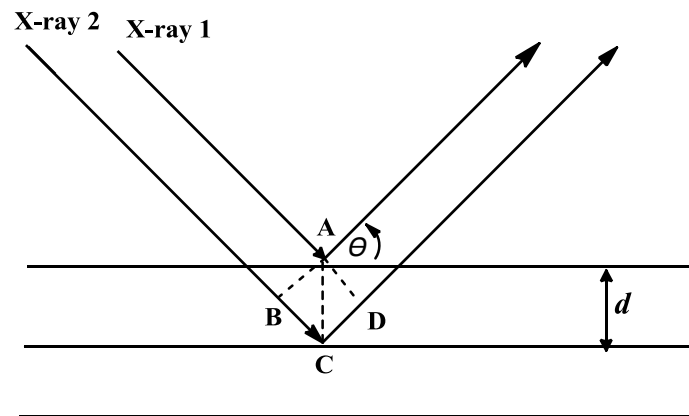
Figure 3.7: Bragg's law of X-rays scattering.

$$\mathbf{n}\lambda = 2\mathbf{d}_{hkl}\sin\theta \qquad\qquad\qquad \dots 3.1$$

Where n is an integer multiple of the wavelength λ, d_{hkl} is the distance between parallel planes, θ is the angle between the plane and the X-ray

3.5.2 Structure factor

The intensity of X-rays in the diffraction pattern can be affected by numerous factors. The one that depends only upon the crystal structure is called the structure factor. Each atom in a crystal scatters X-rays by an amount related to the scattering power, F, of that particular atom. The amplitude F(*hkl*) and the phase(ϕ) of each diffracted wave are important in summing the individual waves to give the resultant diffraction beam. If the atomic positions in the structure are known, the amplitude and the phase appropriate to each atom in the unit cell may be calculated and the summation carried out by various mathematical methods such as,

---

[5] C, Hammond., *The Basics of Crystallography and Diffraction*, Oxford Science Publications, 1998, 125.

$$F(hkl) = \sum_{j=1}^{N} g_i \exp(i\phi_j) = \sum_{j=1}^{N} g_j \exp[i2\pi(hx_j + ky_j + lz_j)] \qquad \text{...3.2}$$

N gives the number of atoms in the unit cell, index j is the numerical value, g_i is the temperature corrected atomic scattering factor.

Equation 3.2 indicates that the magnitude of the structure factor depends on the nature of the atoms in the unit cell and their atomic scattering factors. The phase difference between two atoms depends on two factors: the Miller indices of the reflection that is considered and the fractional coordinates of the atoms in the unit cell.

Equation 3.2 can also be written as:

$$F(hkl) = \sum_{j=1}^{N} g_j \left[\cos 2\pi(hx_j + ky_j + lz_j) + i\sin 2\pi(hx_j + ky_j + lz_j)\right] \qquad \text{...3.3}$$

The intensity of the diffracted X-rays is directly proportional to the square of the structure facture, $[F(hkl)]^2$, since the energy in the cosine waves is proportional to the square of the amplitude of the wave, with I_0 and F_0 are the experimentally observed quantities.

$$I_0(hkl) \propto \left|F_0(hkl)]^2\right| \qquad \text{…3.4}$$

X-rays are diffracted by the electrons associated with the atoms in a crystal. Atoms with a large atomic number provide a higher concentration of electron density compared to atoms with smaller atomic numbers, thus electron density can be expressed as a function of position ρ(x,y,z).

$$F(hkl) = \sum_{j=1}^{N} \exp(i\phi_j) = \sum_{j=1}^{N} \rho(x, y, z)[i2\pi(hx_n + ky_n + lz_n) \qquad \text{…3.5}$$

3.5.3 The Phase Problem

In order to determine a crystal structure, both the amplitude and the phase of different diffractions must be known. The amplitude can be determined from the intensity data. There is however no practical method of directly measuring phases

giving rise to the phase problem dilemma. The Patterson function and the direct methods have been developed to compensate for the phase problem.

3.5.3.1 Direct Methods

Direct methods are normally used to solve molecular structures containing light atoms. The methods calculate phases directly from the amplitudes of normalised structural factors and each reflection is involved in multiple probability distribution. The phases of strongly scattered beams can be estimated from their measured intensities through the correlation between the amplitude and phases of reflections and electron density distribution in a unit cell. Direct methods assume that the electron density is always positive within a unit cell consisting of discrete atoms.

3.5.3.2 Patterson Function

The Patterson function resembles an electron density map since it has peaks of positive intensity. However these do not represent the position of the atoms in the structure, rather a map of vectors between pairs of atoms at (*u, v, w*), whose *x* coordinates differ by *u*, *y* coordinates differ by *v* and the *z* coordinates differ by *w*. Vectors between heavy atoms are often the most prominent in the map.

$$P(u,v,w) = V^{-1} \sum \sum \sum |F(hkl)|^2 \exp -2\pi i(h_u + k_v + l_w)$$ …3.6

Where V is the volume of the unit cell, $F(hkl)^2$ is proportional to the intensity of each reflection, $P(u, v, w)$ is a periodic function in Patterson space.

3.5.3.3 Least Square refinement

The refinement method compares the calculated diffraction pattern relative to the observed one. The similarities between the experimental structure factor and the calculated structure factor are compared in terms of the *residual index* of R-factor through equation 3.17.[6]

$$R = \frac{\sum ||F_0| - |F_c||}{\sum |F_0|}$$ …3.7

An *R-factor* below one is an indication of a good correlation between the experimental and the calculated structure. Better refinement and reliability of the

---

[6] G. H. Stout, L. H. Jensen, *X-ray Structure Determination, A Practical Guide*, The Macmillan Company, London, 1968.

crystal can be obtained by the incorporation the weighing factor which uses the square of the structure factor differences for each reflection, w.

$$wR^2 = \frac{\sum w(F_0^2 - F_c^2)}{\sum w(F_0^2)^2}$$ …3.8

3.6 Chemical kinetics

To measure the rates of reactions, one needs to monitor the concentration of reactants or that of the product as a function of time under specific conditions in order to reduce the number of external parameters. Numerous experimental techniques have been developed to monitor reactions over timescales varying from hours or days all down to femtoseconds (1 Fs = 10 $^{-5}$ s). It is fairly easy to monitor slow reactions spanning around a few minutes to hours or longer, but highly specialised methods such as flow technique, relaxation methods and laser pump probe technique are required in order to study fast reactions.

Kinetic measurements on the UV-Vis spectrometer are based on the principle that unique molecules have independent absorption spectra. A monochromatic light source is passed over the reaction mixture and the ratio of the transmitted to incident light intensity I/I_0 is measured as a function of time. The quantity is defined as transmittance and can be related to the concentration of the absorbing species using the Beer Lambert law.[7]

$$\ln \frac{I}{I_0} = \varepsilon cl = A$$ …3.8

where l is the path length through the sample, ε is the absorption extinction coefficient c is the concentration of the absorbing species. From equation 3.8

$$A = \sum \varepsilon cl$$ …3.9

3.6.1 Reaction rates and orders specific reference to pseudo first order reactions

In a pseudo first order reaction, the concentration of the ligand is orders of magnitude in excess to that of the metal [L]>>[M].

$$a[A] + b[B] \xrightarrow{k_1} c[C] + d[D]$$ …3.10

---

[7] P.W. Atkins, *Physical Chemistry*, Oxford: Oxford University Press Inc., 1994.

From equation 3.10, the rate can be defined as:

$$Rate = \frac{-d[A]}{dt} = \frac{-d[B]}{dt} = \frac{d[C]}{dt} = \frac{d[D]}{dt} = k[A]^a[B]^b \qquad \text{...3.11}$$

Where t represents time, [A], [B], [C] an [D] represents the concentrations of the different species, a is the order of the reaction with respect to A, b is the order of reaction in terms of B, k is the rate constant.

If we consider a pseudo first order reaction which entails changing the concentration of one of the reactants, whilst the other is kept constant, then from equation 3.11 the rate can be defined by as follows:[8]

$$Rate = k_{obs}[A]^a \text{ leading to } k_{obs} = [B]^b \qquad \text{...3.12}$$

And the pseudo first order conditions give:

$$k_{obs} = k_1[B] + k_{-1} \qquad \text{...3.13}$$

Where k_1 and k_{-1} represent the rate of the forward and the reverse reactions respectively.

The equilibrium constant K_{eq} is given by:

$$K_{eq} = \frac{k_1}{k_{-1}} \qquad \text{...3.14}$$

Integrating 3.13 within limits time = 0 and time t gives equation 3.15.

$$\ln\frac{[C]_t}{[C]_0} = -k_{obs}t \text{ or } [C]_t = C_0 e^{k_{obs}t} \qquad \text{...3.15}$$

where $[C]_0$ = concentration change at t = 0 and $[C]_t$ = concentration change at time t.

Relating equation 3.15 to the Beer-Lambert Law which relates the absorption of light to the concentration of a solution,

$$A_t = A_\infty(A_\infty - A_0)e^{k_{obs}t} \qquad \text{...3.16}$$

Where A_t is the absorbance after time t, A_∞ is the absorbance at time infinity.

---

[8] J.W. Moore, R.G. Pearson, *Kinetics and Mechanism*, 3rd Ed., New York: John Wiley & Sons, Inc., 1981.

Now one can reconcile the mathematical kinetic theory with the experimentally obtained data. The data can be translated to a mathematical model to determine the rate constant for the forward and reverse reaction.[9] In accordance with the linear Eyring equation,

$$\ln \frac{k}{T} = \frac{-\Delta H^{\neq}}{RT} + \ln \frac{k_B}{h} + \frac{\Delta S^{\neq}}{R} \qquad \text{...3.17}$$

A plot of $\ln \frac{k}{T}$ vs. $\frac{1}{T}$ would give a linear relation with a slope defined by $\frac{-\Delta H^{\neq}}{RT}$ and intercept of $\ln \frac{k_B}{h} + \frac{\Delta S^{\neq}}{R}$

Where k is the experimentally determined rate constant at temperature T, R is the Universal Gas Constant (8.314 J.K^{-1}. mol^{-1}), k_B is the Boltzmann Constant (1.318 J.K^{-1}) and h h is the Planck's Constant (6.626 J.s). The enthalpy of activation ($\Delta H^{\neq}$) and the entropy of activation ($\Delta S^{\neq}$) can be determined from the graphical data.

3.7 Conclusion

An elementary outline of the theory behind the development of characterization techniques used in the study was presented. The use of these different techniques and a combination thereof are an integrate part in the development of chemistry and science in general. And have been extensively used to characterise the manganese(I) tricarbonyl complexes synthesized and described in the next chapter.

---

[9] Jordan R. B., *Reaction Mechanisms of Inorganic and Organometallic Systems*, Oxford University Press., Inc., Oxford, 1991.

4 SYNTHESIS AND CHARATERIZATION OF LIGANDS AND METAL COMPLEXES

4.1 Introduction

Manganese, rhenium and technetium all belong to the group 7 transition metals. Although the chemistry of technetium is possibly the least developed due to its artificial origin and related radioactivity, a remarkable breakthrough has developed because of its relevance on radiopharmaceutical application. Numerous studies have been performed on rhenium and technetium tricarbonyl systems with a variety of mono-, bi- and tridentate ligands towards radiopharmaceutical application, but only a few references in manganese regards. This is propagated by the desirable properties possessed by both rhenium and technetium. Rhenium and technetium have analogous chemical properties while manganese differs significantly. The difference in the chemistries can be explained by the difference in the structure of the electron shells and sizes of these three elements. Our research group is doing some work of probing into the coordinative and kinetic effects of various bi- and tridentate ligands on the *fac*-$[M(CO)_3]^+$ motif with the notion of gaining valuable insight for the development of radiopharmaceuticals using the *fac*-$[M(CO)_3]^+$ core. Schutte *et al* reported rhenium(I) tricarbonyl complexes containing O,O-, N,N and N,O-bidentate ligands with an elaborate discussion on the effect of bonded ligands on the reactivity of rhenium(I) tricarbonyl core towards the substitution of the coordinated methanol molecule.[1]

The primary aim of this study was to investigate the coordinative and kinetic behaviour of *fac*-$[Mn(CO)_3(L,L^{'})]^+$ ($L,L^{'}$ = bidentate ligands derived from salicylidene

---

[1] M. Schutte, G. Kemp, H. G. Visser, A. Roodt, *Inorg. Chem.*, 2011, 50, 12486.

backbone) relative to rhenium and technetium analogues. A series of Schiff base ligands containing the salicylidene backbone with N,N, N,O and O,N,N donating atoms, have previously been synthesized.[2] The coordination and kinetic properties of these ligands were investigated with the *fac*-[Mn(CO)$_3$]$^+$ core. Our investigations was focused on Schiff base ligands consisting of a phenolic OH group and the azomethine (-RC=N-) group. Another interesting characteristic of these ligands is that they can coordinate either in the neutral (keto) or in the anionic (imido) state depending on the intramolecular hydrogen bonding involved.[3]

This study also extends to the coordinative and kinetic behaviour of β-diketone ligands with the metal tricarbonyl framework. The interaction of diketone ligands with transition metals have relevant application in nuclear industry especially tantalum and niobium. These ligands can also be model complexes for radiopharmaceuticals. The synthesis and characterization of a number of N,O, O,O and N,N will be reported in this chapter. The coordinative and kinetic properties will be discussed in succeeding chapters.

4.2 General considerations

All chemicals used for synthesis and characterization were reagent grade and purchased from Sigma-Aldrich, South Africa, unless stated otherwise. These chemicals were used as purchased without further purification. All solid samples were analysed on a Bruker Tensor 27 Standard spectrophotometer with a laser range of 4000-370 cm^{-1}, at room temperature. ^{1}H and ^{13}C FT-NMR spectra of the ligands and metal complexes were recorded on a Bruker AXS 300 or 600 MHz at 25 ^{0}C in: Acetone (2.05 ppm and 29.92 ppm), Methanol (3.31ppm and 49.15 ppm), DMSO (2.5 ppm and 39.1ppm). Chemical shifts are reported relative to TMS. UV-vis measurements were collected using a Varian 50 Conc UV-Visible spectrophotometer, equipped with a Julabo F12-mV temperature cell regulator (accurate within 0.1°C) in a 1.000 $\pm$ 0.001 cm quartz cuvette cells.

---

[2] A. Brink., *PhD Thesis*, University of the Free State, 2012. Bloemfontein, South Africa.
[3] F. Arod, M. Gardon, P. Pattison, G. Chapuis, *Acta. Cryst.*, C16, o317.

4.3   Synthesis of SalH Ligands

The Schiff base ligands used in the study are synthesised as follows, unless specified otherwise. The respective amine was dissolved in methanol and added dropwise to the aldehyde in [1:1] mole ratio and refluxed for 3 hours at 80 ^{0}C.

(a)

(b)

(c)
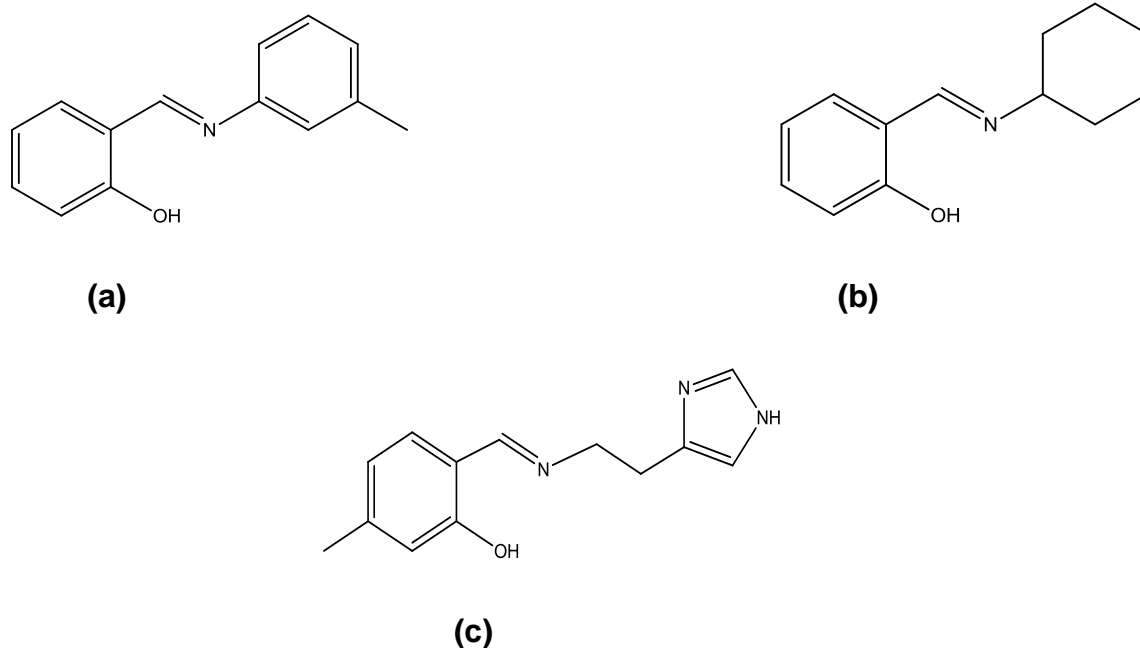
Figure 4.1: Schiff based ligands used in the study, 2-[(*m*-Tolyliminomethyl)]phenol (a), 2-[(Cyclohexyliminomethyl)]phenol (b), 2-[(2-Imidazol-4-yl)ethyliminomethyl]-5-methylphenol (c).

4.3.1   2-(*m*-Tolyliminomethyl)phenol-(SalH-*m*Tol)

The title compound, SalH-*m*Tol, was synthesized as described in 4.3 using *m*-toluidine (0.98 g, 9.144 x 10^{-3} mol) and salicylaldehyde (1.15 g, 9.412 x 10^{-3} mol) in methanol. Anhydrous MgSO$_4$ was added to the solution to remove the water produced by the reaction. An intense yellow colour was observed as soon as the amine was added to the aldehyde. The solution was refluxed at 70-80 ^{0}C for 4 h, MgSO$_4$ was filtered and the solvent removed under reduced pressure, yellow oil was obtained which was dissolved in a minimum of acetone to crystallize. (Yield: 1.541 g, 79.8 %).

^{1}H NMR (300 MHz,CD$_2$Cl$_2$-d_2) δ 8.72 (s, 1H, HC=N), 7.55 (m, 4H, Ar), 7.36 (m, 2H, Ar), 6.92 (m, 2H, Ar), 2.55 (s, 1H, CH$_3$). ^{13}C NMR (300 MHz, Acetone-d_6) δ 169.91,

162.25, 147.15, 131.12, 133.23, 134.12, 134.10, 126.25, 127.51, 119.23, 117.48, 116.25, 115.45 (Ar), 18.2 (CH$_3$).

4.3.2 2-(Cyclohexyliminomethyl)phenol-(SalH-CyHex)

Cyclohexylamine (0.86 g, 8.847 x 10^{-3} mol) in methanol, was added dropwise to salicylaldehyde (1.15 g, 9.412 x 10^{-3} mol). Anhydrous MgSO$_4$ was added and the solution was refluxed at 70-80 ^{0}C for 4 h. MgSO$_4$ was filtered off and solvent removed under reduced pressure, yellow oil was obtained which was dissolved in acetone to crystalize. (yield: 1.278 g, 70.8%).

^{1}H NMR (300 MHz, (CD$_3$)$_2$CO) δ 8.79 (s, 1H, HC=N), 7.57 (m, 2H, Ar), 7.40 (m, 2H, Ar), 3.32 (s, 1H, C21), 1.28-1.83 (m, 10H, cy). ^{13}C NMR (300 MHz, Acetone-d_6) δ 163.33, 161.25, 131.83, 131.49, 119.16, 118.37, 116.42, (Ar), 35.15, 34.12, 33.13, 25,15, 24.12, 18.21(Cy).

4.3.3 2-((2-Imidazol-4-yl)ethyliminomethyl)-5-methylphenol – 5Me-SalH-Hist

Histamine (0.408 g, 3.671 x 10^{-3} mol) was added dropwise to 2-hydroxy-4-methylbenzaldehyde (0.504 g, 3.702 x 10^{-3} mol) in methanol. Anhydrous MgSO$_4$ was added and the reaction was refluxed at 80 ^{o}C for 3 h. The solvent was removed under reduced pressure yielding a yellow powder as product. Yield: (0.732 g, 86.9 %)

^{1}H NMR (300 MHz, Acetone-d_6) δ 8.23, (s,1H, HC=N), 7.60 (s,1H, Ar), 7.11 (d,1H, J = 7.8 Hz, Ar), 6.85 (6,1H, Ar) 6.59 (m, 2H, Ar), 4.46 (m,1H,CH$_2$), 3.85 (t, 2H, J = 6.9 Hz, CH$_2$), 2.96 (t,2H, J = 6.9 Hz, CH$_2$), 2.27(m,1H, CH$_2$), 2.27 (s, 3H, CH$_3$). ^{13}C NMR (600 MHz, CDCl$_3$) δ 165.36, 165.08, 144.42, 131.66, 119.38, 117.87, 115.95, 115.55 (Ar), 56.34, 28.07 (CH$_2$), 20.49 (CH$_2$).

4.4   Synthesis of metal complexes

4.4.1 General Synthesis of *fac*-Manganese(I) tricarbonyl complexes
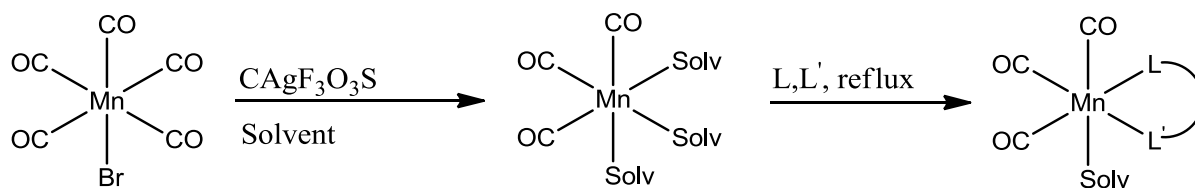
The metal complexes were synthesised as follows unless specified otherwise. The initial step entailed the removal of two CO ligands and the Br ligand with triflic acid under reflux conditions, followed by the subsequent addition of the ligand and further refluxing. The system was covered with aluminium foil to prevent light penetration. Manganese carbonyl complexes are susceptible to photodecomposition.

4.4.2 *fac*-[Mn(Sal-*m*Tol)(CO)$_3$]$_2$

AgF$_3$O$_3$S (0.0934 g, 3.335 x 10^{-4} mol) was added to a solution of [Mn(CO)$_5$Br] (0.1 g, 3.638 x 10^{-4} mol) in acetone. The mixture was refluxed at 70 ^{0}C for 2 h. The precipitated AgBr was filtered. The solvent was removed under reduced pressure yielding a yellow oil to which, SalH-*m*Tol (0.0922 g, 4.364 x10^{-4} mol) in diethyl ether (20ml) was added and refluxed at 70 ^{0}C for 3h. The solvent was removed under reduced pressure. Suitable crystals were obtained through slow diffusion in the dark at room temperature. (Yield: 0.082 g, 32.3 %).

IR(KBr, cm^{-1}): v_{co} = 1952.5, 2003.5, 2017.6, 2012.2, UV-Vis (nm, L.mol^{-1}. cm^{-1}): λ$_{max}$ = 350, ε = 2.998 × 10^3. ^{1}H NMR (300 MHz, DCM) δ 8.61 (s, 1H, HC=N), 7.45-7.29 (m, 6H, Ar), 6.68 (m, 2H, Ar), 2.5 (s, 3H, CH$_3$).
^{13}C (600 MHz, DMSO) 168.36, 168.76, 156.02, 139.54, 134,81, 134,59, 134.54, 127.10, 127.83, 125.35, 122.87, 120.07(Ar), 119.5, 21.25 (CH$_3$).

4.4.3 *fac*-[Mn(Sal-CyHex)(CO)$_3$]$_2$

AgF$_3$O$_3$S (0.0934 g, 3.335 x 10^{-4} mol) was added to a yellow solution of [Mn(CO)$_5$Br] (0.1 g, 3.638 x 10^{-4} mol) in acetone. The solution was refluxed at 70 ^{0}C for 2 h. AgBr precipitated and was filtered off. The solvent was removed under reduced pressure yielding a yellow oil to which SalH-CyHex (0.0889 g, 4.379 x10^{-4} mol) in diethyl ether

was added and refluxed at 70 ^{0}C for 3 h. Majority of the solvent was removed under reduced pressure and suitable crystals were obtained through slow diffusion in the dark at room temperature. Yield: (0.0731 g, 29.5%).

IR(KBr, cm^{-1}): v_{co} = 1907.6, 1924.2, 2022.6. UV-Vis (nm, L.mol^{-1}. cm^{-1}): λ_{max} = 359.7, ε = 1.166× 10^3. ^{1}H NMR (300 MHz, (CD$_3$)$_2$CO) δ8.53 (s, 1H, HC=N), 7.35 (m, 2H, Ar), 6.89 (m, 2H, Ar), 3.32 (s, 1H, C21), 1.28-1.83 (m, 10H, cy). ^{13}C NMR (300 MHz, Acetone-d_6) δ 164.24, 161.52, 132.25, 131.12, 119.23, 118.22, 116.12 (Ar), 35.15, 34.12, 33.13, 25,15, 24.12, 18.21(Cy).

4.4.4 Synthesis of *fac*-[Mn(4-Me-Sal-Hist)(CO)$_3$]

AgF$_3$O$_3$S (0.0934 g, 3.335 x 10^{-4} mol) was added to a yellow solution of [Mn(CO)$_5$Br] (0.1 g, 3.638 x 10^{-4} mol) in acetone. The mixture was refluxed at 70 ^{0}C for 2 h. AgBr precipitated and was filtered off. The solvent was removed under reduced pressure giving yellow oil as product. 4-Me-SalH-Hist (0.0872 g, 3.803 x10^{-4} mol) in diethyl ether was added to the yellow oil and the mixture was refluxed at 70 ^{0}C for 3h. Majority of the solvent was removed. Suitable crystals were obtained through slow evaporation in the dark at room temperature. Yield: (0.09 g, 67.1 %).

IR(KBr, cm^{-1}): v_{co} = 1891.5, 1926.8, 2012.2. UV-Vis (nm, L.mol^{-1}. cm^{-1}): λ_{max} = 359.7, ε = 1.166× 10^3. ^{1}H NMR (300 MHz, acetone-d_6) δ 8.10, (s,1H,HC=N), 8.00 (s,1H,N=CH-N,C$_3$H$_3$N$_2$), 7.10 (s,1H,C=CH-N,C$_3$H$_3$N$_2$) 6.94 (d,1H,J = 7.9, Ar) 6.47 (s,1H,Ar), 6.18 (d,1H,J = 8, Ar), 4.46 (m,1H,CH$_2$), 4.01 (m,1H,CH$_2$), 3.38 (m,1H,CH$_2$), 3.02 (m,1H,CH$_2$), 2.13 (s,3H,CH$_3$). ^{13}C (600 MHz, acetone-d_6) δ (164.34, HC=N), 157.80, 143.41, 138.53, 138.38, 136.30, 133.38, 122.18, 114.47, 60.32 (Ar), 29.58, 27.14 (CH$_2$), 20.97 (CH$_3$).

4.5 Synthesis of *fac*-[Mn(O,O')(CO)₃X] complexes

The complexes were synthesised similarly to the procedure described in section 4.3.

Figure 4.3: Acetylacetone ligands used in the study.

4.5.1 Synthesis of the *fac*-[Mn(CO)₃-2,4-Pentanedione]

AgF$_3$O$_3$S (0.0934 g, 3.335 x 10^{-4} mol) was added to a yellow solution of [Mn(CO)$_5$Br] (0.1 g, 3.638 x 10^{-4} mol) in acetone. The mixture was refluxed at 70 ^{0}C for 2 h. AgBr precipitated and was filtered off. The solvent was removed under reduced pressure yielding a yellow oil. Acetylacetone (0.037 g, 3.700 x10^{-4} mol) in methanol, pH = 7, was added to the yellow solution. The mixture was refluxed at 70 ^{0}C for 24 h. The solvent was removed. Suitable crystals were obtained through slow evaporation in hexane-acetone mixture in the dark at room temperature. Yield: (0.037 g, 37.5 %).

IR(KBr, cm^{-1}): v_{co} = 1910.9, 1927.4, 2042. UV-Vis (nm, L.mol^{-1}. cm^{-1}): λ_{max} = 359.7, ε = 1.594 × 10^3. ^{1}H NMR (300 MHz, DMSO) δ 5.44 (s, 1H, acac), 3.14 (s,3H, OCH$_3$), 1.97 (s, 6H, 2CH$_3$). ^{3}C NMR (600 MHz, CDCl$_3$) δ 188.56, 99.30, 27.94 (2xCH$_3$).

4.5.2 Synthesis of the *fac*-[M(CO)₃-1,1,1-Trifluoro-2,4-pentanedione]

AgF$_3$O$_3$S (0.0934 g, 3.335 x 10^{-4} mol) was added to a yellow solution of [Mn(CO)$_5$Br] (0.1 g, 3.638 x 10^{-4} mol) in acetone. The mixture was refluxed at 70 ^{0}C for 2 h. AgBr precipitated and was filtered off. The solvent was removed under reduced pressure. To the above solution, trifluoroacetylacetone (0.0562g, 3.647 x10^{-4} mol) in diethyl ether (20ml) was added and stirred at 70 ^{0}C for 3h. Suitable crystals were obtained through slow diffusion in the dark at room temperature. Yield: (0.0450 g, 38.1 %).

IR(KBr, cm^{-1}): v_{co} = 1935.1, 2006.7, 2030.1. UV-Vis (nm, L.mol^{-1}. cm^{-1}): λ_{max} = 359.7, ε = 1.166× 10^3. ^{1}H NMR (300 MHz, DMSO) δ 5.93 (s, 1H, acac), 3.16 (s, 3H, OCH$_3$), 2.20 (s, 3H, CH$_3$). ^{13}C NMR (600 MHz, CDCl$_3$) δ 188.56, 99.30, 27.94.

4.6 Results and Discussion

The *fac*-[Mn(CO)$_3$]$^+$ complexes synthesized are reported in this chapter. All the complexes were obtained relatively easy through a two-step reaction procedure described in Paragraph 4.4.1. The reaction between *fac*-manganese(I) tricarbonyl with bidentate Schiff base ligands yielded dimeric species. The kinetic profiles of the formation of the dimeric complexes can be difficult to interpret because of the possibility of multiple reactions forming. Attempts to bypass the formation of the dimeric species for the more direct monomeric abducts were the *fac*-manganese(I) tricarbonyl is stabilised by the anionic bidentate ligand with a vacant 6th coordination site available for a neutral solvent molecule such as methanol, acetonitrile were unsuccessful and a further discussion will be given in Paragraph 4.6.1. The formation of the dimeric complexes carved a path to the exploration of O,O ligands of the acetylacetone derivatives which are also widely studied with rhenium and technetium metal centres.

The main aim of this study was to compare the kinetic and coordination behaviour of *fac*-[Mn(CO)$_3$]$^+$ relative to rhenium analogues hence it was imperative to follow a similar reaction path, however the starting material could not dissolve in methanol which was the major solvent used for rhenium tricarbonyl studies. An alternative solvent had to be used. A major observation made was that the complexes are prone to undergo decomposition in more polar solvent indicated by black deposits of insoluble material. The decomposition might be caused by the loss of one or more CO ligands. When the complexes are exposed to light for periods of time, there is a decrease in intensity of the CO peaks in the infrared spectra indicative of possible structural changes. The stretching frequencies of all the complexes are given by Table 4.1. The data unequivocally proves the coordination of the three CO ligands with three distinctive peaks characteristic of facially coordinated CO ligands. The stretching frequencies are assigned to symmetric and asymmetric binding modes. The bands lie in a range of the standard manganese tricarbonyl complexes with N,O donating ligands spanning around 1987-2089 cm^{-1}.[4] The monomeric and dimeric complexes can have similar stretching frequency profile depending on the symmetry of the complex.

---

[4] Z. D. Reed and M. A. Duncan. *J. Am. Soc. Mass Spectrom.,* 2010, 21, 739.

Table 4.1: Carbonyl stretching frequencies of the *fac*-manganese(I) tricarbonyl complexes.

complex	$v_{(CO)}$ (cm^{-1})
fac-[Mn(Solvent)$_3$(CO)$_3$]	1952.5, 2003,5 2017.6
fac-[Mn(Sal-mTol)(CO)$_3$]$_2$	1907.6, 1924.2, 2022.6
fac-[Mn(Sal-CyHex)(CO)$_3$]$_2$	1891.5, 1926.8, 2012,2
fac-[Mn(4-Me-Sal-Hist)(CO)$_2$]	1896.0, 1920.0, 2021.0
fac-[Mn(Acac)(CO)$_3$](OHCH$_3$)]	1910.9, 1927.4, 2042,1
fac-[Mn(Tfacac)(CO)$_3$(OHCH$_3$)]	1935.1, 2006.7, 2030.1

The reaction between *fac*-manganese(I) tricarbonyl with acetylacetone yielded complexes *fac*-[Mn(Acac)(CO)$_3$)(OHCH$_3$)] and *fac*-[Mn(Tfacac)(CO)$_3$(OHCH$_3$)]. It is interesting to note that analogous rhenium studies required acidic conditions to assure protonation of the ligands and prevention of possible formation of bridging complexes.[5,6] However, manganese complexes were successfully synthesized in almost neutral solutions. It was observed that the acetylacetone complexes are more air and light stable compared to the Schiff base complexes.

4.6.1 Dimer formation

The bidentate Schiff base ligands produced dimeric complexes with *fac*-[Mn(CO)$_3$]$^+$ and their coordinative properties will be discussed. The yellow oils obtained afforded quantifiable yields of yellow prism crystals in cold diethyl ether solution. It is often difficult to crystallise oils but our efforts proved effective. The complexes were crystallised through slow evaporation in a vial covered with aluminium foil to prevent penetration of light. The solid complexes are stable in nonpolar solvents. Black deposits of insoluble material are observed in polar solvents like methanol. The formation of dimeric species is a hindrance to kinetic studies based on the possibility of multiple reactions that could take place which can prove to be difficult or impossible to interpret. The formation of dimers as opposed to monomers may be attributed to the size of the manganese metal centre relative to rhenium metal since monomeric complexes were obtained with rhenium(I).[2]

Analogous studies using *fac*-Rhenium(I) tricarbonyl complex with 8-Oxyquinolate ligands were performed.[7] A Similar approach was employed by not detaching the

[5] A. Manicum, *Msc Thesis*, University of the Free State, 2012. Bloemfontein, South Africa.

[6] L. Helm, *Coord. Chem. Rev.*, 2008, 252, 2346.

[7] H. C. Zhao, B. Mello, B-L Fu, H. Chowdhury, D. J. Szalda, M-K Tsai, D. C. Grills, J. Rochford., *Organomet*, 2013, 32, 1832.

bromine from the starting manganese pentacarbonyl fragment but crystallographic data shows the absence of the bromide ion which implies there is a vacant site that may instigate the dimer formation in order to gain stability. Sekine et al [8] reported the influence of refluxing time on the conversion of monomeric species to dimeric complex. It is by this observation that the refluxing time on one occasion was doubled to 6 hours and on the other halved to 1.5 hours. ^{1}H NMR indicated similar chemical shifts in both extremes, suggesting the formation of the dimeric species once more. This was further validated by single crystal x-ray crystallography.

A twist in the general synthetic procedure was employed in effort to prevent the dimer formation. The idea was to leave the bromine ligand coordinated precluding the possibility of a vacant coordination site implying a five coordinated complex that can dimerize for stability reasons. Single crystal X-ray diffraction indicated once more that a dimeric complex had formed and the bromine ligand had detached from the metal. It was hypothesized that perhaps the reaction conditions were too harsh, as a result the metal centre becomes highly activated prompting the release of the bromine ligand. Based on the hypothesis on the reaction conditions, the reaction was performed at lower temperatures but again single crystal X-ray diffraction showed a dimeric complex. Good coordinating solvents like acetonitrile were also used in attempt to occupy the 6th coordination site. Interestingly, acetonitrile displaces all the CO ligands forming a five coordinated species as revealed by crystal X-ray diffraction. Monoligands pyridine and pyrazole were also tried with no success since crystal X-ray diffraction showed again the formation of dimeric complexes.

---

[8] T. Takayama, A. Harano, T. Sekine, H. kudo, *J. Nucl. Radiochem. Sci.*, 2005, 6,149.

4.7 Conclusion

The main objective of the study was to investigate the coordinative and kinetic properties of *fac*-[Mn(CO)$_3$]$^+$ with Schiff base ligands containing nitrogen and oxygen donor atoms relative to the previously studied rhenium analogues in view of broadening knowledge of the bonding character of the Mn-Triad comprising of manganese, technetium and rhenium. In contrast to the monomeric complexes obtained for rhenium, dimeric complexes were obtained for manganese system. The reasons for the dimeric complexation are still unknown and will be further investigated in the future. Zhao *et al* could switch between monomeric and dimeric rhenium tricarbonyl complex by manipulating reaction conditions such as solvents, pH levels and refluxing times in order to convert the monomeric intermediate to a dimeric complex.[7] Employing similar measures on the *fac*-manganese(I) tricarbonyl did not yield desirable results since dimeric species formed as described earlier. The solid structures of the synthesized complexes will be discussed in the succeeding chapter.

5 X-RAY DIFFRACTION STUDY OF *fac*-MANGANESE(I) TRICARBONYL COMPLEXES

5.1 Introduction

Schiff base ligands have played an immense role, not only in the development of coordination chemistry, but also in numerous fields such as catalysis, biomedical and photo-physical chemistry.[1,2,3,4] The ease of preparation, versatility and chelating abilities are some of the intriguing features rendering these ligands indispensable. A vast number of reports are available on the coordination chemistry of Schiff bases with transition metal complexes containing oxygen, nitrogen and sulphur donor atoms as mono, bi- and multi-dentate ligands. The presence of both hard and soft donor groups increases the coordination efficiency of these ligands towards hard and also soft acidic metal centres. Structure and reactivity of these ligands can be fine-tuned through the alteration of steric and electronic properties around the coordination centre.[5]

The coordination chemistry of the *fac*-[M(CO)$_3$]$^+$ core (where M = Re, Tc) with a variety of bi- and tridentate ligands has been studied extensively in order to gain insight towards radiopharmaceutical development utilizing the *fac*-[M(CO)$_3$]$^+$ fragment. However coordination of these types of ligands to *fac*-[Mn(CO)$_3$]$^+$ is virtually unexplored. Schiff base ligands can serve as models for some important biological species and this affords a window of opportunity to explore the possibilities of utilising these types of ligands. The ease of preparation, versatility and chelating abilities are some of the intriguing features rendering these ligands indispensable.

[1] M. Tumer, H. Koksal, M.K. Sener, S. Serin, *Trans. Met. Chem.,* 1999, 24, 414.
[2] A. Saxena, J. K. Koacher, J. P. Tandon, *J. Antibact Antifung. Agents.*, 1981, 9, 435.
[3] B. De Clercq, F. Verpoort, *Macromolecules.,* 2002, 35, 8943.
[4] T. Opstal, F. Verpoort, *Angew. Chem. Int. Ed.*, 2003, 42. 2876.
[5] S. Chattopadhyay, P. Chakraborty, M. G. B. Drew, A. Ghosh, *Inorg. Chim. Acta.,* 2009, 362, 502.

A primary aim of the study was to synthesize manganese tricarbonyl complexes analogous to those already reported for rhenium and technetium as part of an on-going research on the development of new radiopharmaceuticals using the *fac*-[M(CO)$_3$]$^+$ core. Three new *fac*-manganese(I) tricarbonyl complexes are reported herein. A description of the β-diketone manganese(I) structure will be given in the latter part of this chapter.
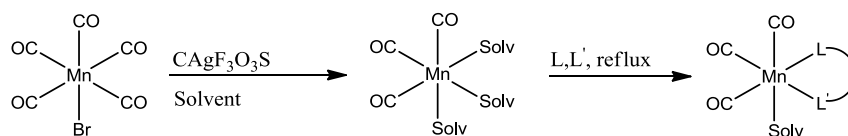
Scheme 5.1: General synthetic procedure of compounds reported.

(1)

(2)

(3)
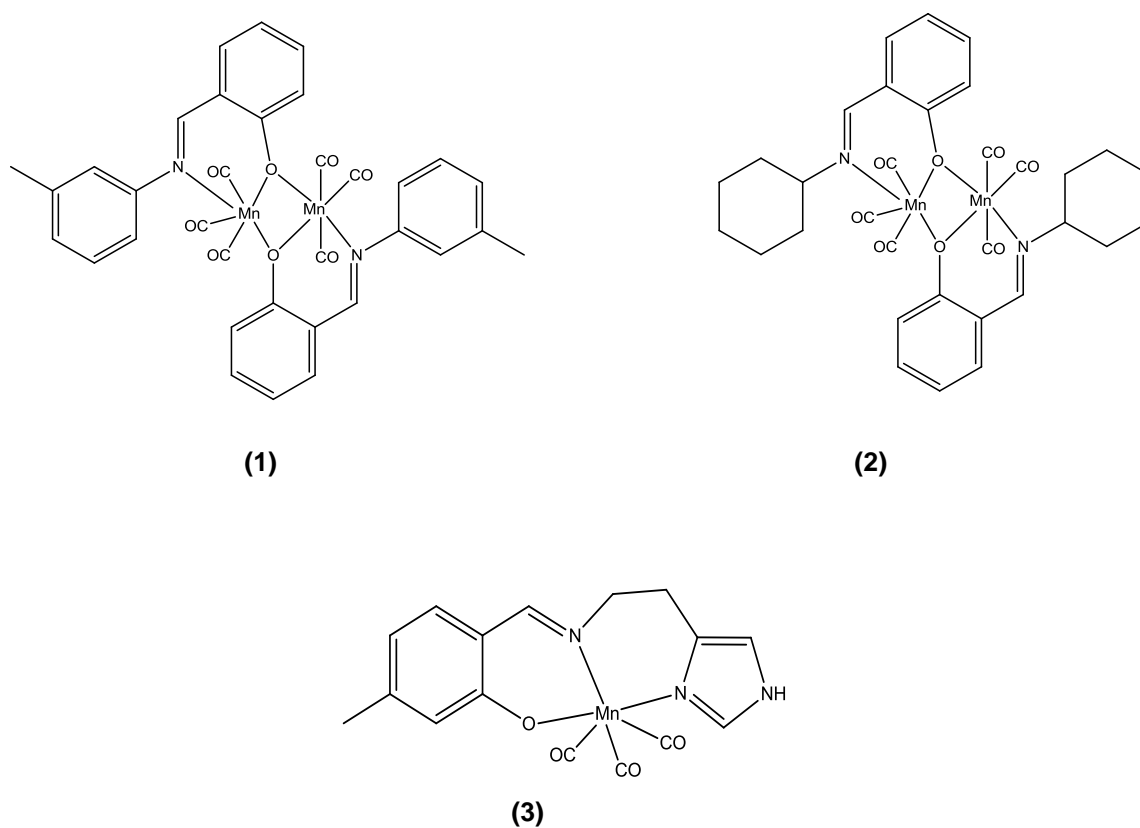
Figure 5.1: The two dimensional sketches of *fac*-[Mn(Sal-*m*Tol)(CO)$_3$]$_2$ (1), *fac*-[Mn(Sal-CyHex)(CO)$_3$]$_2$ (2) and *fac*-[Mn(4-Me-Sal-Hist)(CO)$_3$] (3).

Table 5.1: X-Ray crystallographic data and refinement parameters of *fac*-[Mn(Sal-*m*Tol)(CO)$_3$]$_2$ (1), *fac*-[Mn(Sal-CyHex)(CO)$_3$]$_2$ (2) and *fac*-[Mn-(4-Me-Sal-Hist)(CO)$_3$] (3).

	fac-[Mn(Sal-*m*Tol) (CO)$_3$]$_2$ (1)	*fac*-[Mn(Sal-CyHex) (CO)$_3$]$_2$ (2)	*fac*-[Mn(4-Me (Sal-Hist)(CO)$_3$] (3)
Empirical formula	C$_{34}$H$_{24}$Mn$_2$N$_2$O$_8$	C$_{32}$H$_{32}$Mn$_2$N$_2$O$_8$	C$_{16}$H$_{14}$MnN$_3$O$_4$
Formula weight	698.43	682.47	367.24
Temperature/(K)	100(2)	100(2)	100(2)
wavelength Å	0.71073	0.71073	0.71073
Crystal system	Triclinic	Triclinic	Triclinic
Space group	$P\bar{1}$	$P\bar{1}$	$P\bar{1}$
a/Å	7.737(5)	9.160(2)	7.4262(11)
b/Å	9.483(5)	9.190(2)	9.0038(12)
c/Å	11.309(5)	18.267(4)	13.0780(18)
α/°	101.852(5)	89.90(3)	108.494(4)
β/°	102.514(5)	84.54(3)	104.058(4)
γ/°	101.480(5)	89.83(3)	93.363(4)
Volume/Å^3	766.6(7)	1530.8(6)	795.65(19)
Z	2	2	2
Density calc. (g.cm^{-1})	1.513	1.481	1.533
μ(mm^{-1})	0.88	0.879	0.855
F(000)	356	704	367
Crystal Colour	yellow	yellow	yellow
Crystal Morphology	Cuboid	Plate	Cuboid
Crystal size/mm^3	0.44 × 0.29× 0.25	0.49 × 0.29 × 0.06	0.45 × 0.37 × 0.35
Theta range (°)	2.79 to 28.00	1.120 to 28.00	2.86 to 28.00
Completeness (%)	99.50	99.8	99.9
Index ranges	h = -10 to 10 k = -12 to 11 l = -14 to 14	h = -12 to 12 k = -12 to 12 l = -24 to 24	h = -9 to 9 k = -11 to 11 l = -17 to 17
Reflections collected	15240	30156	23069
Independent reflections	3673	3888	3841
R$_{Int}$	0.0665	0.0942	0.0536
Data/restraints/ parameters	3673/0/209	753/0/398	3841/0/234
Goodness-of-fit on F^2	1.033	1.049	1.061
Final R indexes [I>=2σ (I)]	R1 = 0.0478, wR2 = 0.1159	R1 = 0.0468, wR2 = 0.1055	R1 = 0.0273, wR2 = 0.0760
Final R indexes [all data]	R1 = 0.0736, wR2 = 0.1295	R1 = 0.0780, wR2 = 0.1208	R1 = 0.0305, wR2 = 0.0781
ρ max and ρ min (e.Å^{-3})	0.56 and -0.84	0.62 and -0.62	0.296 and -0.28

5.2 CRYSTAL STRUCTURE OF

fac-[Mn(Sal-*m*Tol)(CO)$_3$]$_2$

The structural determination of complex, *fac*-[Mn(Sal-*m*Tol)(CO)$_3$]$_2$ **(1)**, (Sal-*m*Tol = 2-[(*m*-tolyliminomethyl)]phenolato) was carried out with a yellow plate-like single crystal. The dimeric complex crystallizes in triclinic fashion in $P\bar{1}$ space group with two formula units per unit cell (Z = 2). The asymmetric unit of complex **(1)** consists of one half of the molecule. A structural representation of **(1)** along with the numbering scheme is illustrated by Figure 5.2. Relevant bond distances and bond angles are listed in Table 5.2.
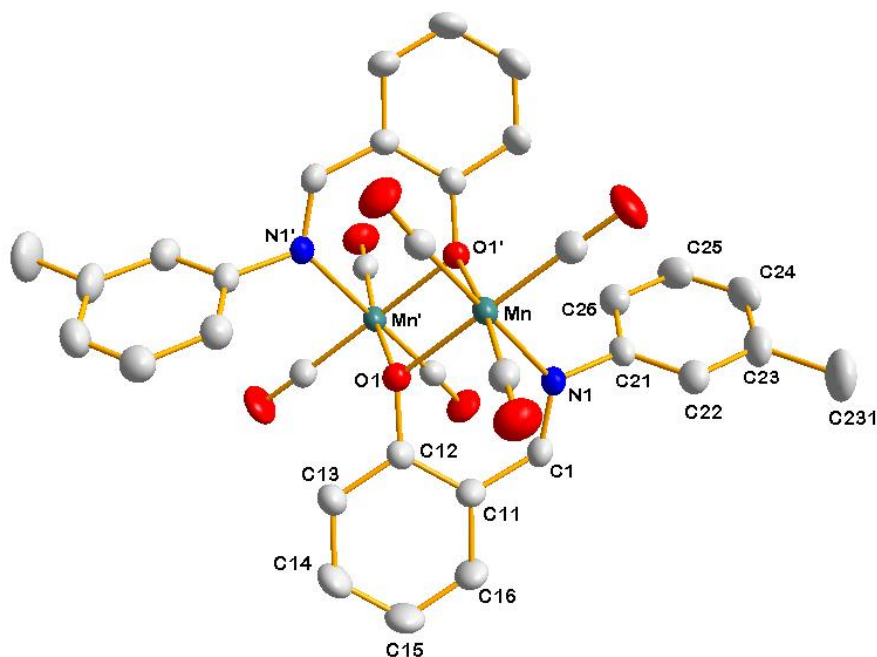
Figure 5.2: Structural representation of *fac*-[Mn(Sal-*m*Tol)(CO)$_3$] with atom numbering scheme and displacement ellipsoids at 50% probability level. For the aromatic rings, the first digit represents the ring number, while the second digit refers to the specific C-atom in the ring.

Table 5.2: Selected bond lengths (Å) and angles (˚) of *fac*-[Mn(Sal-*m*Tol)(CO)$_3$]$_2$ (1).

Atoms	Length (Å)	Atoms	Angle (˚)
Mn-O1	2.0325(19)	N1-Mn-O1	84.64(8)
Mn$^\#$-O1$^\#$	2.066(2)	N1-Mn-C01	178.82(11)
Mn$^\#$-O1	2.066(2)	O1-Mn-C03	95.04(10)
Mn-N1	2.064(2)	O1-Mn-C02	174.92(11)
Mn-C01	1.815(3)	O1-Mn-O1#1	77.96(8)
Mn-C02	1.795(3)	O01-C01-Mn	175.5(2)
Mn-C03	1.789(3)	O03-C03-Mn	177.6(3)
N1-C1	1.282(3)	N1-Mn-O1#1	87.67(9)
C03-O03	1.153(4)	C1-N1-C21	117.41(12)
C01-O01	1.143(4)	C03-Mn-O1#1	172.99(9)
C02-O02	1.143(3)		

(#1) refers to the atoms of the symmetry generated subunit

The dimeric complex **(1)** is composed of two *fac*-[Mn(Sal-*m*Tol)(CO)$_3$] subunits linked together by the oxygen atoms from the phenolato groups of the *m*Tol functionality. The coordination geometry about each manganese atom is a distorted octahedron with two *cis* carbonyl ligands and the two bridging oxygen atoms in the same plane (Figure 5.3).

The deviation from the idealised octahedral geometry is imposed by constraints associated with the ligand as indicated by the N1-Mn-O1 bite angle of 84.64(8)˚ and N1-Mn-C01 angle of 178.82(11)˚. The central unit of the dimeric complex **(1)** is a four membered planar Mn$_2$O$_2$ ring with Mn-O1-Mn$^'$ angle of 101.987(23)˚ and O1-Mn-O1$^'$ angle of 77.96(8)˚ (atom name$^'$ = symmetry generated atoms). A Mn-Mn$^'$ separation of 3.1865(14) Å is long enough to preclude interaction between the two metals. The manganese-carbonyl bond distances are comparable to each other with bond distances of 1.815(3) Å, 1.795(3) Å and 1.789(3) Å for Mn-C01, Mn-C02 and Mn-C03 respectively and are within range for similar complexes.[6,7]

[6] L. A. Garcıa-Escudero, D. Miguel , J. A. Turiel. *J. Organomet. Chem.*, 2006, 691, 3434.
[7] C. M. Alvarez, R. Garcıa-Rodrıguez, D. Miguel, *J. Organomet. Chem.*, 2007, 692, 5717.
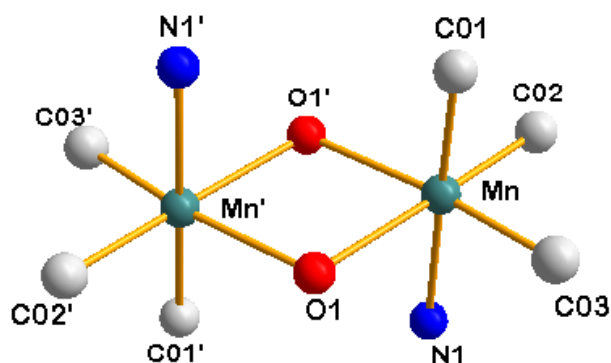
Figure 5.3: View of the coordination octahedron around the manganese atoms. Atoms with an apostrophe were generated by symmetry.

The plane defined by the salicylidene C1 aromatic backbone (Plane 1: C11, C12, C13, C14, C15, C16) is bending relative to the manganese equatorial plane (Plane 2: Mn, N1, O1, C01, C02) with a dihedral angle of 39.02(13)°.
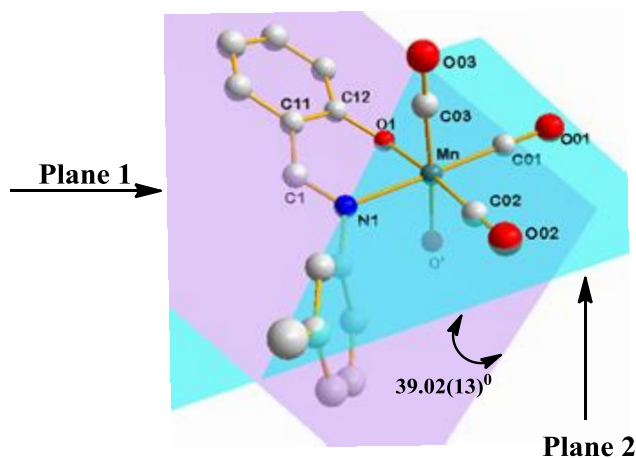
Figure 5.4: Graphical representation of the bending aromatic backbone (Plane 1 is indicated in purple and Plane 2 indicated in blue). Hydrogen atoms were omitted for clarity.

The aromatic ring substituent on the imine N atom is placed almost perpendicular (86.09(11)°) with respect to the manganese equatorial plane (Plane 2) to minimise steric interactions with the coordination sphere.
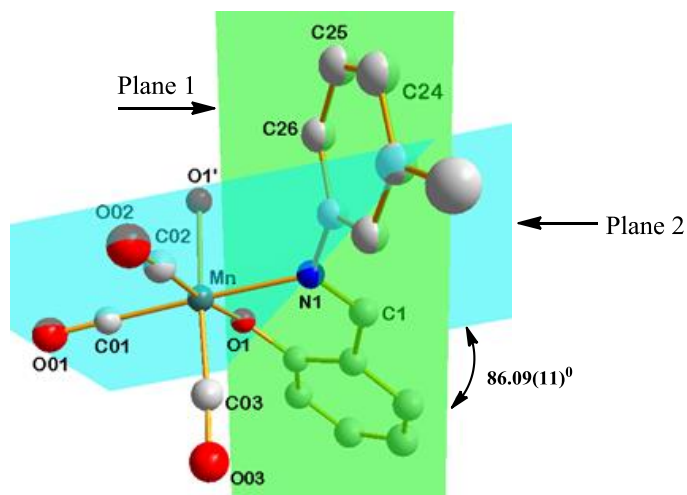
Figure 5.5: Graphical representation of the twist of the imine fragment (Plane 1 indicated in blue and Plane 2 indicated in green). Hydrogen atoms were omitted for clarity.

The conformation in **(1)** leads to the formation of classical intermolecular hydrogen bonding between the atom H26 on the *m*Tol substituent and the oxygen atom of the second subunit O1, (C26…H26…O1[#1]) as illustrated in Figure 5.6 and Table 5.3. No intramolecular hydrogen bonding is observed.

Figure 5.6: Graphical representation of hydrogen bonding interaction between C26…H26…O1[#1]. Some atom labels were omitted for clarity.

Table 5.3: Hydrogen bonds of *fac*-[Mn(Sal-*m*Tol)(CO)₃]₂ [(Å), (˚)].

D-H…A	d(D-H)	d(H…A)	d(D…A)	<(DHA)
C(26)H(26)…O(1)#1	0.93	2.53	3.193(7)	125

Symmetry transformations used to generate equivalent atoms
#1   2 –x, 2-y, 2-z

The crystal lattice is further stabilised by two C-O…π interaction as indicated in Figure 5.7.
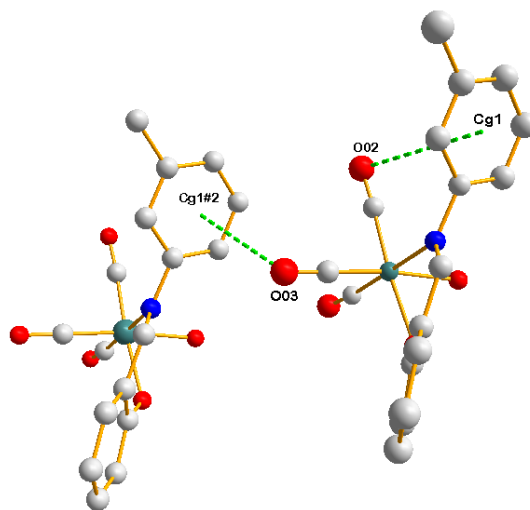
Figure 5.7:   **Graphical representation of the C-O…π interaction indicated by the   green dotted line. Some atom labels were omitted for clarity.**

Table 5.4: C-O…π interactions of *fac*-[Mn(Sal-*m*Tol)(CO)₃]₂ [(Å) and (˚)].

C-O…Cg	Centroid atom	d(O…Cg) Å	d(O…Cg) Å	(C-O…Cg) (˚)
C02-O02	Cg1#1	3.789(6)	3.683(6)	76.0(4)
C03-O03	Cg1#2	3.670(5)	4.211(6)	109.7(4)

Symmetry transformation:
#1   x, y, z   #2   x+1, y, z
Cg1 = centroid atom of C21, C22, C23, C24, C25, C26
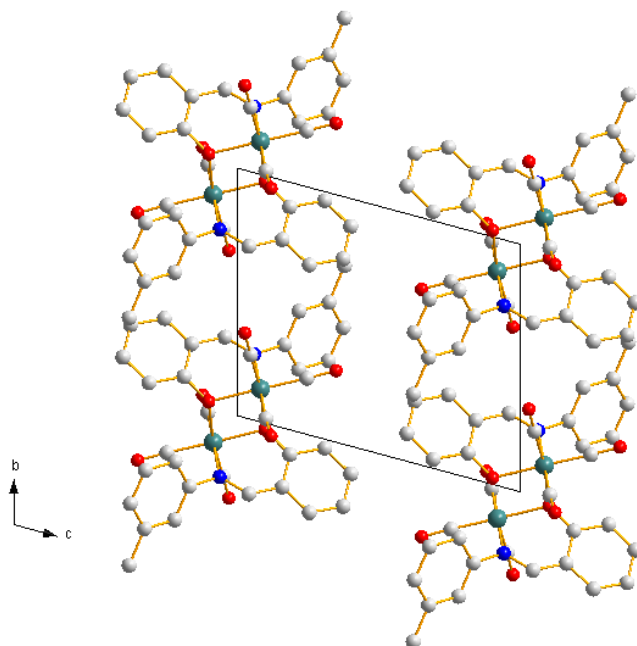
Figure 5.8: Molecular packing of *fac*-[Mn(Sal-*m*Tol)(CO)₃]₂ viewed along the *a*-axis.

5.3 CRYSTAL STRUCTURE OF

fac-[Mn(Sal-CyHex)(CO)₃]₂

The molecular structure of complex, *fac*-[Mn(Sal-CyHex)(CO)$_3$]$_2$ **(2),** (Sal-CyHex = 2-(cyclohexyliminomethyl)phenolato) is illustrated by Figure 5.9. The molecule crystallizes in triclinic crystal system in $P\bar{1}$ space group with two formula units per unit cell (Z=2). The asymmetric unit of **(2)** consists of one half of the manganese molecule. Relevant bond distances and angles are given in Table 5.5.
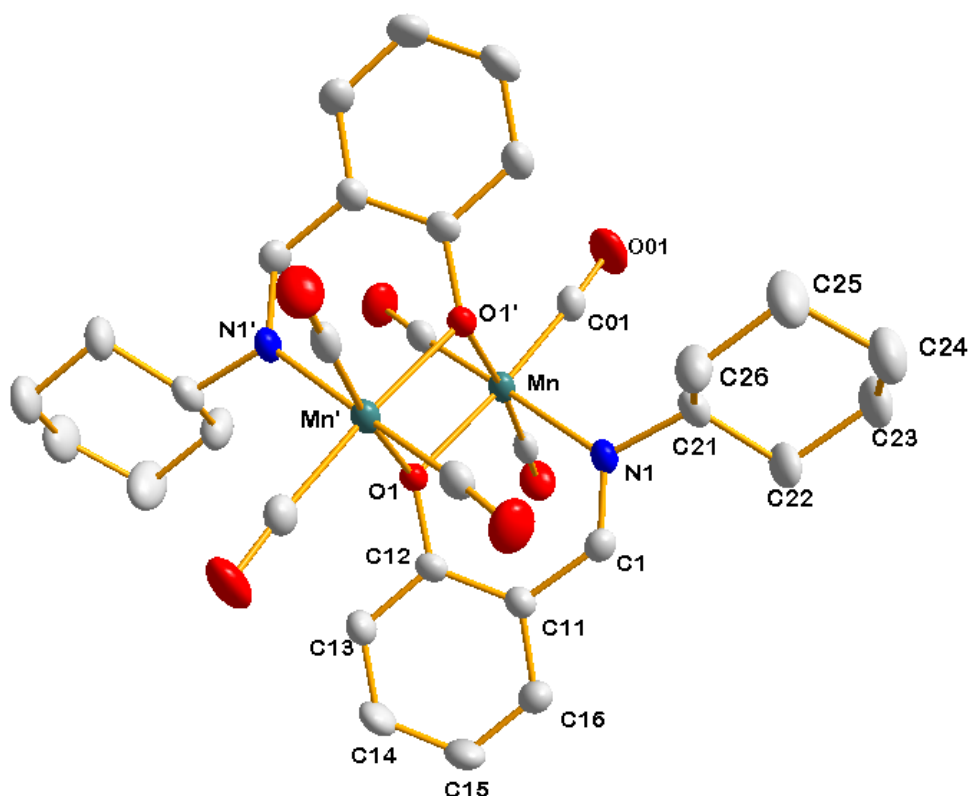
Figure 5.9: Structural representation of fac-[Mn(Sal-CyHex)(CO)₃]₂ complex (2), with atom numbering scheme and displacement ellipsoids at 50% For the aromatic rings, the first digit represents the ring number, while the second digit refers to the specific C-atom in the ring.

Table 5.5: Selected bond distances and angles of *fac*-[Mn(Sal-CyHex)(CO)$_3$]$_2$ (2) [(Å), (˚)]

Atoms	Length (Å)	Atoms	Angle (˚)
Mn1-O1	2.025(19)	N1-Mn-O1	86.15(8)
Mn-O1$^{#1}$	2.062(18)	N1-Mn-O1$^{#1}$	87.67(9)
Mn-N1	2.086(2)	O1-Mn-C03	96.49(10)
Mn-C01	1.802(3)	N1-Mn-C02	176.74 (11)
Mn-C02	1.809(3)	O1-Mn-O1$^{#2}$	76.89(8)
Mn-C03	1.796(3)	O1-Mn-C02	93.92.92(10)
N1-C1	1.287(3)	O03-C03-Mn	177.6(3)
C03-O03	1.153(4)	N1-Mn1-C01	176.74(11)
C02-O02	1.144(3)	N1-Mn1-O1	86.15(8)
C01-O01	1.152(3)	C1-N1-C21	117.3(2)

#1 refers to the symmetry generated subunit.

The molecule consists of two Mn metal [Mn((Cyhex)(CO)$_3$)] units merged by two bridging phenolato oxygen atoms of the CyHex ligand. The coordination sphere about the manganese atoms are distorted from idealised octahedral geometry with two *cis* carbonyl groups and two linking oxygen atoms in the [C-C-Mn-O-O] chelation plane. The third carbonyl ligand and the imine nitrogen atom occupy the axial positions of the plane consisting of Mn-O1$^{'}$-O1-C02-C03.
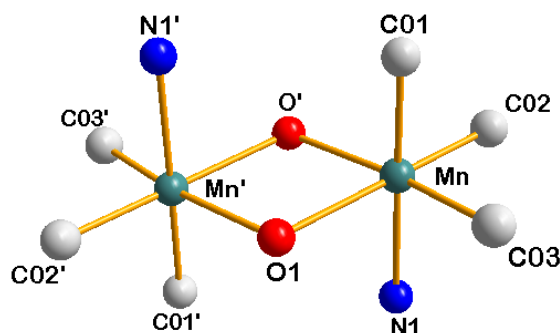
Figure 5.10: View of the coordination octahedron around the manganese atoms. The apostrophe indicates the symmetry generated subunit.

The distortion around each manganese metal centre can primarily be associated with the ligand bite angle of 86.15(8)˚, 87.67(9)˚ for N1-Mn-O1 and N1-Mn-O1$^{'}$ which is smaller than the expected 90˚. A deviation from linearity in N1-Mn-C01, 176.74(11)˚ was also observed.

The two Mn(I) atoms with a Mn-Mn' separation of 3.2007(10) Å, are projecting slightly from the equatorial plane defined by atoms Mn-C02-C03-O1'-O1 with an average out-of-plane displacement of 0.0271 (4) Å. The metal ions seem to be both electronically and geometrically equivalent in that corresponding bond lengths and angles are comparable.

The plane defined by the salicylidene C1 aromatic backbone (Plane 1: C11, C12, C13, C14, C15, C16) is bending relative to the manganese equatorial plane (Plane 2: Mn, N1, O1, C01, C02) with a dihedral angle of 39.33(11)° as indicated by Figure 5.11.
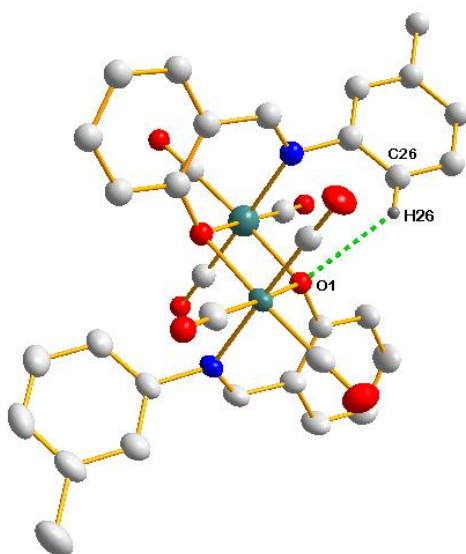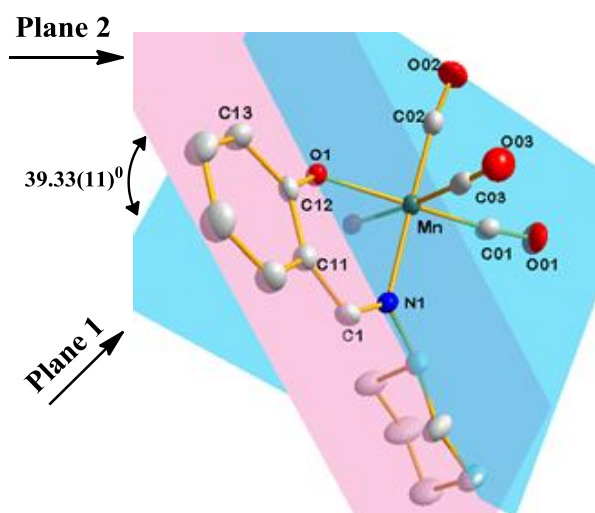

Figure 5.11: Graphical representation of the bending aromatic backbone (Plane 1 is indicated in purple and plane 2 indicated in blue). Hydrogen atoms were omitted for clarity.

The crystal lattice of complex **(2)** is stabilised by intermolecular hydrogen bonding between the H1 on the CyHex substituent and the oxygen atom of the adjacent molecule (C1…H1…O1$^{\#1}$) as illustrated in Figure 5.12 and Table 5.6. The other molecule in the asymmetric unit is also stabilised by intermolecular hydrogen bonds between H1 on the *m*-tolyl substituent and the oxygen atom of the adjacent molecule (C3…H3…O05$^{\#1}$).
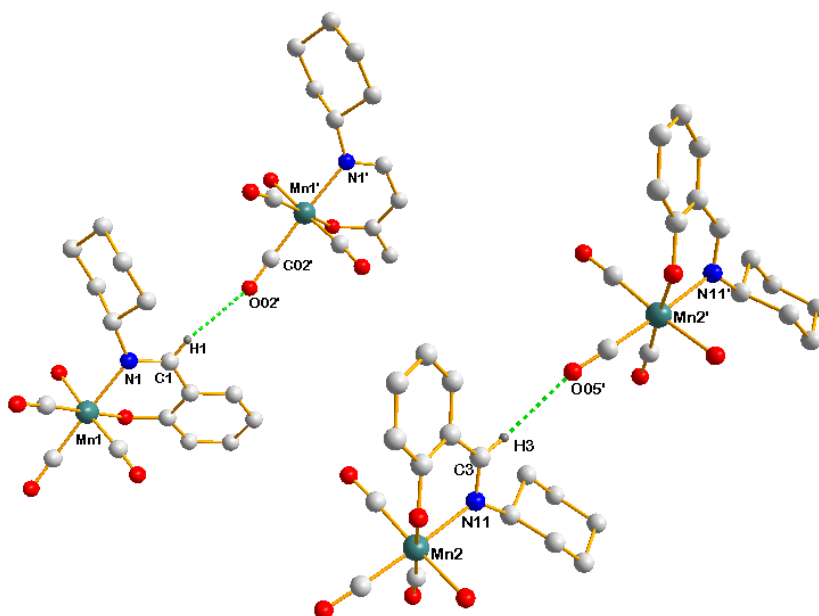
Figure 5.12:   **Graphical representation of intermolecular hydrogen bond interaction Hydrogen interaction is illustrated by the green dotted line. Certain atoms were omitted for clarity.**

Table 5.6: Hydrogen bonds for *fac*-[Mn(Sal-CyHex)(CO)$_3$] (Å,˚).

D-H…A	d(H…A)	d(H…A)	d(D…A)	<(DHA)
C(1)-H(1)…O(02)'#1	0.93	2.59	3.412(3)	148
C(3)-H(3)…O(05)'#1	0.93	2.58	3.406(3)	148

Symmetry transformation used to generate equivalent atoms:
#1 x, y-1,z

5.4 CRYSTAL STRUCTURE OF

fac-[Mn(4-Me-Sal-Hist)(CO)₃]

The complex, *fac*-[Mn-(4-Me-Sal-Hist)(CO)₃] **(3), (**4-Me-Sal-Hist = 2-[(2-Imidazol-4-yl)ethyliminomethyl]-5-methylphenolato) crystallises in a triclinic crystal system in $P\bar{1}$ space group with two formula units per unit cell (Z = 2). The asymmetric unit of complex **(3)** consists of one independent molecule. The molecular structure of **(3)** is illustrated by Figure 5.13 along with atom numbering scheme. Relevant bond distances and angles are listed in Table 5.7.
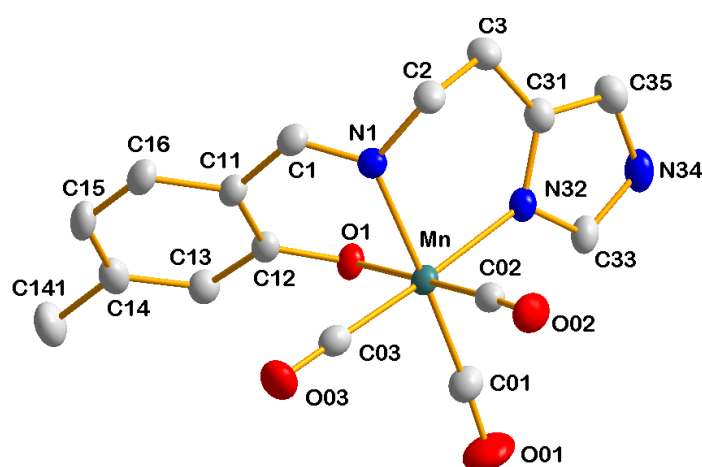
Figure 5.13: Molecular structure of *fac*-[Mn-(4-Me-Sal-Hist)(CO)₃] (3) showing atom numbering scheme and displacement ellipsoids at 50% probability level. For the aromatic rings, the first digit represents the ring number, while the second digit.

Table 5.7: Selected geometric parameters [Å, ˚].

Atoms	Length (Å)	Atoms	Angle (˚)
Mn-O1	2.0440(10)	N1-Mn-O1	84.08(5)
Mn-N1	2.0287(12)	N1-Mn-N32	85.10(5)
Mn-N32	2.0707(12)	N1-Mn-C02	96.48(6)
Mn-C01	1.8120(16)	N32-Mn-C02	91.51(6)
Mn-C02	1.7990(16)	O1-Mn-C02	179.41(6)
Mn-C03	1.8091(16)	N32-Mn-C03	176.95(6)
N1-C1	1.2890(18)	N1-Mn-C01	175.55(6)
N1-C2	1.4623(19)	N1-Mn-O1	88.72(4)
C01-O01	1.140(2)	Mn-O02-C02	176.55(14)
C02-O02	1.496(19)	C1-N1-C2	117.41(12)
C1-C11	1.441(2)	C1-N1-C2	117.41(12)
O1-C12	1.3231(17)	C01-Mn-O1	91.49(6)

The molecule affords a distorted octahedral configuration around the manganese atom with three carbonyl ligands in facial arrangement and a tridentate 5Me-SalH-Hist ligand with two N atoms and one O atom. The deviation from the ideal octahedral geometry is evident from the observed angles of 84.08(5)°, 85.10(5)° and 176.95(6)° for N1-Mn1-O1 and N1-Mn-N32 and N32-Mn1-C03 respectively. The Mn-N1 and Mn-O1 bond distances of [(2.0287(12) Å, 2.0440(10) Å)] are typical for similar complexes. The manganese carbonyl bond distances are comparable with bond distances of 1.8120 (16) Å, 1.7990 (16) Å and 1.8091(16) Å for Mn-C01, Mn-C02 and Mn-C03 respectively and are consistent with those observed in similar complexes.[6,7,16] The manganese atom lies at the centre of the equatorial plane defined by N1, N32, Mn, C01, C03 with an out-of-plane displacement of 0.0373(1) Å.
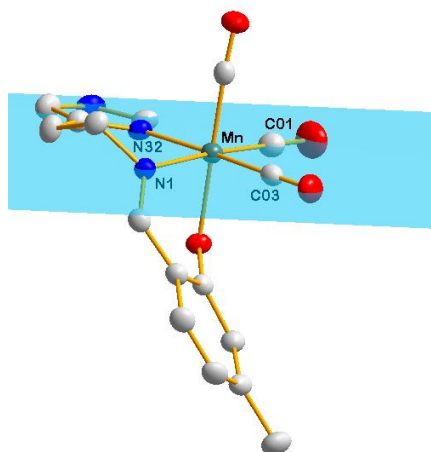
Figure 5.14: **Graphical representation of the out of the planarity in the equatorial plane. Hydrogen atoms were omitted for clarity.**

The plane formed by the salicylidene aromatic backbone (Plane 1: C11, C12, C13, C14, C15, C16) is tilted relative to the Mn equatorial plane (Plane 2: Mn, N1, O1, C01, C02) with a dihedral angle of the 47.940°.
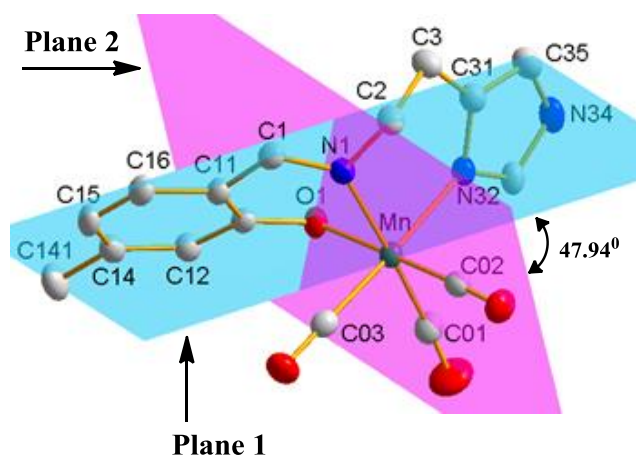
Figure 5.15: Graphical representation of the bending of the salicylidene aromatic backbone (Plane 1 indicated by purple, Plane 2 indicated by blue). Hydrogen atoms were omitted for clarity.

The histamine ring is almost perpendicular (88.406°) to the equatorial plane. The salicylidene backbone forms a dihedral angle of 51.783 °with the 5-membered histamine ring (plane 3: C31, N32, C33, N34, C35).
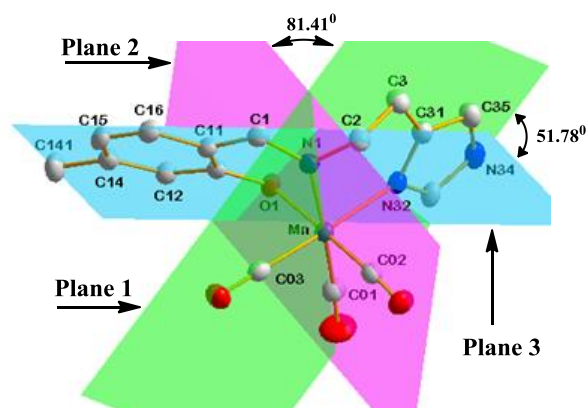
Figure 5.16: Graphical representation of the bending of the histamine moiety (Plane 1 indicated   by purple, plane 2 indicated by blue). Hydrogen atoms were omitted for clarity.

In the molecular packing of **(3)**, the hydrogen atom and the oxygen atom from adjacent molecules are aligned face-to-face. This conformation leads to the formation of classical intermolecular hydrogen between the atom H34 on the histamine substituent and the adjacent chelating oxygen atom O1, (N34-H34…O1[#1]) as illustrated in Figure 5.17 and Table 5.8. No intramolecular hydrogen bonding is observed.
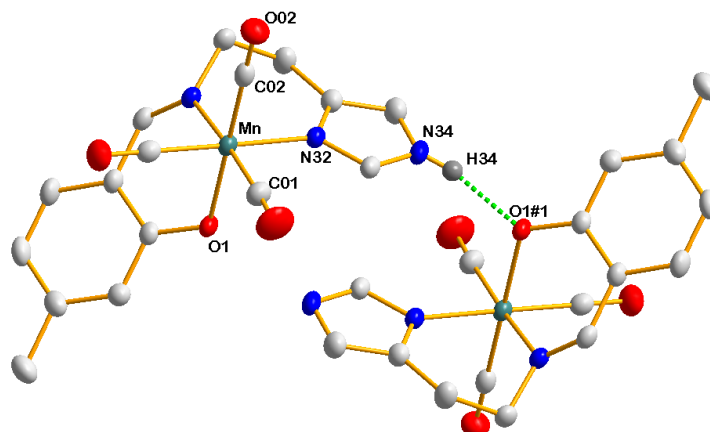
Figure 5.17: Graphical representation of intermolecular hydrogen bond interaction indicated between N34-H34…O1[#1]. Hydrogen interaction is illustrated by the green dotted line. Certain hydrogen atoms were omitted for clarity.

Table 5.8: Hydrogen bonds for *fac*-[Mn-(4-Me-Sal-Hist)(CO)$_3$] [Å, ˚].

D-H…A	d(D-H)	d(H…A)	d(D…A)	<(DHA)
N(34)-H(34)…O(1)#1	0.79	1.93	2.6929(17)	164(21)

Symmetry transformations used to generate equivalent atoms:
#1 1-x, -y, -z

A π-π interaction exists between the five-membered histamine rings and the symmetry generated counterparts of adjacent molecule, with a centroid to centroid distance of 3.8860(11) Å as indicated in Figure 5.18.
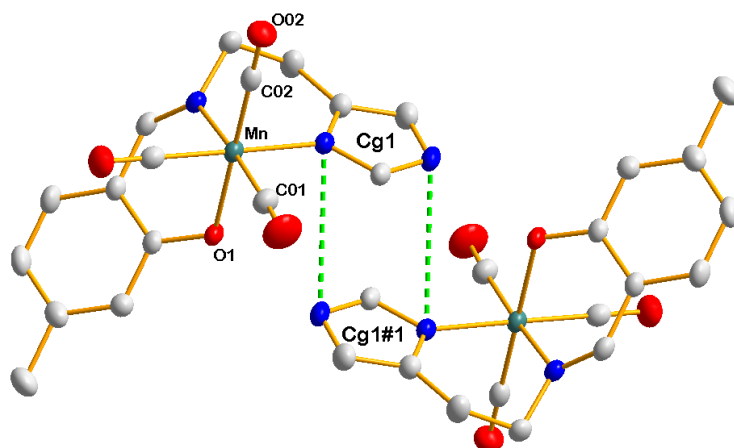
Figure 5.18: Graphical representation of the π-π interactions of five membered rings. Certain hydrogen atoms were omitted for clarity.

Table 5.9: π-π interaction in *fac*-[Mn(4-Me-Sal-Hist)(CO)$_3$] [(Å)].

Centroid atom	Centroid atom	Distance between centroid atoms
Cg1	Cg1#1	3.886(11)

Cg1 centroid atom of C31, N32, C33, N34, C35

#1 –x, -y, -z

The molecule displays two C-O…π interactions between C01-O01…Cg1[#2], the histamine ring, and C03-O03…Cg4, the salicylidene C1 backbone aromatic ring, and as indicated by green dotted lines in Figure 5.19 and Table 5.10.
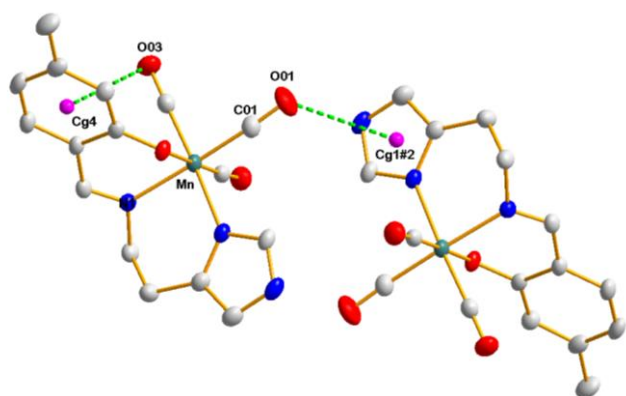
Figure 5.19: Graphical representation of C-O…π interaction indicated by the green dotted lines. Hydrogen atoms were omitted for clarity.

Table 5.10: C-O…π interactions of *fac*-[Mn-(4-Me-Sal-Hist)(CO)$_3$] [(Å), (˚)].

C-H…Cg	d(H…Cg)	d(C-H…Cg)	d(C-H…Cg)
C01-O01…Cg1	3.894(18)	4.389(18)	108
C03-O03…Cg2#1	3.788(16)	3.635(17)	74

Symmetry transformations:
#1 –x,-y,-z
Cg1 = Centroid atom of C11, C12, C13, C14, C15, C16; Cg2 = C31, C33, N32, N34, C35
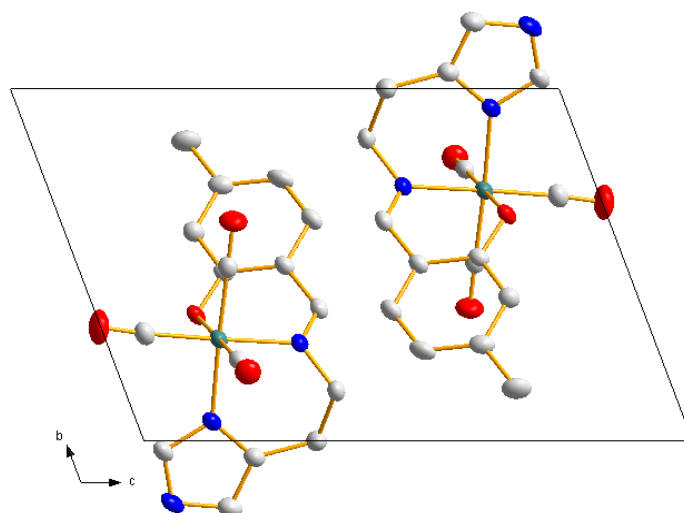
Figure 5.20: Molecular packing of *fac*-[Mn-(4-Me-Sal-Hist)(CO)$_3$] viewed along the *c*-axis. Hydrogen atoms were omitted for clarity.

5.5 INTERPRETATION AND CORRELATION OF PARAMETERS

The coordination properties of two new *fac*-[Mn(L,L'-Bid(CO)$_3$]$_2$ (L,L'-Bid = N,O Sal bidentate ligand) and one *fac*-[Mn(O,N,N')(CO)$_3$] (N,N,O Sal tridentate ligand) were evaluated and presented in this chapter. All three complexes contain an aromatic ring substituent attached to the nitrogen atom of the imine group. The three complexes have a distorted octahedral geometry about the manganese ion with three carbonyl ligands in facial arrangement. The remaining coordination sites are occupied by the phenolato oxygen atom and the imine nitrogen atom. The octahedron is completed by the nitrogen atom of the bound histamine moiety in the tridentate complex forming a six-membered chelate for complex **(3)**. In the two dimeric complexes **(1, 2)**, the ligand acts as both a chelate and a bridging ligand satisfying the octahedral configuration around the metal centre.

The crystal lattices of the complexes are stabilised by intermolecular hydrogen bonding interactions. Complex **(1)** and **(3)** are further stabilised by C-O…π interactions

Table 5.11: **Relevant crystallographic parameters of the *fac*-manganese(I) complex reported in this chapter.**

Complex	*fac*-[Mn(Sal-*m*Tol) (CO)$_3$]$_2$ (1)	*fac*-[Mn(Sal-CyHex) (CO)$_3$]$_2$ (2)	*fac*-[Mn(4-Me (Sal-Hist)(CO)$_3$]$_2$ (3)
Crystal system	Triclinic	Triclinic	Triclinic
Space group	$P\bar{1}$	$P\bar{1}$	$P\bar{1}$
a/Å	7.737(5)	9.160(2)	7.4262(11)
b/Å	9.483(5)	9.190(2)	9.0038(12)
c/Å	11.309(5)	18.267(4)	13.0780(18)
α/°	101.852(5)	89.90(3)	108.494(4)
β/°	102.514(5)	84.54(3)	104.058(4)
γ/°	101.480(5)	89.83(3)	93.363(4)
Volume/Å^3	766.6(7)	1530.8(6)	795.65(19)
Z	2	2	2

Figure 5.21: A graphical representation of the octahedral nature around the metal centre (atom label' = symmetry generated fragments).

The distortion from the idealised octahedral geometry in complexes **(1)**, **(2)** and **(3)** is evidenced by the reduction of the N1-Mn-O1 bond angle due to the restraints imposed by the coordinating ligands. The distorted octahedral configuration in **(1)** and **(2)** is given in Figure 5.21. The central unit of the **(1)** and **(2)** is a four membered planar Mn-O-Mn-O ring. The metal centres in both complexes are electronically and geometrically equivalent as evidenced by the corresponding bond parameters, for example, Mn-O1-Mn' angle of 101.987(23)° and 103.11(8)° for **(1)** and (**2**) respectively. The Mn-Mn' distances of 3.1865(14) Å for **(1)** and 3.2007(10) Å for **(2)** are too long to qualify any significant metal-metal interactions.

Table 5.12: Comparison of corresponding bond distances and angles of *fac*-manganese(I) tricarbonyl and fac-rhenium(I) tricarbonyl complex.[8]

Complex	(1)	Re-(a)	(2)	Re-(b)	(3)	Re-(c)
Bond Distance(Å)						
Mn-O1	2.044(10)	2.199(3)	2.025(19)	2.202(9)	2.0440(10)	2.1454(16)
Mn-N1	2.066(2)	2.157(4)	2.086(2)	2.131(7)	2.0287(12)	2.1599(15)
Mn-C01	1.815(3)	1.913(6)	1.802(3)	1.896(11)	1.8120(16)	1.924(2)
Mn-C02	1.795(3)	1.919(6)	1.809(3)	1.894(13)	1.7990(16)	1.905(2)
Mn-C03	1.789(3)	1.890(6)	1.796(3)	1.896(10)	1.8091(16)	1.911(2)
N1-C1	1.282(3)	1.290(6)	1.287(3)	1.282(12)	1.2890(18)	1.285(3)
C01-O01	1.143(4)	-	1.152(3)	-	1.140(2)	-
Mn-Mn'	3.1865(14)	-	3.2007(10)	-	-	--
C02-O02	1.143(3)	-	1.144(3)	-	1.496(19)	-
Bond angle (°)						
N1-Mn-O1	84.64(8)	84.6(1)	86.15(8)	84.0(2)	84.08(5)	80.11(7)
N1-Mn-C01	178.82(11)	-	176.74(11)	-	175.55(6)	-
O1-Mn-O1#1	77.96(8)	-	76.89(8)	-	-	-
O1-Mn-C02	174.92(11)	-	176.74 (11)	-	179.41(6)	-
O03-C03-Mn	177.6(3)	179.4(5)	177.6(3)	175.8(10)	179.17(15)	-
Mn-O1-Mn'	101.987(23)	-	103.11(8)	-	-	

Re-(b): *fac*-[Re(Sal-mTol(CO)₃(OHCH₃], Re-(b): *fac*-[Re(Sal-CyHex(CO)₃(OHCH₃), Re-(c) [Re(5-Me-Sal-Hist(CO)₃

[8] A. Brink, *PhD Thesis*, University of the Free State, Bloemfontein, South Africa, 2011.

The Mn-O1 and Mn-O1$'$ bond distances of [2.0325(19) Å, 2.066(2) Å] for **(1)** and [2.025(19) Å, 2.0619(18) Å] for **(2)** indicate that each *fac*-Mn[(CO)$_3$]$^+$ core is bound more tightly to the oxygen atom within the subunit.

5.6 Conclusion

Three new *fac*-manganese(I) tricarbonyl complexes were analysed and discussed herein. The observed coordination properties of **(1)** and **(2)**, are to some extend similar to the reported rhenium(I) monomeric analogues, for example, the bite angles of corresponding complexes are similar which implies little enhancement in the electronic and steric properties of the dimeric complexes relative to the monomeric complexes. The slight increase in rhenium complexes bond distances is most likely due to differences in ionic radii between the two metals.

5.7 CRYSTAL STRUCTURE OF *fac*-ACETYLACETONE COMPLEXES

The coordination chemistry of β-diketones with a variety of metal ions is well documented.[9,10,11,12,13] These ligands have the ability to stabilise various metal complexes through mononegative O_2-chelation. A key feature of these compounds is the keto-enol equilibrium. The equilibrium can be affected by factors such as solvent polarity and functionalities on both the methylene and the peripheral carbon atoms.
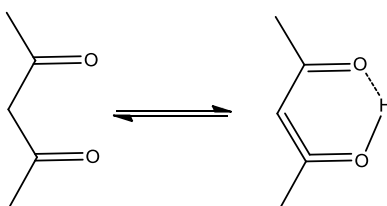
Figure 5.22: Keto-enol tautomerism in β-diketones.

There is growing interest in the possible application of these ligands in the designs of new materials such as contrast agents for magnetic resonance imaging, transport carriers of alkali metals across biological membranes.[14] The chelation process reduces the polarity on the metal ions by coordination, subsequently increasing the lipophilicity nature of the metals. It is suggested that the functionalization of the β-diketone system with two or more pharmacophore sites has some effect in their antifungal, antibacterial and antioxidant activity.

Two new complexes of the type, *fac*-[Mn(O,O')(CO)$_3$(X)] (where O,O'= acetylacetonatido, X = methanol) are presented herein. Their crystallographic data is listed in Table 5.13. The β-diketone ligands can be systematically modified to incorporate a target biomolecule at the alkyl carbon and also at the terminal carbons. Another interesting prospect is the possibility of linking a biomolecule to the monodentate ligand which might have a significant effect on the overall properties of the β-diketone complexes.

[9] R.M. Pike, *Coord. Chem. Rev.,1967,* 2,163.

[10] F. Bonati, *Organomet. Chem. Rev.*, 1996, 1, 379.

[11] C. Gkioni,V. Psycharis, C. P. Raptopoulou, *Polyhedron.,* 2009, *28*,3425.

[12] H. T. Zhang, J. H. Yang, R. V. Shpanchenko, A. M. Abakumov, J. Hadermann, R. Clérac, E. V. Dikarev., *Inorg. Chem.* 2009, *48*, 8480.

[13] C. P. Cheng, S. R. Wang, J. C. Lin, S. L. Wang, *J. Organomet. Chem.*, 1988, 349, 375.

[14] P. A. Vigato, V. Peruzzo, S. Tamburini. *Coord. Chem. Rev.*, 2009, 253, 1099.

Table 5.13: X-Ray crystallographic data and refinement parameters of *fac*-Manganese(I) β-diketone tricarbonyl complexes.

	fac-[Mn(Acac)(CO)$_3$(OHCH$_3$)]	*fac*-[Mn(TFA)(CO)$_3$(OHCH$_3$)]
Empirical formula	C$_8$H$_7$MnO$_5$	C$_8$H$_5$F$_3$MnO$_5$
Formula weight	271.3	325.10
Temperature/K	293(2)	293(2)
wavelength Å	0.71073	0.71073
Crystal system	triclinic	Monoclinic
Space group	$P\bar{1}$	$P2_1$/n
a/Å	7.513(5)	7.878(2)
b/Å	8.629(5)	19.556(5) Å
c/Å	9.771(5)	8.665(2) Å
α/°	81.914(5)	90°
β/°	80.707(5)	107.154(10)°
γ/°	69.715(5)	90°
Volume/Å3	583.9(6)	1275.5(6)
Z	2	4
Density calc g.cm^{-1}	1.809	1.526
μ/mm-1	4.548	1.076
F(000)	310	580
Crystal Colour	yellow	yellow
Crystal Morphology	Cuboid	Plate
Crystal size/mm^3	0.44 × 0.29× 0.25	0.49 × 0.29 × 0.06
Theta range (°)	2.121 to 24.9	2.083 to 28.00
Completeness (%)	88.6	100
Index ranges	h= -6 to 8	h= -10 to 10
	k= -9 to 10	k=-25 to 25
	l= -11 to 11	l= -11 to 11
Reflections collected	15240	22319
Independent reflections	1873	3075
R$_{Int}$	0.0878	0.0866
Data/restraints/parameters	3673/0/209	3075/0/174
Goodness-of-fit on F^2	1.047	0.874
Final R indexes [I>=2σ (I)]	R1 = 0.0835, wR2 = 0.2375	R1 = 0.0493, wR2 = 0.1474
Final R indexes [all data]	R1 = 0.1091, wR2 = 0.2818	R1 = 0.0818, wR2 = 0.1781
ρ max and ρ min (e.Å-3)	0.890 and -0.958	0.459 and -0.629

5.8 CRYSTAL STRUCTURE OF

fac-[Mn(Acac)(CO)₃(OHCH₃)]

The structural determination of complex, *fac*-[Mn(Acac)(CO)$_3$(OHCH$_3$)] **(4)**, (Acac = acetylacetone) was carried out with a yellow cuboid single crystal. The complex crystallises in triclinic crystal system in $P\bar{1}$ space group with two formula units per unit cell (Z = 2). The asymmetric unit of complex **(4)** consists of one independent molecule. The molecular structure of **(4)** is illustrated by Figure 5.23 along with atom numbering scheme. Selected bonds and bond distances are listed in Table 5.14 and 5.15.
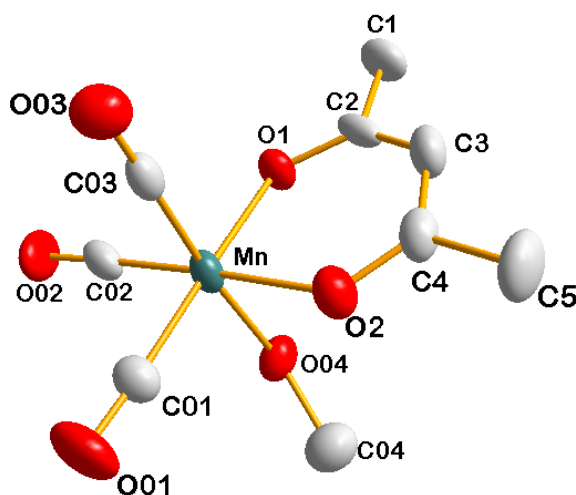
Figure 5.23:   .Molecular structure of *fac*-[Mn(Acac)(CO)$_3$(OHCH$_3$)] (4) showing atom numbering scheme and displacement ellipsoids at 50% probability level. Hydrogen atoms were omitted for clarity

Table 5.14:   Selected bond distances of *fac*-[Mn(Acac)(CO)$_3$(OHCH$_3$)] (4) (Å).

Atoms	Length (Å)	Atoms	Length (Å)
Mn-O1	2.022(5)	O01-C01	1.137(11)
Mn-O2	2.003(7)	O02-O02	1.171(12)
Mn-C01	1.802(9)	O03-O03	1.128(10)
Mn-C02	1.793(10)	C1-C2	1.263(11)
Mn-C03	1.801(8)	C3-C4	1.527(14)
Mn-O04	2.085(6)	O2-C4	1.263(11)
O04-C04	1.474(12)	O1-C2	1.296(11)

The molecular geometry about the manganese atom in complex **(4)** is a distorted octahedral comprising of the O,O' bidentate chelator, acetylacetone, the methanol molecule and three carbonyl ligands arranged in a *facial* manner. The apical positions of the octahedron are occupied by the methanol ligand and one of the carbonyl groups. This O,O' structure coordinates as a monomeric species unlike the N,O bidentate ligands reported in section 5.1-5.6. The six-membered ring in the coordination sphere defined by the O1-C2-C3-C4-O2 atoms of the acetylacetone chelate and the manganese ion are almost planer with the largest displacement of C3 being 0.2362(3) Å from the plane defined by atoms Mn-O1-C2-C3-C4-O2. The C2-C3-C4 angle, 125.5(10)° of the chelating acetylacetone ligands deviates from the expected 120°. The molecular distortion from the ideal octahedral geometry is indicated by the C03-Mn-C02 bite angle of 88.4(4)° and the C01-Mn-O1, C02-Mn-O2 bond angles of 176.9(3)° and 177.6(3)° respectively. The Mn-O1 and Mn-O2 bond distances 2.022(5) Å, 2.003(7) Å are within the expected range for Mn-Acac type complexes spanning around 1.860(2)-2.072(2) Å.[15,16,17] The C4-O2 and C2-O1 bond distances of 1.263(11) Å and 1.296(11) Å for the C4-O2 and C2-O1 are well within range for related complexes.[18] The Mn-CO bonds are within the normal range spanning from 1.793(10) to 1.801(8) Å.

Table 5.16: Selected bond angles of *fac*-[Mn(Acac)(CO)$_3$(OHCH$_3$)] (4) (°).

Atoms	Angle (Å)	Atoms	Angle (°)
O1-Mn-O2	89.6(3)	C4-O2-Mn	127.7(6)
C01-Mn-O2	91.4(3)	O2-C4-C3	125.5(10)
C02-Mn-O1	92.6(3)	O1-C2-C3	125.6(8)
C03-Mn-C02	88.4(4)	O2-C4-C5	115.8(8)
C03-Mn-C01	89.8(4)	C01-Mn-O1	176.9(3)
C03-Mn-O1	93.0(3)	C02-Mn-O2	177.6(3)
C03-Mn-O2	92.5(3)	O1-Mn-O04	83.0(2)
C2-C3-C4	124.7(10)	O2-Mn-O04	84.8(2)
C04-O04-Mn1	125.7(6)		

[15] Y. Cheng, S. Xia, J. Feng, Jun, S. Du, L. An, X. Lu, *Chin. J. Chem.,* 2012, *30,* 1063.
[16] S. Geremia, N. Demitri. *J. Chem. Educ,* 2005, 82, 460.
[17] B. Morosin, J. R. Brathovde, *Acta Crystallogr.,* 1964, *17,* 705.
[18] B. R. Stults, R. S. Marianelli, V. W. Day. *Inorg. Chem* ., 1979, 18, 1853.

The carbon atom of the coordinated methanol molecule is bending outwards relative to the manganese atom with a Mn-O04-C04 angle of 125.7(6). The Mn-O04 bond distance of 2.085(6) Å compares well with the aqua complexes with distances of 2.108(5) and 2.099 Å.[19,20] The molecular packing of *fac*-[Re(Acac)(CO)$_3$(OHCH$_3$)] within the unit cell is illustrated by Figure 5.24. No π-π interactions or classical hydrogen bonds are observed in the structure.
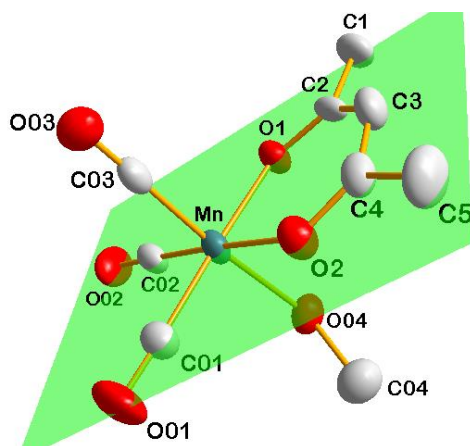
Figure 5.24: **Graphical representation of the out-of-plane displacement of C3 atom.**
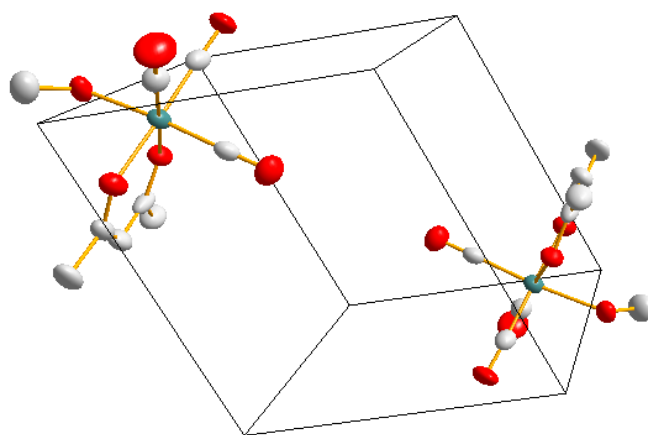
Figure 5.25: **An illustration of the diagonal packing in the unit cell viewed along the *c*-axis.**

[19] M. L. Valín, D. Moreiras, X. Solans, M. Font-Altaba, F. J. García-Alonso, *Acta Crystallogr.*, 1986, C42, 417.

[20] G. Ara, S.E. Kabir, K. Kundu, K.M.A. Malik, *J. Chem. Cryst.*, 2003, 33, 851.

5.9 CRYSTAL STRUCTURE OF

fac-[Re(Tfacac)(CO)$_3$(OHCH$_3$)]

The solid state structure determination of complex, *fac*-[Mn(Tfacac)(CO)$_3$(OHCH$_3$)] **(5)**, (Tfacac = trifluoroacetylacetone) was carried out with a yellow prism single crystal. The complex crystallises in the monoclinic crystal system in *P*2$_1$/n space group with four formula units per unit cell (Z = 4). The asymmetric unit of complex **(5)** consists of one independent molecule. A structural representation of **(5)** along with atom numbering scheme is illustrated by Figure 5.26. Selected bond angles and bond distances are listed in Tables 5.17 and 5.18.
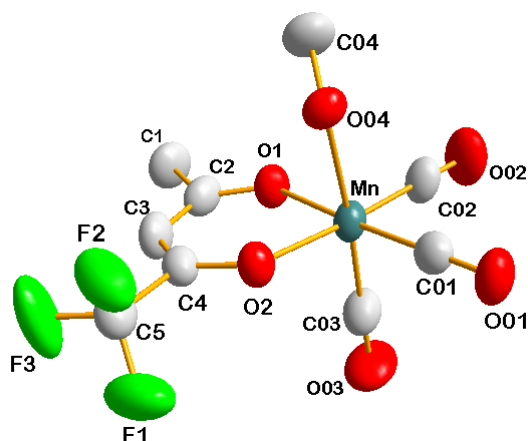
Figure 5.26: Molecular structure of *fac*-[Mn(Tfacac)(CO)$_3$(OHCH$_3$)] (5) showing atom numbering scheme and displacement ellipsoids at 50% probability level. Hydrogen atoms were omitted for clarity.

Table 5.17: Selected bond lengths of *fac*-[Mn(Tfacac)(CO)$_3$(OHCH$_3$)] (Å).

Atoms	Length (Å)	Atoms	Length (°)
Mn-O1	2.005(4)	O03-C03	1.153(8)
Mn-O2	2.016(4)	C5-F1	1.335(8)
Mn-C01	1.808(7)	C5-F2	1.318(7)
Mn-C02	1.817(2)	C5-F3	1.315(7)
Mn-C03	1.800(7)	C1-C2	1.499(8)
Mn-O04	2.092(4)	C3-C4	1.346(8)
O04-C04	1.406(7)	C2-C3	1.417(8)
O01-C01	1.130(8)	O1-C2	1.259(7)
O02-C02	1.148(6)	O2-C4	1.300(6)

The coordination around the manganese atom is a distorted octahedron consisting of two oxygen atoms from the triflouroacetylacetone bidentate chelate, the methanol molecule and three carbonyl ligands arranged facially around the metal ion. One carbonyl ligand and the coordinated methanol molecule occupy the axial positions. The six-membered ring in the coordination sphere defined by O1-C2-C3-C4-O5 atoms of the triflouroacetylacetone chelate and the manganese ion are almost planar with the largest displaced atom C3 being 0.0526(1) Å. The C2-C3-C4 angle, 125.5(10) ° of the chelating acetylacetone ligands deviates from the expected 120°.

Table 5.18: Selected bond angles of *fac*-[Mn(Tfacac)(CO)$_3$(OHCH$_3$)] [°].

Atoms	Angle (°)	Atoms	Angle (°)
O1-Mn-O2	88.97(14)	C4-O2-Mn	124.9(3)
C01-Mn-O2	93.04(19)	O2-C4-C3	128.1(5)
C02-Mn-O1	92.6(3)	O1-C2-C3	124.3(5)
C03-Mn-C02	93.4(2)	O2-C4-C5	112.2(5)
C03-Mn-C01	89.8(4)	C01-Mn-O1	93.8(2)
C01-Mn-O1	176.9(3)	C02-Mn-O2	176.3(2)
C02-Mn-O2	177.6(3)	O1-Mn-O04	84.60(14)
C2-C3-C4	124.7(10)	O2-Mn-O04	82.26(16)
C04-O04-Mn1	125.7(6)	O1-Mn-O2	88.97(14)

The Mn-O1 and Mn-O2 bond distances are 2.005(4) Å and 2.016(4) Å. These are comparable to other Mn-acac type complexes which span around 2.161(4)-2.186 (4) Å.[21] The angular distortion from the ideal octahedral is indicated by the O1-Mn-C03 and O1-Mn-O04 bond angles of 89.4(2)° and 84.60(14)° respectively. The distortion is further supported by the C02-Mn-O1 and C03-Mn-O2 bond angles of 177.5(2)° and 176.3(2)° respectively. The Mn-O bond distances 2.005(4) Å and 2.016(4) Å are well within the normal range for similar complexes.[16] All three Mn-CO bonds are equivalent with distances 1.800(7) Å, 1.817(2) Å and 1.808(7) Å for Mn-C01, Mn-C02 and Mn-C03 respectively.

The coordinated methanol with a Mn-O04 bond distance of 2.092(4) Å, is bent away from the equatorial plane constructed through atoms (plane 1: Mn, C01, C03, O1, O04) with a Mn-O04-C04 bond angle of 126.8(4)°.

---

[21] M. D. Carducci , R. J. Doedens. *Inorg. Chem.* 1989, *28,* 2492.
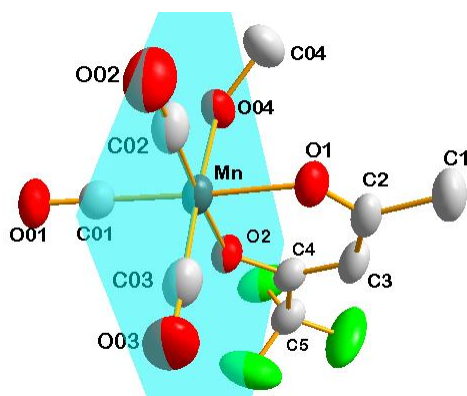
Figure 5.27: Graphical representation of the bending of the methanol molecule relative to the drawn equatorial plane. Hydrogen atoms were omitted for clarity.

The plane formed by the trifluoroacetylacetone bidentate ligand (Plane 1: O1, C2, C3, C4, O2, Mn) forms a dihedral angle of 1.058˚ with the equatorial plane (Plane 2: C01, C02, Mn, O1, O2).
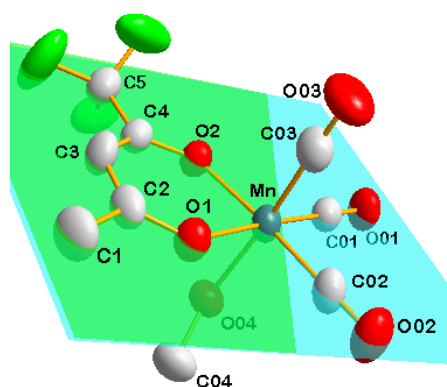
Figure 5.28: Graphical representation of the bending of the triflouroacetylacetone (Plane 1 indicated by green, Plane 2 indicated by blue). Hydrogen atoms were omitted for clarity.

The arrangement of complex **(5)** in the unit cell leads to the formation of intramolecular C-H…F hydrogen bonding between the hydrogen atom of the acetylacetone chelate ring and the fluorine atom as illustrated in Figure 5.29 and Table 5.19. No intermolecular hydrogen bonding observed.
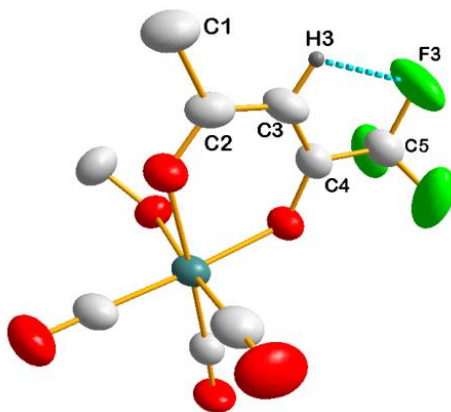
Figure 5.29: **Graphical representation of intramolecular hydrogen bond interaction indicated by the green dotted line. Certain atom labels were omitted for clarity.**

Table 5.19: Hydrogen bonding for *fac*-[Re(Tfacac)(CO)$_3$(OHCH$_3$)] [Å and ˚]

D-H…A	d(D-H)	d(H…A)	d(D…A)	
C(3)-H(2)…F(3)#1	0.93	2.35	2.726(8)	104

Symmetry transformations:
#1 x, y, z

The molecule is stabilised by the formation of C-F…π interactions defined by C5-F3…Cg1#1 of the acetylacetone chelate ring. The interactions are depicted by the blue dotted line in Figure 5.30 and Table 5.20.
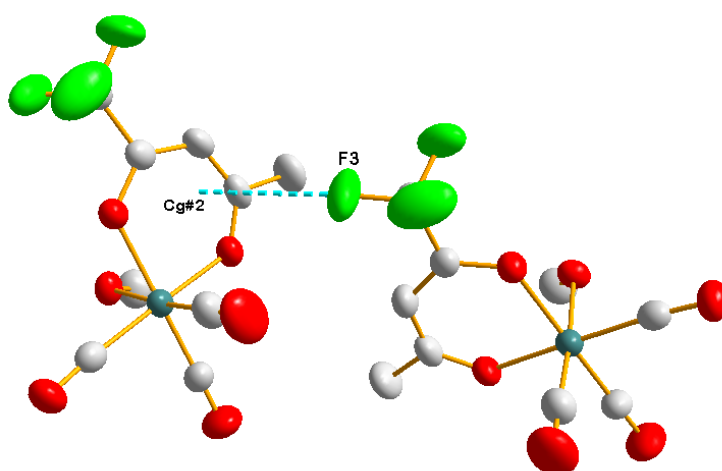
Figure 5.30: **Graphical representation of intermolecular fluorine interaction with the chelate ring indicated by the blue dotted line. Certain atom labels were omitted for clarity.**

Table 5.20: C-F…π bonding [Å and ˚].

C-O…Cg	Centroid atom(Cg)	d(O…Cg)	d(C…Cg)	<(CO…Cg)
C5-F3	Cg1#2	3.512(6)	4.800(7)	166.4(4)

Symmetry transformations:
#2 1/2+x, ½-y, ½+z

The molecules in the unit cell pack in an antiparallel fashion where the fluorine atoms of adjacent molecule are facing in the opposite direction when viewed along the *c*-axis.
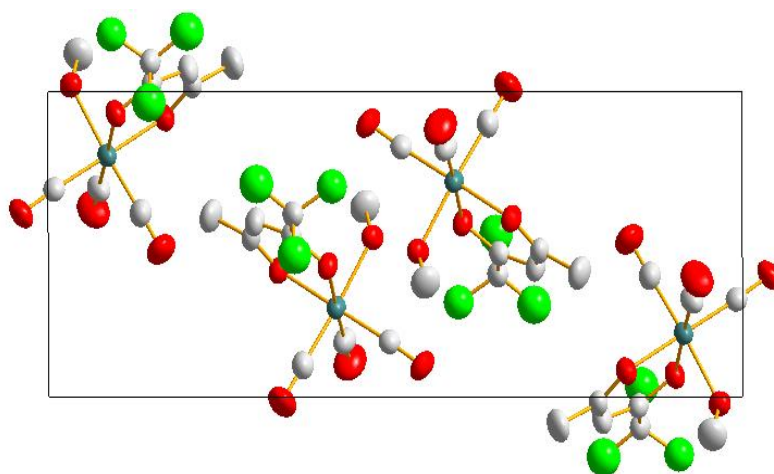
Figure 5.31:   Molecular packing in the unit cell viewed along the *c*-axis.

5.10 Discussion

Complexes **(4)** and **(5)** both have a distorted octahedral geometry around the central atom with the coordinated methanol molecule and one carbonyl ligand occupying the apical positions. The equatorial plane is defined by the manganese atom and the bidentate chelate. Complex **(4)** has two molecules per unit cell (Z = 2) and crystallizes in $P\bar{1}$ space group, whilst **(5)** has four molecules per unit cell (Z = 4) and crystallizes in the P2$_1$/n space group.

Table 5.21: Cell dimension overview for complex (4) and (5).

Complex	(4)	(5)
Crystal system	Triclinic	Monoclinic
Space group	$P\bar{1}$	P2$_1$/n
a/Å	7.513(5)	7.878(2)
b/Å	8.629(5)	19.556(5) Å
c/Å	9.771(5)	8.665(2) Å
α/°	81.914(5)	90°
β/°	80.707(5)	107.154(10)°.
γ/°	69.715(5)	90°
Volume/Å3	583.9(6)	1275.5(6)
Z	2	4

Table 5.22: A comparison of selected bond distances and angles for synthesized compounds with rhenium analogues.[22]

Complex	(4)	*fac*-[Re(Acac)(Py)-(CO)$_3$]	(5)	*fac*[Re(Tfacac)(Py)-(CO)$_3$]
Bond Lengths (Å)				
M-O1	2.022(5)	2.1189(19)	2.005(4)	2.135(3)
M-O2	2.003(7)	2.1226(19)	2.016(4)	2.117(3)
M-O04	2.085(6)	-	2.092(4)	-
M-C01	1.802(9)	1.926(3)	1.808(7)	1.932(5)
M-C02	1.793(10)	1.896(13)	1.817(2)	1.906(4)
O1-C2	1.296(11)	1.276(4)	1.259(7)	1.263(5)
O2-C4	1.263(11)	1.274(4)	1.300(6)	1.269(5)
Bond angle (°)				
C03-Mn-C02	90.1(3)	-	88.4(4)	90.32(18)
O1-Mn-C03	93.8(2)	95.29(10)	93.0(3)	95.20(15)
O1-Mn-O04	84.60(14)	-	83.0(2)	-
C02-Mn-O2	176.3(2)	94.55(10)	177.6(3)	92.70(14)
C2-C3-C4	128.1(5)	125.3(3)	125.5(10)	129.2(4)
O1-Mn-O2	88.97(14)	85.07(8)	89.6(3)	84.99(11)

[22] A. Manicum, M. Schutte-Smith, G. Kemp, H. G. Visser, *Polyhedron.*, 2015, 85, 190.

The six-membered ring in the coordination sphere defined by the O1-C2-C3-C4-O2 atoms of the acetylacetone ligand and the metal ion is almost planar with a minimum manganese atom deviation of 0.0332(3) Å and 0.0317(1) Å for *fac*-[Mn(Acac)(CO)$_3$(OHCH$_3$)] **(4)** and *fac*-[Mn(Tfacac)(CO)$_3$(OHCH$_3$)] respectively. The distortion in the octahedral geometry around the central metal ion in complex **(4)** and **(5)** is comparable with a slight decrease in bite angles going from **(4)** to **(5)** indicated by 177.5(2)° > 176.9(3)° for C02-Mn-O1 and 93.4(2)° > 92.6(3)° for C03-Mn-C02 respectively. The observed Mn-O1 and Mn-O2 bond distances [**(4)** 2.022(5), 2.005(4) Å; **(5)** 2.003(7), 2.016(4) Å] are well within the range for Mn-O complexes.[23] The Mn-O bond distances are comparable to analogous *fac*-rhenium(I) tricarbonyl complex with Re-O bond distances of 2.117(3) and 2.135(3) Å. The slight increase in bond lengths is characteristic when going down in the Mn-triad group due to the differences in atomic radii. The O2-C4 and O1-C2 bond distances 1.259(6) Å and 1.300(6) Å are comparable to those observed in *fac*-rhenium tricarbonyl with acetylacetone ligands spanning around 1.269(5) Å.

5.11 Conclusion

Two new *fac*-manganese(I) tricarbonyl acetylacetone and its fluorinated analogue complexes were analysed and discussed in this chapter. Both complexes present an octahedral geometry around the metal centre with three carbonyls in *facial* orientation. The chelating bidentate ligand and a methanol molecule complete the octahedral geometry. An overarching observation made was the insignificant influence of the functionalised acetylacetone ligand on the bond lengths within the complex.

---

[23] C. Yifeng, X. Sifeng, F. Jun, D. Shizhen. *Chin. J. Chem.*, 2012, 30, 1063

6 METHANOL SUBSTITUTION KINETICS OF MANGANESE (I) COMPLEXES

6.1 Introduction

Chemical reaction kinetics deals with the rates of chemical processes, that is, the change in some chemical characteristic of a species involved, with respect to time. These studies can reveal some facet regarding the property of a chemical reaction such as the mechanism of chemical changes and the transition from one state to another. The rate of reaction can be affected by factors such as homogeneity, concentration, temperature and sensitivity to light. It is thus imperative to study the fundamental reactivity of complexes which include the rates of complex formation, electronic and steric effects of the entering ligands on the rates of reaction under specifically determined reaction conditions.

6.2 Background information on previous studies

Several studies were undertaken after the first kinetic studies on the water exchange of fac-[M(CO)$_3$(H$_2$O)]$^+$ by a variety of nucleophiles.[1,2] A more detailed description of these studies can be found in Paragraph 2.7. This present study serves as a continuation of the investigations on the effect of coordinated bidentate ligands on the methanol substitution in complexes fac-[M(CO)$_3$(X)(L,L$^{'}$-Bid)] where X = methanol and L,L$^{'}$–Bid = bidentate ligand.

Manicum and co-workers[3] pointed out the influence of substituted fluorine atoms in the β-diketone bidentate ligands on the rate of methanol substitution by a variety of

[1] L. Helm, *Coord. Chem. Rev.*, 2008, 252, 2346.
[2] M. Schutte, G. Kemp, H. G. Visser, A. Roodt, *Inorg. Chem.,* 2011, 50, 12486.
[3] A. Manicum, M. Schutte-Smith, G. kemp, H. G. Visser, *Polyhedron.*, 2015, 85, 190.

mono-coordinating ligands to the rhenium(I) complexes. It was concluded that the rate of methanol substitution is in direct correlation with the degree of substitution on the acetylacetone backbone and principally on the nature of the coordinated ligand. These findings were verified by analogues studies using the *fac*-[Mn(CO)$_3$(N,N-Bid)(OHCH$_3$)]^n complex with a variety of ligands Br$^-$, pyridine and thiourea.[4] The study revealed that the nature of the donating functionalities on the bidentate ligands influence the rate of methanol substitution independently, that is, the *O,O'*-Bid donating functionalities are able to activate the methanol substitution reaction more than *N,O'*-Bid functions.

The interesting results obtained in the above mentioned studies fuelled the synthesis of the new *fac*-[Mn(O,O'-Bid)(CO)$_3$(OHCH$_3$)] where *O,O'*-Bid = acetylacetone backbone. The coordination of acetylacetone with a variety of transition metals is well documented.[5,6] These ligands have the ability to stabilise metal complexes through *O,O'* chelation. The systematic modification of these ligands may induce a significant effect in the overall activity of the complexes specific reference to the modeling of biological complexes in the [2+1] labeling approach.

(4) **(5)**
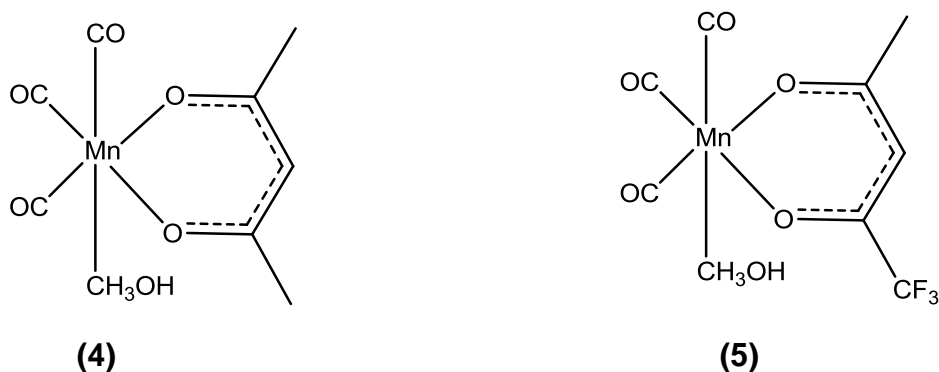
Figure 6.1: A schematic representation of *fac*-[Mn(Acac)(CO)$_3$(OHCH$_3$)] and *fac*-[Mn(Tfacac)(CO)$_3$(OHCH$_3$)] where Acac = acetylacetone and Tfacac = trifluoroacetylacetone.

[4] T. N. Twala, M. Schutte-Smith, A. Roodt, H. G. Visser, Dalton Trans, DOI: 10.1039/C4DT03524K.

[5] F. Bonati, *Organomet. Chem. Rev.*, 1996, 1, 379.

[6] C. Gkioni,V. Psycharis, C. P. Raptopoulou, *Polyhedron.*, 2009, *28*,3425

6.3 Experimental

6.3.1 Procedure

All chemicals used in this study were of analytical grade and used as purchased from Sigma-Aldrich, South Africa, unless stated otherwise. The UV-vis measurements were collected using a Varian 50 Conc UV-Visible spectrophotometer, equipped with a Julabo F12-mV temperature cell regulator (accurate within 0.1°C) in a 1.000 $\pm$ 0.001 cm tandem quartz cuvette cells. The kinetic experiments were performed under *pseudo* first order conditions and the data was fitted to selected functions using the Scientist Micromath version 2.01.[7] The solid lines represent the least square fits and the experimental data is represented by individual points.

6.3.2 Data treatment

The Beer-Lambert Law relates the absorption of light to the concentration of a solution, by the following equations,

$$A_t = A_\infty (A_\infty - A_0)e^{k_{obs}t} \qquad \qquad \text{...6.1}$$

where A_t is the absorbance after time t, A_∞ is the absorbance at time infinity and k_{obs} is the pseudo first order rate constant of the reaction determined from a least-squares fit of absorbance *vs* time data.

6.4 Results

The substitution kinetics of the coordinated methanol molecule in neutral complexes of the type *fac*-[Mn(O,O$^{'}$-Bid)(CO)$_3$(OHCH$_3$)] (where O,O'-Bid = acetylacetone backbone) by a neutral monodentate ligand, imidazole, was studied under simple pseudo first order conditions.

---

[7] Micromath Scientist for Windows, Version 2.01, copyright © 1986-1995, MicorMath, Inc

$$[Mn(O,O'\text{-Bid})(CO)_3(OHCH_3)] + Im \underset{k_{-1}}{\overset{k_1, K_1}{\rightleftharpoons}} [Mn(O,O'\text{-Bid})(CO)_3(Im)] + CH_3OH$$
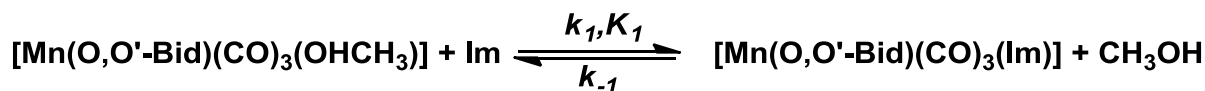
Scheme 6.1: Schematic illustration of the predicted methanol substitution in complexes of the type *fac*-[Mn(O,O'-Bid)(CO)₃(OHCH₃)].

The rate of reaction can be written as:

Rate = k₁[Mn(O,O'-Bid)(CO)₃(X)] – *k*₋₁[Mn(O,O'-Bid)(CO)₃(OHCH₃)]   …6.2

Pseudo first order reaction conditions entails changing the concentration of one of the reactants, whilst the other is kept constant. The concentration dependence of the *pseudo* first order observed rate for the methanol substitution by a monodentate ligand (L) is defined by Eq 6.3.

$$k_{obs} = k_1[L] + k_{-1} \qquad \qquad …6.3$$

Where k_1 and k_{-1} represent the rate of the forward and the reverse reactions respectively.

The equilibrium constant, K_1, was determined from equation 6.4. A plot of k_{obs} vs [L] gives a linear relationship with a slope of k_1 and an intercept of k_{-1}. The equilibrium constant, for one reaction per metal complex was alternatively determined from a non-linear least-squares fit to confirm that the kinetically (Eq. 6.4) and thermodynamically (Eq. 6.5) equilibrium constant are the same.

$$K_1 = \frac{k_1}{k_{-1}} \qquad \qquad …6.4$$

$$A_{obs} = (A_M + A_{ML}K_1[L]/K_1[L] \qquad \qquad …6.5$$

The experimentally obtained data is translated into the linear Eyring equation from which the standard activation enthalpy ($\Delta H^{\neq}$) and the standard activation entropy change ($\Delta S^{\neq}$) are determined.[8]

$$\ln \frac{k}{T} = \frac{-\Delta H^{\neq}}{RT} + \ln \frac{k_B}{h} + \frac{\Delta S^{\neq}}{R} \qquad \qquad \text{...6.6}$$

A plot of $\ln \frac{k}{T}$ vs $\frac{1}{T}$ gives a linear relation with a slope defined by $\frac{-\Delta H^{\neq}}{R}$ and intercept of $\ln \frac{k_B}{h} + \frac{\Delta S^{\neq}}{R}$

Where k is the experimentally determined rate constant at temperature T, R is the Universal Gas Constant (8.314 J.K^{-1}. mol^{-1}), k_B is the Boltzmann Constant (1.318 J.K^{-1}) and h is the Planck's Constant (6.626 J.s).

6.4.1 The reaction between *fac*-[Mn(O,O$^{'}$)(CO)$_3$(OHCH$_3$)] and Imidazole in methanol

Complex *fac*-[Mn(Acac)(CO)$_3$(OHCH$_3$)] **(4)** and *fac*-[Mn(Tfacac)(CO)$_3$(OHCH$_3$)] **(5)** (where Acac = acetylacetone, Tfacac = trifluoroacetylacetone) were synthesized as described in Paragraph 4.5. The coordinated bidentate ligands were consciously selected to investigate the effect of the electron withdrawing fluorine atoms on the overall rate of methanol substitution. The methanol substitution reaction with imidazole was studied at average temperatures of 15, 25, 35 and 45 ^{0}C for complex **(4)** and **(5)**. The standard activation enthalpy ($\Delta H^{\neq}$) and the standard activation entropy change ($\Delta S^{\neq}$) were determined from the Eyring equation described above. Substitution with other entering ligands like bromide ions (Br$^-$), pyridine (Py) and thiourea (Tu) did not yield reliable data since the observed change in reaction was too small..

---

[8] Jordan R. B., *Reaction Mechanisms of Inorganic and Organometallic Systems*, Oxford University Press., Inc., Oxford, 1991.

6.4.2 The reaction between *fac*-[Mn(Acac)(CO)$_3$(OHCH$_3$)] and Imidazole in methanol

Figure 6.2 shows a typical absorbance change scan of the methanol substitution reaction between *fac*-[Mn(CO)$_3$(Acac)(OHCH$_3$)] and imidazole for all the reactions in this study. The k_{obs} *vs* [L] data at exact temperatures of 15.1, 24.5, 34.5 and 44.5 ^{0}C were obtained and fitted to Eq. 6.4. Analysis of the absorbance vs time data for individual kinetic traces indicates unequivocally, only one overall reaction. The linear behavior for the pseudo first order reaction was obtained and is illustrated in Figure 6.2. The activation parameters of the reaction between *fac*-[Mn(CO)$_3$(Acac)(OHCH$_3$)] and Im were determined by least-squares fits of temperature-dependent data of the pseudo first order rate constants to the Eyring equation 6.6 and are illustrated in Figure 6.3.
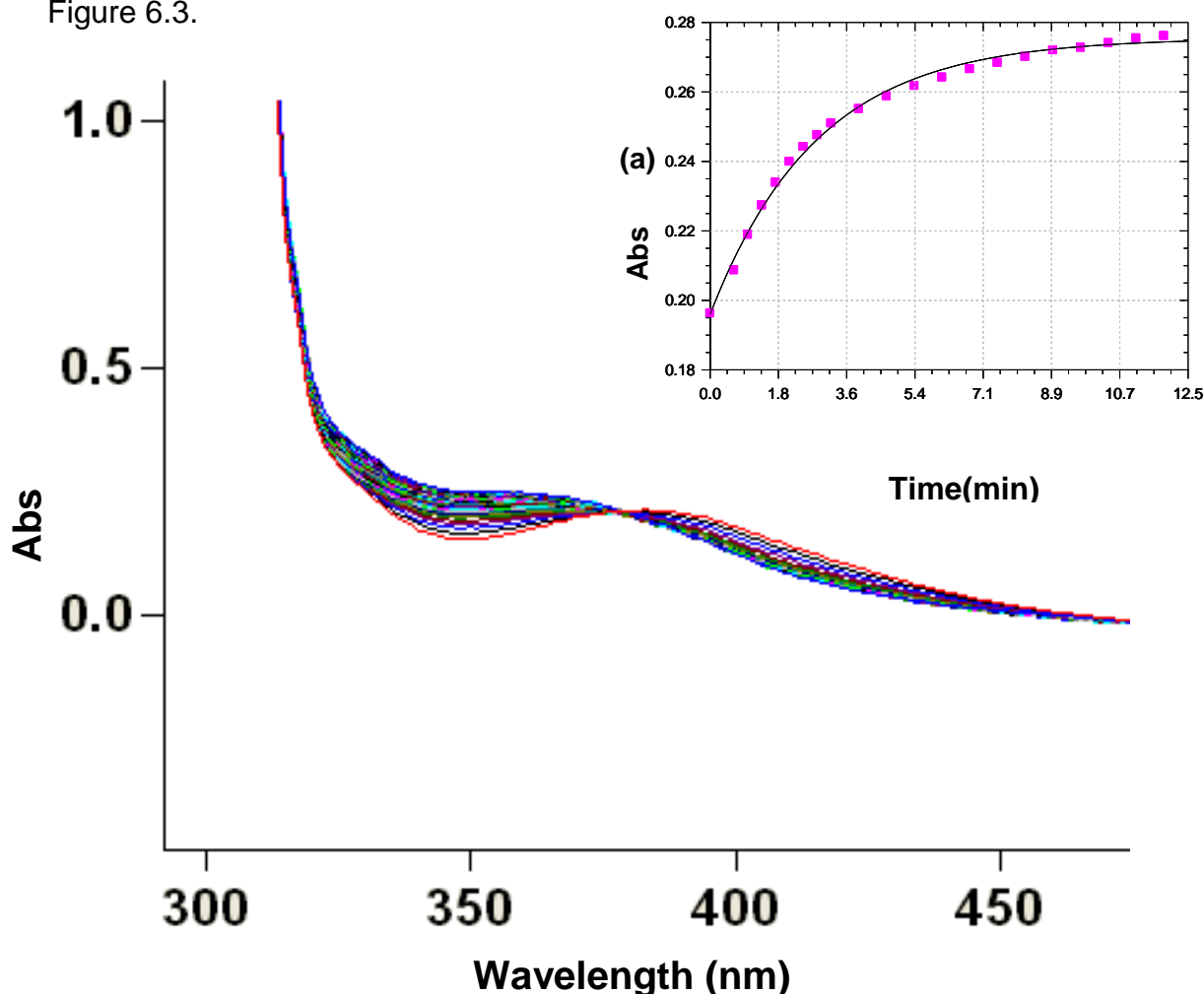
Figure 6.2: A typical UV/vis spectral change for the methanol substitution reaction between *fac*-[Mn(CO)$_3$(Acac)(CH$_3$OH)] (2 x 10^{-3} M) and imidazole (0.125 M) in methanol at 24.5 °C and (a) a fit of absorbance *vs* time data for this reaction at 350 nm.
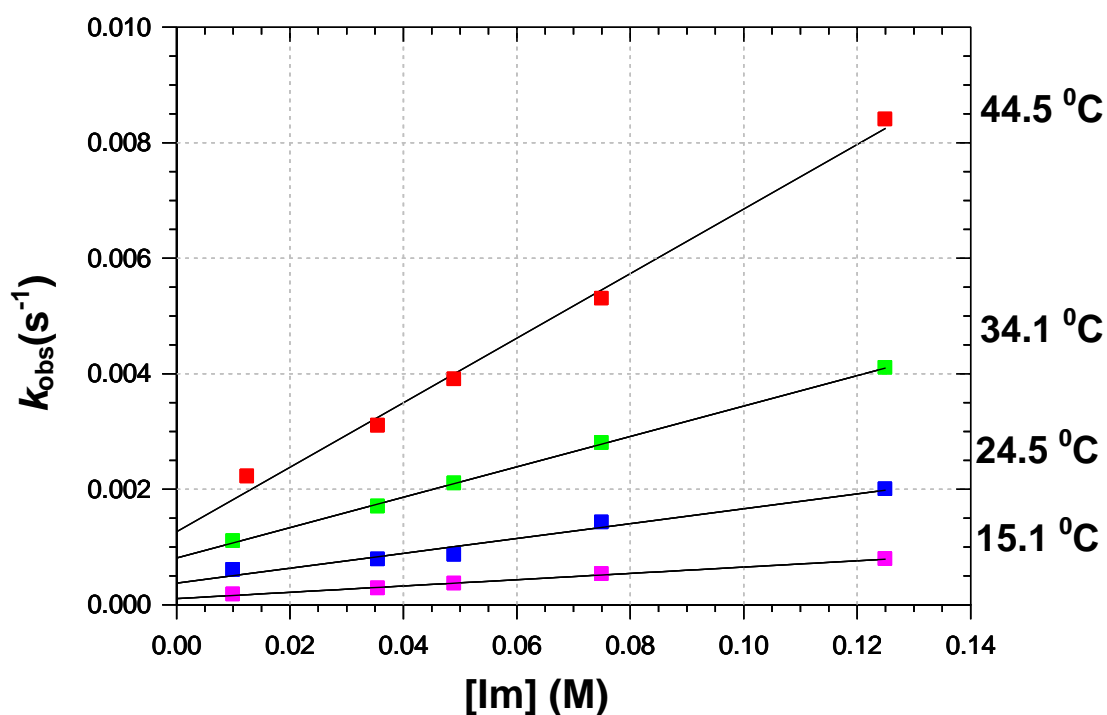
Figure 6.3: A plot of k_{obs} *vs* [Im] for the reaction between *fac*-[Mn(CO)$_3$(Acac)(OHCH$_3$)] and Im at various temperatures; [Mn] = 2 x 10^{-3} M, (λ = 350 nm) and [Im] = 0.01-0.125 M, Δt = 12 s.

Table 6.1: A summary of the rate constant and activation parameters of the reaction between *fac*-[Mn(CO)$_3$(Acac)(CH$_3$OH)] and Im at various temperatures; [Mn] = 2 x 10^{-3} M, (λ = 350 nm) and [Im] = 0.01-0.125 M.

Constants	14.5 ^{0}C	24.5 ^{0}C	34.5 ^{0}C	45.5 ^{0}C
10^3 k_1 (M^{-1}.s^{-1})	5.5(3)	13(1)	26.3(4)	56(3)
10^3 k_{-1} (s^{-1})	0.11(1)	0.38(9)	0.8(2)	1.3(2)
K_1 (M^{-1})^a	51(7)	34(9)	32(1)	44(7)
K_1 (M^{-1})^b		86(30)		
$\Delta H^{\neq}$ (kJ mol^{-1})		58(3)		
$\Delta S^{\neq}$ (J K^{-1} mol)		-88(1)		

^{a} and ^{b} represent the kinetic and thermodynamic activation parameters respectively.
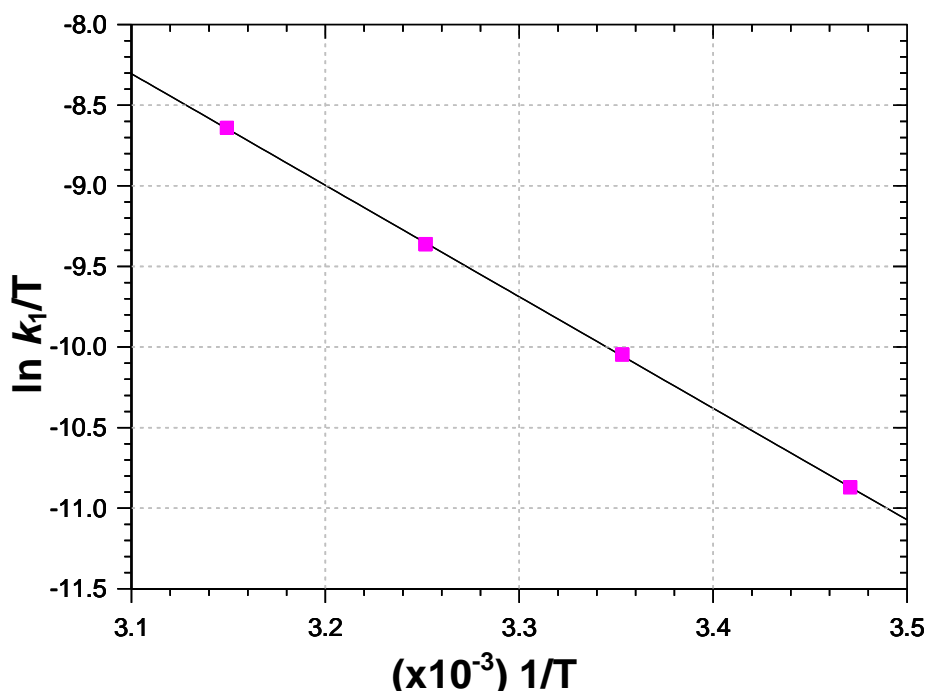
Figure 6.4: Eyring plot for the reaction between *fac*-[Mn(CO)$_3$(Acac)(OHCH$_3$)] and Imidazole at various temperatures; [Mn] = 2 x 10^{-3} M, (λ = 350 nm) and [Im] = 0.01-0.125 M.
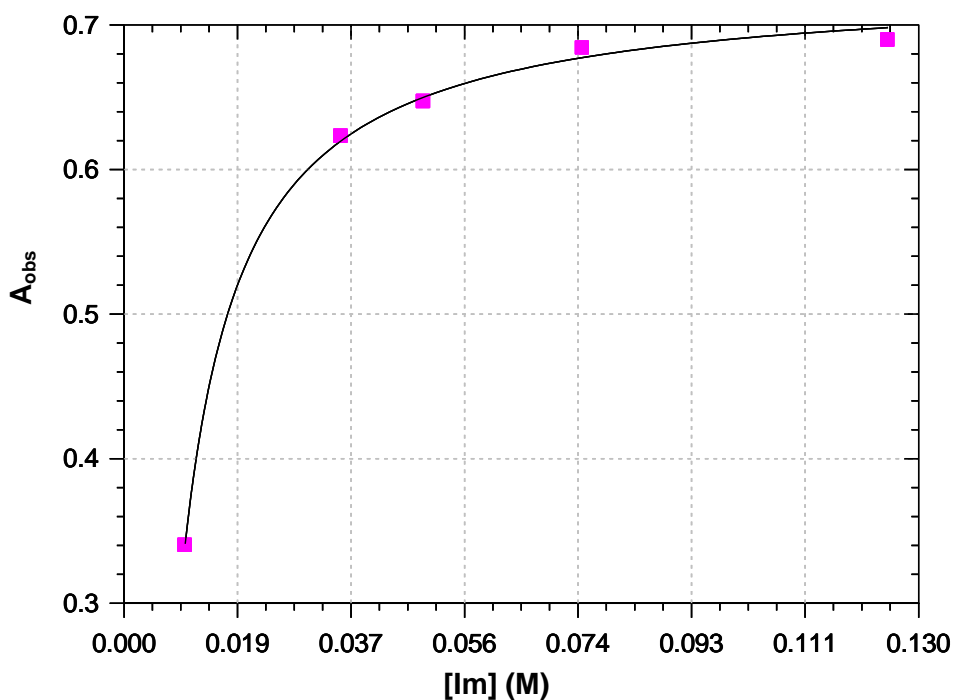
Figure 6.5: Thermodynamic determination of the equilibrium constant, K_1, for the reaction between *fac*-[Mn(CO)$_3$(Acac)(CH$_3$OH)] and Im at 25 ^{0}C ; [Mn] = 2 x 10^{-3} M, (λ = 350 nm) and [Im] = 0.125 M in methanol.

6.4.3 The reaction between *fac*-[Mn(Tfacac)(CO)$_3$(OHCH$_3$)] and Im in methanol

A characteristic UV-Vis spectrum of the methanol substitution reaction between *fac*-[Mn(CO)$_3$(Tfacac)(CH$_3$OH)] and imidazole is illustrated in Figure 6.6.
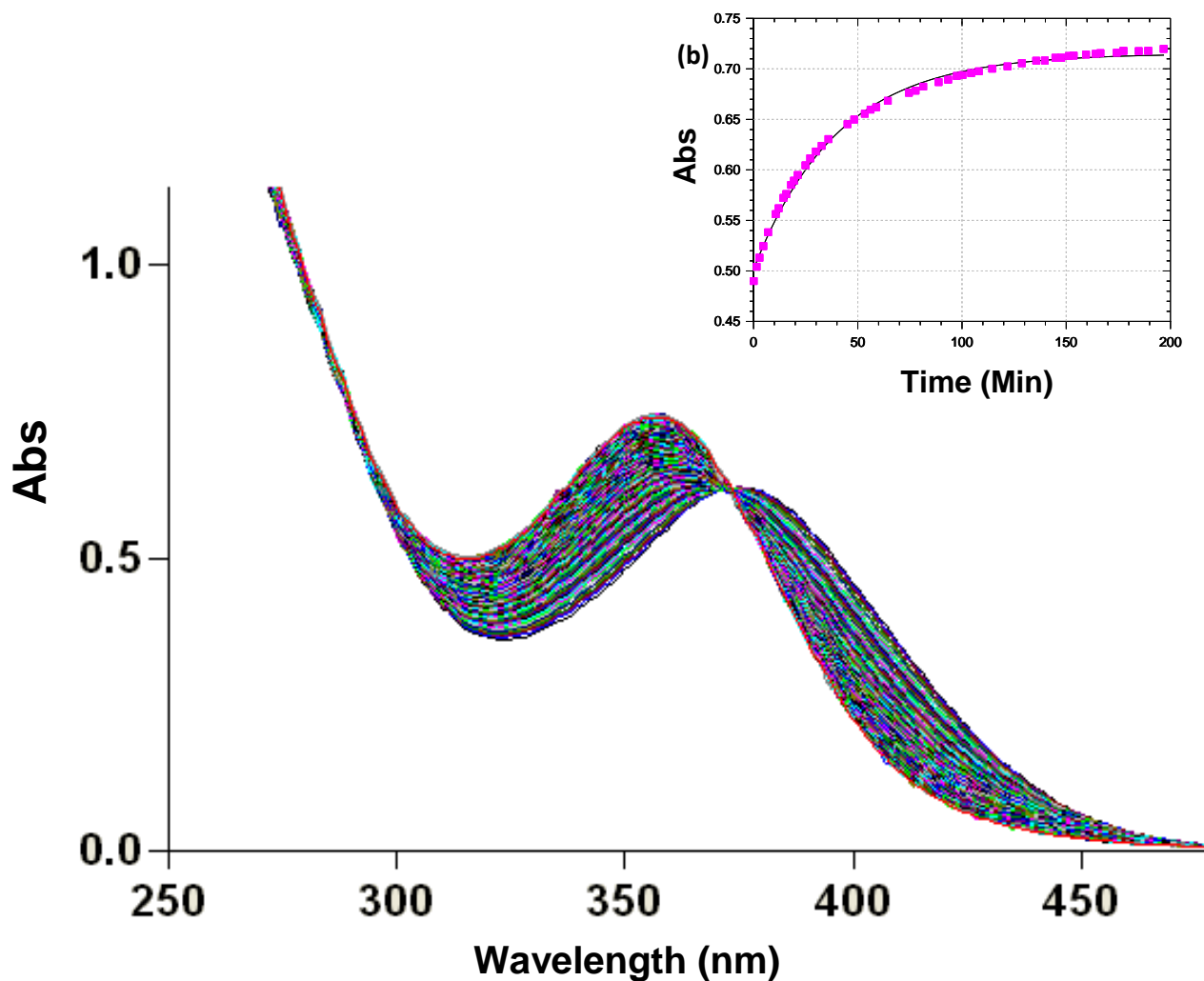
Figure 6.6: A typical UV/vis spectral change for the methanol substitution reaction between *fac*-[Mn(CO)$_3$(TfAcac)(OHCH$_3$)] (2 x 10^{-3} M) and imidazole (0.125 M) in methanol at 24.5 °C and (b) a fit of absorbance *vs* time data for this reaction at 350 nm.
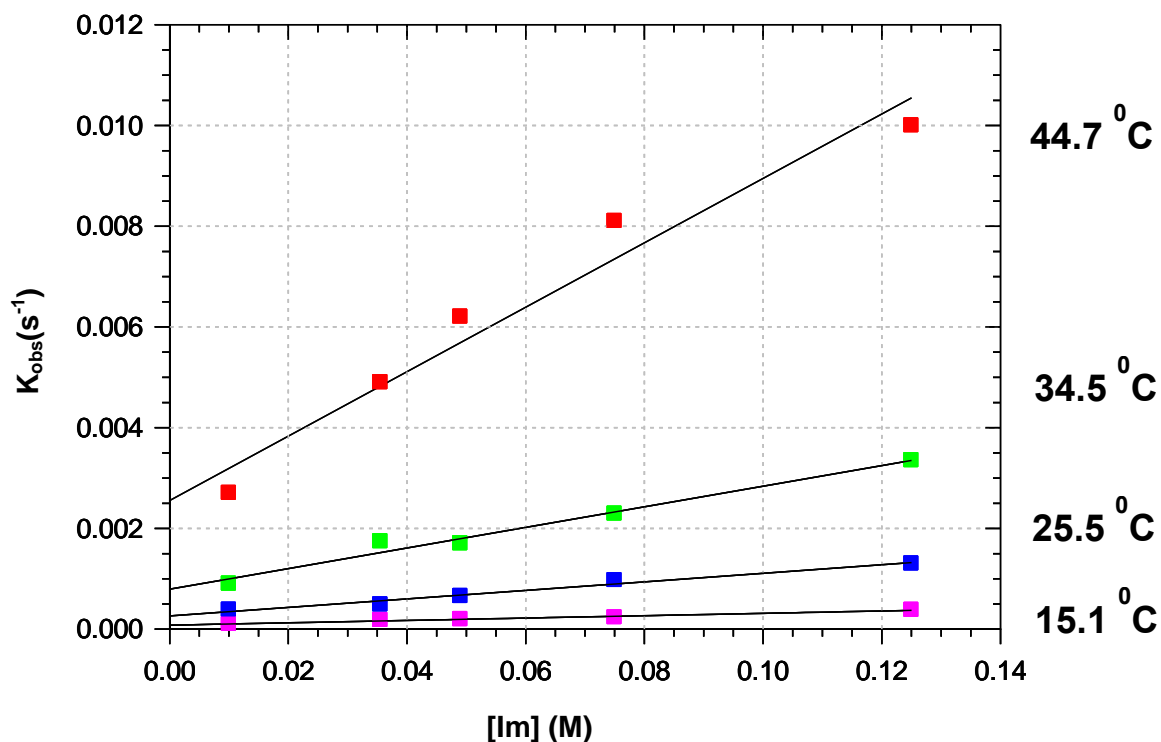
Figure 6.7: A plot of k_{obs} *vs* [Im] for the reaction between *fac*-[Mn(CO)$_3$(Tfacac)(CH$_3$OH)] and Im at various temperatures; [Mn] = 2 x 10^{-3} M, (λ = 350 nm) and [Im] = 0.01-0.125 M, Δt =12 s.

Table 6.2: A summary of the rate constant and activation parameters of the reaction between *fac*-[Mn(CO)$_3$(Tfacac)(CH$_3$OH)] and Im at various temperatures; [Mn] = 2 x 10^{-3} M, λ = 350 nm and [Im] = 0.01-0.125 M.

Constants	14.7 ^{0}C	25.5 ^{0}C	34.5 ^{0}C	44.7 ^{0}C
10^3 k_1 (M^{-1}.s^{-1})	2.56(4)	8.5(8)	20(1)	63(8)
10^3 k_{-1} (s^{-1})	0.09(3)	0.26(5)	0.8(1)	2.67(6)
K_1 (M^{-1})[a]	30(12)	33(7)	26(5)	24(6)
K_1 (M^{-1})[b]		79(2)		
Δ$H^{\neq}$ (kJ mol^{-1})		-18(6)		
Δ$S^{\neq}$ (J K^{-1} mol)				

[a] **and** [b] **represent the kinetic and thermodynamic activation parameters respectively.**
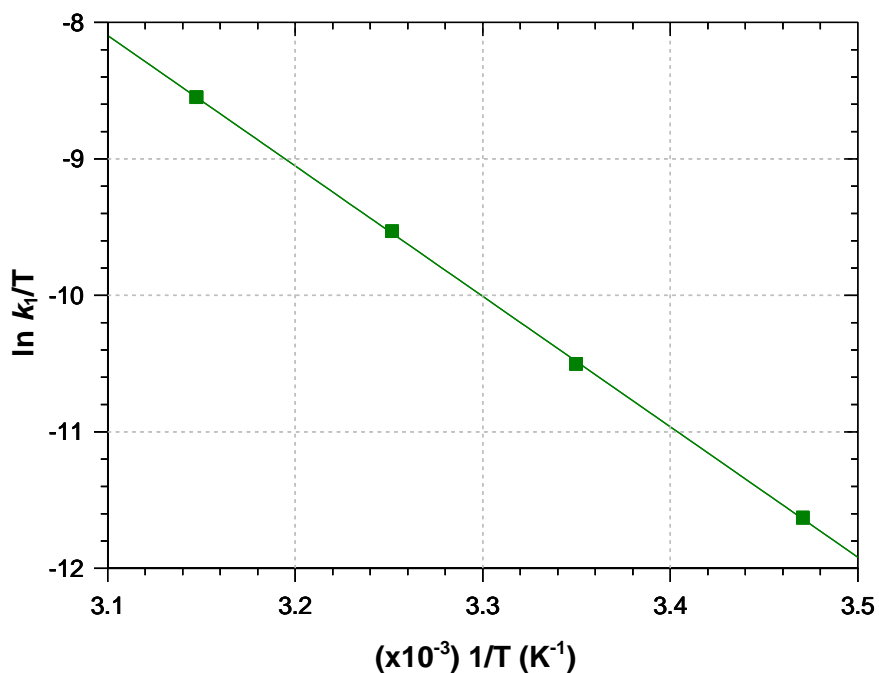
Figure 6.8: Eyring plot for the reaction between *fac*-[Mn(CO)$_3$(Tfacac)(CH$_3$OH)] and Im in methanol.
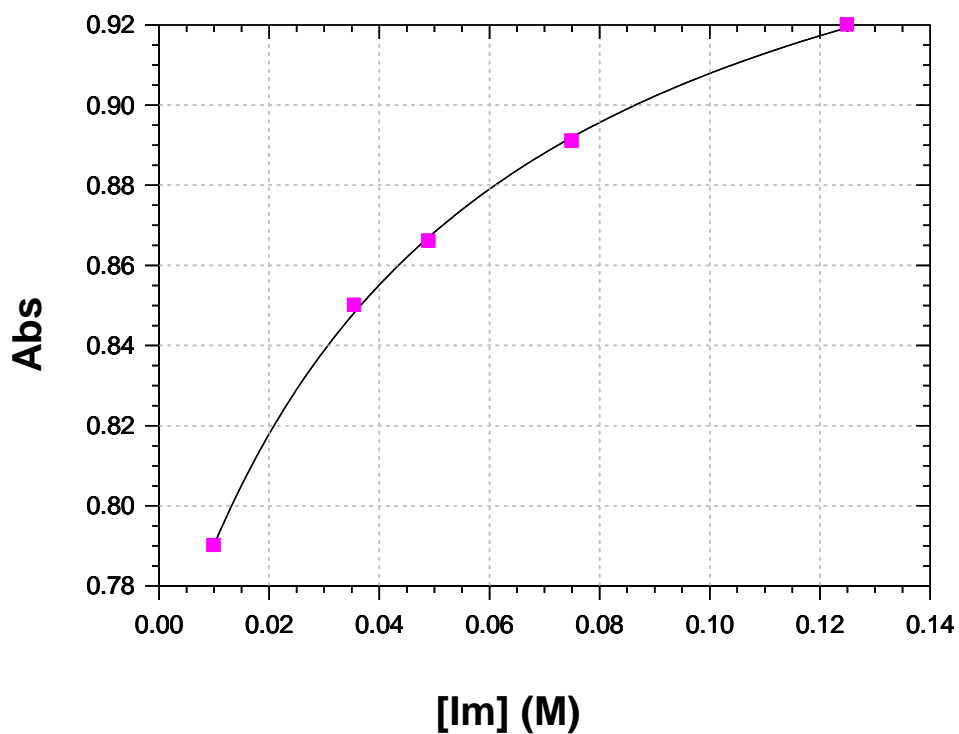
Figure 6.9: An illustration of the thermodynamic determination of the stability constant (*K$_1$*) for the reaction between *fac*-[Mn(CO)$_3$(Tfacac)(CH$_3$OH)] and Im at various temperatures; [Mn] = 2 x 10^{-3} M, (λ = 350 nm).

6.5 Discussion

A primary aim of this study was to investigate the substitution kinetics of the coordinated methanol molecule in complexes of the type fac-[Mn(O,O'-Bid)(CO)$_3$(OHCH$_3$)], by the neutral mono-coordinating ligands. The two neutral manganese(I) tricarbonyl complexes contains a β-diketone backbone with various substituents. The methanol substitution reactions between fac-[Mn(CO)$_3$(Tfacac)(OHCH$_3$)] **(4)** and fac-[Mn(CO)$_3$(Tfacac)(OHCH$_3$)] **(5)** with imidazole were monitored in methanol as solvent. The evaluations were performed under pseudo first order reaction conditions defined by the single equilibrium described in Scheme 6.1. Analysis of the time vs absorbance data for individual kinetic traces indicates, unequivocally, that only one overall reaction is taking place. The rate and stability constants have been calculated as described above and are compared in Table 6.3. The second order rate constant, k_1, of the fluorinated complex **(5)** (8.5(8) x 10^{-3} M^{-1}s^{-1}), is 1.5 times slower than the non-fluorinated equivalent, complex **(4)** (k_1 = 1.3(1) x 10^{-2} M^{-1}s^{-1}). The decrease in methanol substitution rate was anticipated due to the presence of electron withdrawing fluorine atoms on the ligand backbone in **(5)**. These atoms decrease electron density from the metal ion, resulting in the strengthening of the metal-methanol bond henceforth, this effect slows down the rate of methanol substitution. The decrease in the methanol substitution going from the non-fluorinated ligand backbone is consistent with the decrease in pK_a values of 8.95 and 6.40 for acetylacetone and trifluoroacetylacetone respectively.[9]

---

[9] P. Mushak, M. T. Glenn, J. Savory, *Chem. Rev.* 1973, 6, 43.

Table 6.3: A summary of the rate constant and activation parameters of the reaction between fac-[M(CO)$_3$(O,O$^{'}$)(OHCH$_3$)] (M = Mn, Re) with Py and Im at ± 25 ^{0}C.

Compounds	(10^3) k_1 (M^{-1}.s^{-1})	(10^3) k_{-1} (M^{-1}.s^{-1})	K_1 (M^{-1})	IR Data (v_{co})
fac[Mn(CO)$_3$(Acac)(OHCH$_3$)][a]	13(1)	0.38(9)	34(9)	1910,1927,2042
fac-[Mn(CO)$_3$(Tfacac)(OHCH$_3$)][a]	8.5(8)	0.26(5)	33(7)	1935,2006,2030
fac-[Re(CO)$_3$(Acac)(OHCH$_3$)][b]	13.7(1)	0.03(2)	457(305)	2015,1907,1879
fac[Re(CO)$_3$(Tfacac)(OHCH$_3$)][b]	0.35(3)	0.0018(4)	19(5)	2018,1895,1878
fac[Re(CO)$_3$(Hfacac)(OHCH$_3$)][b]	0.17(3)	0.013(4)	13(5)	2025, 1893

*Acac = acetylacetone, Tfacac = trifluoroacetylacetone, Hfacac = hexaflouroacetylacetone

a = complexes in this study; b = rhenium complexes with pyridine.

There is no systematic trend observed in the IR stretching frequencies of these complexes. The overall rate constants, k_1, obtained in this study are in general faster than those obtained for methanol substitution reaction in complex fac-[Mn(CO)$_3$(Bipy)(CH$_3$OH)]$^+$ and fac-[Mn(CO)$_3$(Phen)(OHCH$_3$)]$^+$ (where Phen = 1,10-phenanthrolineand Bipy = 2,2′-bipyridine) with pyridine.[4] One can, right off the bat, attribute the difference in rates to the steric and electronic differences between the ligand systems. Schutte et al. reported an increase in activation of the metal center going from the N,N to N,O-Bid and finnaly O,O$^{'}$-Bid complexes. The study indicated that positively charged metal complexes have a slower methanol substitution rate with neutral substituting ligands. A striking feature is the slower methanol substitution in complex **(4)** when compared to the rhenium complex. Previous studies indicated a decrease in the water exchange reactions (methanol in our case), when proceeding down the periodic table from manganese to rhenium, k_{ex} was determined to be 23 s^{-1} for Mn, 0.49 s^{-1} for Tc and 0.054 s^{-1} for Re. The decrease in exchange rate was credited to the charge increase of the isoelectric complexes when following the Mn-Triad.[10,11] With this in consideration, the trend of the Mn-Acac and Mn-Tfacac with respect to the rhenium analogue is not fully understood at present. Further studies, including other solvents, could possibly cast more light in this regard.

[10] P. V. Grundler, L. Helm, R. Alberto, A. E. Merbach, *Inorg. Chem.* 2006, *45*, 10378.

[11] B. Salignac, P. V. Grundler, S. Cayemittes, U. Frey, R. Scopelliti, A. E. Merbach, R. Hedinger, K. Hegetschweiler, R. Alberto, U. Prinz, G. Raabe, U. Kolle, S. Hall, *Inorg. Chem.* 2003, *42*, 3516.

At a first glance, the negative values obtained for the activation entropy ($\Delta S^{\neq}$) (-88(1) J K^{-1} mol^{-1}) and (-18(6) J K^{-1} mol^{-1}) for complex **(4)** and **(5)** respectively, points out towards an associative type mechanism, the use of high pressure activation volume studies is required to confirm the suggested associative mechanism.

General remarks:

First order rate constants, k_1, for the methanol substitution with neutral ligand imidazole were obtained for complex *fac*-[Mn(CO)$_3$(Acac)(OHCH$_3$)] **(4)** and *fac*[Mn(CO)$_3$(Tfacac)(OHCH$_3$)] **(5)**. The observed rate decreases with the introduction of electron withdrawing fluorine atoms on the ligand backbone.

The negative activation parameters ($\Delta S^{\neq}$) (-88(1) J K^{-1} mol^{-1}) and (-18(6) J K^{-1} mol^{-1}) for complex **(4)** and **(5)** respectively, indicate the likelihood of an associative type mechanism, however other factors such as the decrease in the second order rate constant are suggestive of a more dissociative mechanism. Intricate investigations need to be done in the future in order to verify the intimate mechanism of methanol substitution.

An underlying factor of the results in this study is that, systematic alteration of the O,O'-Bid ligands can influence the overall reactivity of the metal centre. This presents a great opportunity to explore other ligand systems.

7   <u>EVALUATION OF THE STUDY</u>

7.1 Introduction

The primary objective of this study was to evaluate the coordinative and kinetic properties of *fac*-[Mn(L,L'-Bid(CO)$_3$]$_2$ (L,L'-Bid = Salicydene, Sal, bidentate ligand) and one *fac*-[Mn(O,N,N')(CO)$_3$] (N,N,O Sal tridentate ligand) relative to the corresponding rhenium analogues in view of modelling potential therapeutic and diagnostic radiopharmaceuticals. The coordination chemistry of the *fac*-[M(CO)$_3$]$^+$ core (where M = Re, Tc) with a variety of bi- and tridentate ligands has received significant attention, however coordination of these types of ligands to *fac*-[Mn(CO)$_3$]$^+$ is practically unexplored. Schiff base ligands can serve as models for some important biological species and this grants a window of opportunity to explore the possibilities of using these types of ligands as modelling agents.

7.2 Synthesis and Crystallography

Three new *fac*-manganese(I) tricarbonyl complexes containing Schiff base ligands derived from salicylidene were synthesized via a two-step reaction. These complexes appear to be light sensitive as suggested by the formation of black deposits of insoluble material implying decomposition. For this reason, reaction mixtures were covered with aluminium foil to prevent the penetration of light. The coordinative properties of these complexes are to some extend similar to the reported rhenium(I) monomeric analogues, for example, the bite angles of corresponding complexes are comparable. The slight increase in the rhenium complexes bond distances is possibly due to the differences in ionic radii between the two metals. However a primary difference was the formation of dimeric Mn species whereby the O-donor atom of the salicylidene complex acting as a chelate and a bridging ligand. Numerous synthetic attempts were made to break the

dimer into a monomeric species was not successful. An intricate part of this study was to evaluate the kinetic properties of the Schiff base complexes relative to the reported rhenium(I) complexes. The formation of dimeric species derailed the course since the kinetic profiles of dimeric complexes were difficult to interpret due to the possibility of multiple reactions forming. For this reason, two new *fac*-manganese(I) tricarbonyl of the type *fac*-$[Mn(CO)_3(O,O')(OHCH_3)]$, $O,O' = $ acetylacetone and its fluorinated analogue were synthesized and characterised by means of single X-ray diffraction and other spectroscopy techniques (IR, NMR and Uv-Vis) in order to expand the knowledge on the bonding character of the group 7 metals comprising of manganese, technetium and rhenium. Both complexes afford an octahedral geometry around the metal centre with three carbonyls in *facial* orientation. The chelating bidentate ligand and a methanol molecule complete the octahedral geometry. An overarching observation made was the insignificant influence of the functionalised acetylacetone ligand on the bond lengths within the complex.

7.3 Substitution kinetics

First order rate constants, k_1, for the methanol substitution with neutral ligand imidazole were obtained for complex *fac*-$[Mn(CO)_3(Acac)(OHCH_3)]$ and *fac*$[Mn(CO)_3(Tfacac)(OHCH_3)]$. The effect of the attached electron withdrawing fluorine atoms was clearly demonstrated through the overall larger k_1 and K_1 for non-fluorinated complex relative to the fluorinated complex. These values are indicative of the strengthening of the methanol-manganese bond due to the removal of electron density by the fluorine atoms. The negative activation parameters ($\Delta S^{\neq}$) (-88(1) J K^{-1} mol^{-1}) and (-18(6) J K^{-1} mol^{-1}) obtained for both complexes, indicates the likelihood of an associative type mechanism. The results are however not conclusive and for this reason more intricate investigations using activation changes in volume need to be done in the future in order to verify the intimate mechanism of methanol substitution. The rates of methanol substitution were expected to be orders of magnitude greater than the

corresponding rhenium complexes as suggested by the water exchange reaction conducted by Salignac *et al.*[1]

7.4 Future work

Numerous aspects that need further investigations have been identified. These include;

- Investigation of the formation of dimeric complexes contrary to the monomeric species obtained in corresponding rhenium studies
- Expanding the scope of the ligand systems to further investigate the effects of different donor ligands on the reactivity of the metal centre.
- In-depth kinetic evaluation in order to increase the knowledge of the mechanism of the methanol substitution reaction using a series of entering ligands.

---

[1] L. Helm, *Coord. Chem. Rev.,2008*, 252, 2346.

APPENDIX

Supplementary Data of Crystal Structures

---

1 Crystallographic data for *fac*-[Mn(Sal-*m*Tol)(CO)₃]₂

Table 1: Atomic coordinates (x 10^4) and equivalent isotropic displacement parameters ($Å^2$x 10^3) for *fac*-[Mn(Sal-*m*Tol)(CO)₃]₂.

	x	y	z	U(eq)
Mn(1)	538(1)	3669(1)	4171(1)	26(1)
N(1)	-1763(3)	2334(2)	4392(2)	27(1)
O(01)	3873(3)	5457(2)	3799(2)	44(1)
O(1)	922(2)	4746(2)	5994(2)	26(1)
O(02)	-291(3)	2112(3)	1507(2)	51(1)
O(03)	2757(3)	1579(3)	4714(2)	48(1)
C(1)	-1808(4)	1963(3)	5415(2)	31(1)
C(01)	2586(4)	4813(3)	3981(2)	29(1)
C(02)	-4(4)	2739(3)	2535(3)	33(1)
C(03)	1863(4)	2387(3)	4516(2)	33(1)
C(11)	-431(4)	2607(3)	6598(2)	31(1)
C(12)	810(4)	4005(3)	6863(2)	28(1)
C(13)	1901(4)	4634(3)	8093(3)	37(1)
C(14)	1820(5)	3880(4)	9011(3)	44(1)
C(15)	660(5)	2488(4)	8738(3)	47(1)
C(16)	-475(5)	1870(3)	7553(3)	40(1)
C(21)	-3329(4)	1614(3)	3327(2)	30(1)
C(22)	-3724(4)	105(3)	2809(3)	37(1)
C(23)	-5213(4)	-579(4)	1757(3)	42(1)
C(24)	-6251(4)	294(4)	1252(3)	45(1)
C(25)	-5856(4)	1785(4)	1777(3)	43(1)
C(26)	-4393(4)	2465(3)	2823(3)	36(1)
C(231)	-5663(5)	-2231(4)	1206(4)	61(1)

Table 2: Bond lengths [Å] and angles [°] for *fac*-[Mn(Sal-*m*Tol)(CO)₃]₂.

Atoms	Length	Atom	Angle
Mn(1)-C(03)	1.789(3)	C(03)-Mn(1)-C(02)	89.05(13)
Mn(1)-C(02)	1.795(3)	C(03)-Mn(1)-C(01)	87.23(14)
Mn(1)-C(01)	1.815(3)	C(02)-Mn(1)-C(01)	87.63(12)
Mn(1)-O(1)	2.0325(19)	C(03)-Mn(1)-O(1)	95.04(10)
Mn(1)-N(1)	2.064(2)	C(02)-Mn(1)-O(1)	174.92(11)
Mn(1)-O(1)#1	2.066(2)	C(01)-Mn(1)-O(1)	95.57(10)
Mn(1)-Mn(1)#1	3.1865(14)	C(03)-Mn(1)-N(1)	91.60(12)
N(1)-C(1)	1.282(3)	C(02)-Mn(1)-N(1)	92.24(11)
N(1)-C(21)	1.444(3)	C(01)-Mn(1)-N(1)	178.82(11)
O(01)-C(01)	1.143(4)	O(1)-Mn(1)-N(1)	84.64(8)
O(1)-C(12)	1.329(3)	C(03)-Mn(1)-O(1)#1	172.99(9)
O(1)-Mn(1)#1	2.066(2)	C(02)-Mn(1)-O(1)#1	97.94(12)
O(02)-C(02)	1.143(3)	C(01)-Mn(1)-O(1)#1	93.51(11)
O(03)-C(03)	1.153(4)	O(1)-Mn(1)-O(1)#1	77.96(8)
C(1)-C(11)	1.444(4)	N(1)-Mn(1)-O(1)#1	87.67(9)
C(1)-H(1)	0.95	C(03)-Mn(1)-Mn(1)#1	134.40(9)
C(11)-C(16)	1.404(4)	C(02)-Mn(1)-Mn(1)#1	136.46(11)
C(11)-C(12)	1.405(4)	C(01)-Mn(1)-Mn(1)#1	95.83(9)
C(12)-C(13)	1.398(4)	O(1)-Mn(1)-Mn(1)#1	39.36(6)
C(13)-C(14)	1.381(4)	N(1)-Mn(1)-Mn(1)#1	85.07(7)
C(13)-H(13)	0.95	O(1)#1-Mn(1)-Mn(1)#1	38.59(5)
C(14)-C(15)	1.373(5)	C(1)-N(1)-C(21)	116.7(2)
C(14)-H(14)	0.95	C(1)-N(1)-Mn(1)	122.70(18)
C(15)-C(16)	1.368(4)	C(21)-N(1)-Mn(1)	120.11(17)
C(15)-H(15)	0.95	C(12)-O(1)-Mn(1)	121.44(16)
C(16)-H(16)	0.95	C(12)-O(1)-Mn(1)#1	119.88(17)
C(21)-C(22)	1.375(4)	Mn(1)-O(1)-Mn(1)#1	102.04(8)
C(21)-C(26)	1.379(4)	N(1)-C(1)-C(11)	125.3(2)

C(22)-C(23)	1.398(4)	N(1)-C(1)-H(1)	117.3
C(22)-H(22)	0.95	C(11)-C(1)-H(1)	117.3
C(23)-C(24)	1.384(5)	O(01)-C(01)-Mn(1)	175.5(2)
C(23)-C(231)	1.501(4)	O(02)-C(02)-Mn(1)	176.9(3)
C(24)-C(25)	1.360(5)	O(03)-C(03)-Mn(1)	177.6(3)
C(24)-H(24)	0.95	C(16)-C(11)-C(12)	119.3(3)
C(25)-C(26)	1.383(4)	C(16)-C(11)-C(1)	118.0(2)
C(25)-H(25)	0.95	C(12)-C(11)-C(1)	122.3(3)
C(26)-H(26)	0.95	O(1)-C(12)-C(13)	120.1(2)
C(231)-H(23A)	0.98	O(1)-C(12)-C(11)	121.9(2)
C(231)-H(23B)	0.98	C(13)-C(12)-C(11)	118.0(3)
C(231)-H(23C)	0.98	C(14)-C(13)-C(12)	121.1(3)
		C(14)-C(13)-H(13)	119.4
		C(12)-C(13)-H(13)	119.4
		C(15)-C(14)-C(13)	120.7(3)
		C(15)-C(14)-H(14)	119.6
		C(13)-C(14)-H(14)	119.6
		C(16)-C(15)-C(14)	119.3(3)
		C(16)-C(15)-H(15)	120.3
		C(14)-C(15)-H(15)	120.3
		C(15)-C(16)-C(11)	121.4(3)
		C(15)-C(16)-H(16)	119.3
		C(11)-C(16)-H(16)	119.3
		C(22)-C(21)-C(26)	120.7(3)
		C(22)-C(21)-N(1)	120.1(3)
		C(26)-C(21)-N(1)	119.2(2)
		C(21)-C(22)-C(23)	119.8(3)
		C(21)-C(22)-H(22)	120.1
		C(23)-C(22)-H(22)	120.1
		C(24)-C(23)-C(22)	118.8(3)
		C(24)-C(23)-C(231)	121.5(3)
		C(22)-C(23)-C(231)	119.8(3)

		C(25)-C(24)-C(23)	121.0(3)
		C(25)-C(24)-H(24)	119.5
		C(23)-C(24)-H(24)	119.5
		C(24)-C(25)-C(26)	120.5(3)
		C(24)-C(25)-H(25)	119.7
		C(26)-C(25)-H(25)	119.7
		C(21)-C(26)-C(25)	119.3(3)
		C(21)-C(26)-H(26)	120.4
		C(25)-C(26)-H(26)	120.4
		C(23)-C(231)-H(23A)	109.5
		C(23)-C(231)-H(23B)	109.5
		H(23A)-C(231)-H(23B)	109.5
		C(23)-C(231)-H(23C)	109.5
		H(23A)-C(231)-H(23C)	109.5
		H(23B)-C(231)-H(23C)	109.5

Table 3 Anisotropic displacement parameters ($Å^2$ x 10^3) for *fac*-[Mn(Sal-*m*Tol)(CO)$_3$]$_2$.

	U^{11}	U^{22}	U^{33}	U^{23}	U^{13}	U^{12}
Mn(1)	28(1)	25(1)	20(1)	3(1)	7(1)	1(1)
N(1)	29(1)	24(1)	24(1)	3(1)	7(1)	2(1)
O(01)	36(1)	42(1)	57(1)	16(1)	22(1)	2(1)
O(1)	30(1)	24(1)	21(1)	3(1)	6(1)	1(1)
O(02)	53(1)	64(2)	24(1)	-5(1)	11(1)	5(1)
O(03)	59(2)	40(1)	56(1)	18(1)	22(1)	23(1)
C(1)	34(1)	24(1)	30(1)	4(1)	11(1)	-2(1)
C(01)	35(2)	28(1)	24(1)	6(1)	7(1)	8(1)
C(02)	32(1)	34(2)	30(1)	6(1)	9(1)	1(1)
C(03)	38(2)	30(2)	28(1)	6(1)	10(1)	-1(1)
C(11)	37(2)	30(1)	26(1)	8(1)	12(1)	3(1)
C(12)	32(1)	28(1)	23(1)	4(1)	8(1)	7(1)
C(13)	40(2)	36(2)	27(1)	7(1)	3(1)	2(1)
C(14)	52(2)	51(2)	23(1)	7(1)	5(1)	6(2)

C(15)	61(2)	52(2)	33(2)	22(1)	16(2)	9(2)
C(16)	48(2)	37(2)	34(1)	14(1)	15(1)	0(1)
C(21)	29(1)	30(2)	25(1)	3(1)	10(1)	-2(1)
C(22)	38(2)	33(2)	35(1)	4(1)	13(1)	1(1)
C(23)	36(2)	37(2)	41(2)	-4(1)	14(1)	-5(1)
C(24)	33(2)	56(2)	34(2)	5(1)	4(1)	-3(2)
C(25)	34(2)	51(2)	42(2)	16(1)	8(1)	3(1)
C(26)	31(2)	39(2)	36(1)	9(1)	10(1)	3(1)

2. Crystallographic data for *fac*-[Mn(Sal-CyHex)(CO)$_3$]$_2$

Table 4: Atomic coordinates (x 10^4) and equivalent isotropic displacement parameters (Å^2 x 10^3) for *fac*-[Mn(Sal-CyHex)(CO)$_3$]$_2$.

	x	y	z	U(eq)
Mn(2)	8342(1)	336(1)	9847(1)	21(1)
Mn(1)	1657(1)	5336(1)	5153(1)	21(1)
N(11)	7938(2)	-1879(2)	10012(1)	20(1)
N(1)	2061(2)	3120(2)	4988(1)	22(1)
O(05)	8684(2)	3473(2)	9532(1)	44(1)
O(06)	6673(2)	336(2)	8544(1)	40(1)
O(04)	5676(2)	1444(2)	10694(1)	49(1)
O(2)	10289(2)	-276(2)	9322(1)	21(1)
O(02)	1316(2)	8469(2)	5469(1)	44(1)
O(01)	4326(2)	6443(2)	4304(1)	49(1)
O(03)	3326(2)	5337(2)	6456(1)	40(1)
O(1)	-290(2)	4725(2)	5680(1)	21(1)
C(04)	6707(3)	947(3)	10384(2)	28(1)
C(05)	8646(3)	2245(3)	9657(2)	28(1)
C(06)	7327(3)	294(3)	9054(2)	27(1)
C(42)	10364(3)	-1341(3)	8807(1)	22(1)
C(43)	11401(3)	-1249(3)	8199(2)	29(1)
C(44)	11490(3)	-2309(3)	7659(2)	35(1)
C(45)	10552(3)	-3509(3)	7721(2)	35(1)
C(46)	9565(3)	-3637(3)	8330(2)	32(1)
C(41)	9438(3)	-2559(3)	8877(2)	23(1)
C(3)	8418(3)	-2830(3)	9530(2)	27(1)
C(31)	6982(3)	-2423(3)	10662(2)	26(1)
C(32)	5999(3)	-3716(3)	10528(2)	36(1)

C(33)	4963(3)	-4024(4)	11219(2)	41(1)
C(34)	5811(4)	-4316(4)	11878(2)	48(1)
C(35)	6875(4)	-3080(4)	11995(2)	54(1)
C(36)	7884(3)	-2777(3)	11297(2)	39(1)
C(02)	1356(3)	7250(3)	5344(2)	26(1)
C(01)	3295(3)	5946(3)	4618(2)	29(1)
C(03)	2676(3)	5293(3)	5946(2)	27(1)
C(12)	-366(3)	3661(3)	6196(2)	22(1)
C(13)	-1404(3)	3752(3)	6805(2)	30(1)
C(14)	-1492(3)	2692(3)	7340(2)	36(1)
C(15)	-558(3)	1492(3)	7281(2)	37(1)
C(16)	435(3)	1368(3)	6671(2)	31(1)
C(11)	560(3)	2442(3)	6123(2)	24(1)
C(1)	1576(3)	2172(3)	5471(2)	25(1)
C(21)	3023(3)	2576(3)	4334(2)	28(1)
C(22)	4002(3)	1281(3)	4471(2)	35(1)
C(23)	5035(3)	972(3)	3781(2)	40(1)
C(24)	4185(4)	686(4)	3121(2)	47(1)
C(25)	3126(4)	1914(4)	3001(2)	53(1)
C(26)	2120(3)	2226(3)	3701(2)	38(1)

Table 5: Bond lengths [Å] and angles [°] for *fac*-[Mn(Sal-CyHex)(CO)$_3$]$_2$

Atoms	Length	Atoms	Angle
Mn(2)-C(06)	1.795(3)	C(06)-Mn(2)-C(04)	88.81(13)
Mn(2)-C(04)	1.800(3)	C(06)-Mn(2)-C(05)	87.17(13)
Mn(2)-C(05)	1.806(3)	C(04)-Mn(2)-C(05)	84.73(13)
Mn(2)-O(2)	2.0216(18)	C(06)-Mn(2)-O(2)	96.40(10)
Mn(2)-O(2)#1	2.0602(18)	C(04)-Mn(2)-O(2)	174.49(11)
Mn(2)-N(11)	2.086(2)	C(05)-Mn(2)-O(2)	93.70(10)
Mn(2)-Mn(2)#1	3.1984(10)	C(06)-Mn(2)-O(2)#1	173.17(10)
Mn(1)-C(03)	1.796(3)	C(04)-Mn(2)-O(2)#1	97.99(11)
Mn(1)-C(01)	1.802(3)	C(05)-Mn(2)-O(2)#1	94.09(11)
Mn(1)-C(02)	1.809(3)	O(2)-Mn(2)-O(2)#1	76.82(8)
Mn(1)-O(1)	2.0248(19)	C(06)-Mn(2)-N(11)	89.69(11)
Mn(1)-O(1)#2	2.0619(18)	C(04)-Mn(2)-N(11)	95.57(11)

Mn(1)-N(1)	2.086(2)	C(05)-Mn(2)-N(11)	176.84(11)
Mn(1)-Mn(1)#2	3.2007(10)	O(2)-Mn(2)-N(11)	86.29(8)
N(11)-C(3)	1.287(3)	O(2)#1-Mn(2)-N(11)	88.99(8)
N(11)-C(31)	1.493(3)	C(06)-Mn(2)-Mn(2)#1	135.24(9)
N(1)-C(1)	1.287(3)	C(04)-Mn(2)-Mn(2)#1	135.95(10)
N(1)-C(21)	1.501(3)	C(05)-Mn(2)-Mn(2)#1	94.98(9)
O(05)-C(05)	1.150(3)	O(2)-Mn(2)-Mn(2)#1	38.84(5)
O(06)-C(06)	1.154(3)	O(2)#1-Mn(2)-Mn(2)#1	37.98(5)
O(04)-C(04)	1.148(3)	N(11)-Mn(2)-Mn(2)#1	87.00(6)
O(2)-C(42)	1.355(3)	C(03)-Mn(1)-C(01)	88.51(13)
O(2)-Mn(2)#1	2.0601(18)	C(03)-Mn(1)-C(02)	86.80(12)
O(02)-C(02)	1.144(3)	C(01)-Mn(1)-C(02)	84.50(12)
O(01)-C(01)	1.152(3)	C(03)-Mn(1)-O(1)	96.49(10)
O(03)-C(03)	1.153(3)	C(01)-Mn(1)-O(1)	174.67(10)
O(1)-C(12)	1.355(3)	C(02)-Mn(1)-O(1)	93.92(10)
O(1)-Mn(1)#2	2.0619(18)	C(03)-Mn(1)-O(1)#2	173.32(10)
C(42)-C(43)	1.394(4)	C(01)-Mn(1)-O(1)#2	98.13(11)
C(42)-C(41)	1.405(4)	C(02)-Mn(1)-O(1)#2	94.57(10)
C(43)-C(44)	1.384(4)	O(1)-Mn(1)-O(1)#2	76.89(8)
C(44)-C(45)	1.397(4)	C(03)-Mn(1)-N(1)	89.96(10)
C(45)-C(46)	1.370(4)	C(01)-Mn(1)-N(1)	95.72(11)
C(46)-C(41)	1.404(4)	C(02)-Mn(1)-N(1)	176.74(11)
C(41)-C(3)	1.466(4)	O(1)-Mn(1)-N(1)	86.15(8)
C(31)-C(36)	1.521(4)	O(1)#2-Mn(1)-N(1)	88.62(8)
C(31)-C(32)	1.528(4)	C(03)-Mn(1)-Mn(1)#2	135.35(9)
C(32)-C(33)	1.532(4)	C(01)-Mn(1)-Mn(1)#2	136.14(10)
C(33)-C(34)	1.516(4)	C(02)-Mn(1)-Mn(1)#2	95.42(9)
C(34)-C(35)	1.528(4)	O(1)-Mn(1)-Mn(1)#2	38.86(5)
C(35)-C(36)	1.529(4)	O(1)#2-Mn(1)-Mn(1)#2	38.03(5)
C(12)-C(13)	1.395(4)	N(1)-Mn(1)-Mn(1)#2	86.67(7)
C(12)-C(11)	1.402(4)	C(3)-N(11)-C(31)	116.9(2)
C(13)-C(14)	1.375(4)	C(3)-N(11)-Mn(2)	121.28(19)
C(14)-C(15)	1.392(4)	C(31)-N(11)-Mn(2)	121.63(16)
C(15)-C(16)	1.373(4)	C(1)-N(1)-C(21)	117.3(2)
C(16)-C(11)	1.403(4)	C(1)-N(1)-Mn(1)	121.10(18)
C(11)-C(1)	1.462(4)	C(21)-N(1)-Mn(1)	121.46(17)
C(21)-C(26)	1.520(4)	C(42)-O(2)-Mn(2)	120.90(15)
C(21)-C(22)	1.523(4)	C(42)-O(2)-Mn(2)#1	119.99(14)
C(22)-C(23)	1.530(4)	Mn(2)-O(2)-Mn(2)#1	103.18(8)

C(23)-C(24)	1.520(4)	C(12)-O(1)-Mn(1)	121.09(14)
C(24)-C(25)	1.515(4)	C(12)-O(1)-Mn(1)#2	119.84(15)
C(25)-C(26)	1.530(4)	Mn(1)-O(1)-Mn(1)#2	103.11(8)
		O(04)-C(04)-Mn(2)	174.2(3)
		O(05)-C(05)-Mn(2)	172.9(2)
		O(06)-C(06)-Mn(2)	176.8(2)
		O(2)-C(42)-C(43)	119.7(2)
		O(2)-C(42)-C(41)	121.6(2)
		C(43)-C(42)-C(41)	118.7(2)
		C(44)-C(43)-C(42)	120.9(3)
		C(43)-C(44)-C(45)	120.4(3)
		C(46)-C(45)-C(44)	119.2(3)
		C(45)-C(46)-C(41)	121.3(3)
		C(46)-C(41)-C(42)	119.4(3)
		C(46)-C(41)-C(3)	117.5(3)
		C(42)-C(41)-C(3)	122.8(2)
		N(11)-C(3)-C(41)	126.2(2)
		N(11)-C(31)-C(36)	110.9(2)
		N(11)-C(31)-C(32)	116.3(2)
		C(36)-C(31)-C(32)	109.2(2)
		C(31)-C(32)-C(33)	109.9(2)
		C(34)-C(33)-C(32)	111.3(3)
		C(33)-C(34)-C(35)	111.3(3)
		C(34)-C(35)-C(36)	111.2(3)
		C(31)-C(36)-C(35)	110.2(3)
		O(02)-C(02)-Mn(1)	173.0(2)
		O(01)-C(01)-Mn(1)	174.4(3)
		O(03)-C(03)-Mn(1)	176.8(2)
		O(1)-C(12)-C(13)	119.9(2)
		O(1)-C(12)-C(11)	121.2(2)
		C(13)-C(12)-C(11)	118.9(2)
		C(14)-C(13)-C(12)	120.9(2)
		C(13)-C(14)-C(15)	120.7(3)
		C(16)-C(15)-C(14)	118.8(3)
		C(15)-C(16)-C(11)	121.6(3)
		C(12)-C(11)-C(16)	119.0(3)
		C(12)-C(11)-C(1)	123.1(2)
		C(16)-C(11)-C(1)	117.8(2)
		N(1)-C(1)-C(11)	126.5(2)

	N(1)-C(21)-C(26)	110.9(2)
	N(1)-C(21)-C(22)	116.0(2)
	C(26)-C(21)-C(22)	109.3(2)
	C(21)-C(22)-C(23)	109.6(2)
	C(24)-C(23)-C(22)	111.3(2)
	C(25)-C(24)-C(23)	111.5(3)
	C(24)-C(25)-C(26)	111.2(3)
	C(21)-C(26)-C(25)	110.3(3)

Table 6: Anisotropic displacement parameters (Å^{2}x 10^3) for *fac*-[Mn(Sal-CyHex)(CO)$_3$]$_2$

	U^{11}	U^{22}	U^{33}	U^{23}	U^{13}	U^{12}
Mn(2)	17(1)	19(1)	27(1)	0(1)	1(1)	0(1)
Mn(1)	17(1)	19(1)	27(1)	-1(1)	2(1)	-1(1)
N(11)	17(1)	20(1)	23(1)	1(1)	2(1)	-2(1)
N(1)	18(1)	23(1)	25(1)	-4(1)	2(1)	0(1)
O(05)	43(1)	22(1)	66(2)	7(1)	-2(1)	-1(1)
O(06)	33(1)	50(1)	37(1)	4(1)	-10(1)	-4(1)
O(04)	30(1)	47(1)	66(2)	4(1)	18(1)	10(1)
O(2)	17(1)	19(1)	26(1)	-3(1)	3(1)	0(1)
O(02)	44(1)	23(1)	64(2)	-9(1)	-1(1)	-2(1)
O(01)	30(1)	50(1)	65(2)	-2(1)	18(1)	-12(1)
O(03)	35(1)	50(1)	34(1)	-6(1)	-8(1)	2(1)
O(1)	19(1)	19(1)	25(1)	2(1)	2(1)	-1(1)
C(04)	24(1)	24(2)	36(2)	4(1)	0(1)	-1(1)
C(05)	21(1)	28(2)	34(2)	-6(1)	3(1)	0(1)
C(06)	21(1)	22(1)	37(2)	1(1)	6(1)	-2(1)
C(42)	20(1)	23(1)	22(1)	-1(1)	-2(1)	6(1)
C(43)	28(2)	28(2)	29(2)	0(1)	3(1)	-5(1)
C(44)	37(2)	38(2)	28(2)	-5(1)	10(1)	0(1)
C(45)	41(2)	32(2)	31(2)	-9(1)	3(1)	0(1)
C(46)	36(2)	27(2)	32(2)	-7(1)	1(1)	-3(1)
C(41)	24(1)	23(1)	23(2)	-3(1)	2(1)	1(1)
C(3)	25(1)	19(1)	35(2)	-1(1)	1(1)	-5(1)
C(31)	25(1)	23(1)	29(2)	1(1)	6(1)	0(1)
C(32)	28(2)	44(2)	34(2)	5(1)	-2(1)	-11(1)
C(33)	31(2)	45(2)	45(2)	10(2)	6(2)	-9(1)
C(34)	48(2)	54(2)	41(2)	16(2)	4(2)	-13(2)

C(35)	61(2)	69(3)	31(2)	11(2)	-2(2)	-29(2)
C(36)	39(2)	44(2)	35(2)	7(2)	-5(1)	-16(1)
C(02)	20(1)	29(2)	29(2)	-1(1)	1(1)	-3(1)
C(01)	26(2)	26(2)	34(2)	-3(1)	1(1)	3(1)
C(03)	19(1)	21(1)	38(2)	-2(1)	8(1)	-1(1)
C(12)	20(1)	22(1)	24(2)	1(1)	0(1)	-6(1)
C(13)	26(2)	28(2)	32(2)	-1(1)	5(1)	2(1)
C(14)	36(2)	41(2)	28(2)	2(1)	11(1)	-2(1)
C(15)	38(2)	37(2)	33(2)	12(1)	4(1)	-3(1)
C(16)	30(2)	25(2)	38(2)	6(1)	1(1)	1(1)
C(11)	22(1)	24(1)	25(2)	0(1)	2(1)	-2(1)
C(1)	26(2)	18(1)	31(2)	-1(1)	0(1)	0(1)
C(21)	24(1)	29(2)	28(2)	-6(1)	6(1)	-3(1)
C(22)	24(2)	43(2)	37(2)	-5(1)	0(1)	9(1)
C(23)	27(2)	47(2)	44(2)	-12(2)	3(1)	8(1)
C(24)	47(2)	52(2)	40(2)	-15(2)	4(2)	12(2)
C(25)	61(2)	66(2)	33(2)	-15(2)	-2(2)	22(2)
C(26)	39(2)	44(2)	32(2)	-6(1)	-6(1)	14(1)

3. Crystallographic data for *fac*-[Mn-(4-Me-Sal-Hist)(CO)$_3$]

Table 7: Atomic coordinates (x 10^4) and equivalent isotropic displacement parameters (Å^2 x 10^3) for *fac*-[Mn-(4-Me-Sal-Hist)(CO)$_3$]

	x	y	z	U(eq)
Mn(1)	3304(1)	2892(1)	2067(1)	20(1)
O(01)	1128(2)	3236(2)	-34(1)	55(1)
O(03)	2957(2)	6240(1)	3147(1)	37(1)
O(02)	-346(2)	1961(2)	2373(1)	35(1)
O(1)	5792(1)	3575(1)	1820(1)	24(1)
N(1)	4959(2)	2777(1)	3515(1)	21(1)
N(32)	3659(2)	556(1)	1373(1)	23(1)
N(34)	3550(2)	-1757(2)	90(1)	29(1)
C(01)	1989(2)	3054(2)	755(1)	31(1)
C(02)	1103(2)	2298(2)	2274(1)	24(1)
C(03)	3105(2)	4945(2)	2734(1)	25(1)
C(12)	6933(2)	4792(2)	2623(1)	21(1)
C(13)	7893(2)	5940(2)	2353(1)	26(1)
C(14)	9038(2)	7269(2)	3174(1)	28(1)

C(141)	9950(3)	8520(2)	2846(2)	39(1)
C(15)	9313(2)	7438(2)	4301(1)	31(1)
C(16)	8473(2)	6295(2)	4590(1)	28(1)
C(11)	7243(2)	4978(2)	3773(1)	23(1)
C(1)	6464(2)	3761(2)	4105(1)	24(1)
C(2)	4559(2)	1420(2)	3853(1)	26(1)
C(3)	5257(2)	-3(2)	3144(1)	31(1)
C(31)	4431(2)	-459(2)	1904(1)	26(1)
C(35)	4372(2)	-1887(2)	1108(1)	32(1)
C(33)	3148(2)	-289(2)	281(1)	26(1)

Table 8. Bond lengths [Å] for *fac*-[Mn-(4-Me-Sal-Hist)(CO)₃].

Mn(1)-C(02)	1.7990(16)	C(02)-Mn(1)-C(03)	89.84(7)
Mn(1)-C(03)	1.8091(16)	C(02)-Mn(1)-C(01)	87.95(7)
Mn(1)-C(01)	1.8120(16)	C(03)-Mn(1)-C(01)	87.61(7)
Mn(1)-N(1)	2.0287(12)	C(02)-Mn(1)-N(1)	96.48(6)
Mn(1)-O(1)	2.0440(10)	C(03)-Mn(1)-N(1)	92.03(6)
Mn(1)-N(32)	2.0707(12)	C(01)-Mn(1)-N(1)	175.55(6)
O(01)-C(01)	1.140(2)	C(02)-Mn(1)-O(1)	179.41(6)
O(03)-C(03)	1.1432(19)	C(03)-Mn(1)-O(1)	89.95(5)
O(02)-C(02)	1.1496(19)	C(01)-Mn(1)-O(1)	91.49(6)
O(1)-C(12)	1.3231(17)	N(1)-Mn(1)-O(1)	84.08(5)
N(1)-C(1)	1.2890(18)	C(02)-Mn(1)-N(32)	91.51(6)
N(1)-C(2)	1.4623(19)	C(03)-Mn(1)-N(32)	176.95(6)
N(32)-C(33)	1.3321(18)	C(01)-Mn(1)-N(32)	95.17(6)
N(32)-C(31)	1.384(2)	N(1)-Mn(1)-N(32)	85.10(5)
N(34)-C(33)	1.331(2)	O(1)-Mn(1)-N(32)	88.73(4)
N(34)-C(35)	1.368(2)	C(12)-O(1)-Mn(1)	117.60(8)
N(34)-H(3)	0.79(2)	C(1)-N(1)-C(2)	117.41(12)
C(12)-C(13)	1.403(2)	C(1)-N(1)-Mn(1)	123.28(10)
C(12)-C(11)	1.4172(19)	C(2)-N(1)-Mn(1)	118.97(9)
C(13)-C(14)	1.389(2)	C(33)-N(32)-C(31)	105.52(13)
C(13)-H(13)	0.93	C(33)-N(32)-Mn(1)	125.37(11)
C(14)-C(15)	1.395(2)	C(31)-N(32)-Mn(1)	129.11(9)
C(14)-C(141)	1.506(2)	C(33)-N(34)-C(35)	107.37(13)
C(141)-H(14A)	0.96	C(33)-N(34)-H(3)	125.3(17)
C(141)-H(14B)	0.96	C(35)-N(34)-H(3)	126.0(17)

C(141)-H(14C)	0.96	O(01)-C(01)-Mn(1)	175.90(16)
C(15)-C(16)	1.371(2)	O(02)-C(02)-Mn(1)	176.55(14)
C(15)-H(15)	0.93	O(03)-C(03)-Mn(1)	179.17(15)
C(16)-C(11)	1.4060(19)	O(1)-C(12)-C(13)	120.31(13)
C(16)-H(16)	0.93	O(1)-C(12)-C(11)	121.83(13)
C(11)-C(1)	1.441(2)	C(13)-C(12)-C(11)	117.86(13)
C(1)-H(1)	0.992(17)	C(14)-C(13)-C(12)	121.95(14)
C(2)-C(3)	1.525(2)	C(14)-C(13)-H(13)	119
C(2)-H(2A)	0.97	C(12)-C(13)-H(13)	119
C(2)-H(2B)	0.97	C(13)-C(14)-C(15)	119.26(14)
C(3)-C(31)	1.496(2)	C(13)-C(14)-C(141)	120.18(15)
C(3)-H(3A)	0.97	C(15)-C(14)-C(141)	120.56(14)
C(3)-H(3B)	0.97	C(14)-C(141)-H(14A)	109.5
C(31)-C(35)	1.364(2)	C(14)-C(141)-H(14B)	109.5
C(35)-H(2)	0.96(2)	H(14A)-C(141)-H(14B)	109.5
C(33)-H(4)	0.932(18)	C(14)-C(141)-H(14C)	109.5
		H(14A)-C(141)-H(14C)	109.5
		H(14B)-C(141)-H(14C)	109.5
		C(16)-C(15)-C(14)	120.11(14)
		C(16)-C(15)-H(15)	119.9
		C(14)-C(15)-H(15)	119.9
		C(15)-C(16)-C(11)	121.34(14)
		C(15)-C(16)-H(16)	119.3
		C(11)-C(16)-H(16)	119.3
		C(16)-C(11)-C(12)	119.32(14)
		C(16)-C(11)-C(1)	119.65(13)
		C(12)-C(11)-C(1)	120.74(12)
		N(1)-C(1)-C(11)	124.21(13)
		N(1)-C(1)-H(1)	119.3(10)
		C(11)-C(1)-H(1)	116.3(10)
		N(1)-C(2)-C(3)	108.68(12)
		N(1)-C(2)-H(2A)	110
		C(3)-C(2)-H(2A)	110
		N(1)-C(2)-H(2B)	1
		C(3)-C(2)-H(2B)	110
		H(2A)-C(2)-H(2B)	108.3
		C(31)-C(3)-C(2)	114.98(13)
		C(31)-C(3)-H(3A)	108.5
		C(2)-C(3)-H(3A)	108.5

		C(31)-C(3)-H(3B)	108.5
		C(2)-C(3)-H(3B)	108.5
		H(3A)-C(3)-H(3B)	107.5
		C(35)-C(31)-N(32)	108.54(14)
		C(35)-C(31)-C(3)	126.93(15)
		N(32)-C(31)-C(3)	124.48(13)
		C(31)-C(35)-N(34)	106.94(15)
		C(31)-C(35)-H(2)	132.3(13)
		N(34)-C(35)-H(2)	120.7(13)
		N(34)-C(33)-N(32)	111.63(14)
		N(34)-C(33)-H(4)	123.9(11)
		N(32)-C(33)-H(4)	124.5(11)

Table 9. Anisotropic displacement parameters for for *fac*-[Mn-(4-Me-Sal-Hist)(CO)₃]

	U_{11}	U_{22}	U_{33}	U_{23}	U_{13}	U_{12}
Mn(1)	22(1)	21(1)	15(1)	3(1)	4(1)	2(1)
O(01)	60(1)	75(1)	31(1)	27(1)	0(1)	12(1)
O(03)	41(1)	27(1)	42(1)	6(1)	14(1)	11(1)
O(02)	25(1)	40(1)	39(1)	13(1)	10(1)	1(1)
O(1)	26(1)	24(1)	16(1)	0(1)	7(1)	-2(1)
N(1)	25(1)	21(1)	17(1)	4(1)	7(1)	4(1)
N(32)	25(1)	22(1)	18(1)	3(1)	7(1)	0(1)
N(34)	34(1)	25(1)	24(1)	-3(1)	13(1)	-2(1)
C(01)	33(1)	34(1)	23(1)	7(1)	7(1)	2(1)
C(02)	29(1)	22(1)	19(1)	5(1)	3(1)	4(1)
C(03)	23(1)	29(1)	22(1)	9(1)	7(1)	4(1)
C(12)	21(1)	21(1)	21(1)	3(1)	6(1)	4(1)
C(13)	26(1)	26(1)	25(1)	7(1)	9(1)	2(1)
C(14)	24(1)	22(1)	36(1)	6(1)	11(1)	4(1)
C(141)	40(1)	28(1)	48(1)	10(1)	14(1)	-4(1)
C(15)	25(1)	23(1)	31(1)	-2(1)	3(1)	-2(1)
C(16)	28(1)	28(1)	20(1)	0(1)	2(1)	2(1)
C(11)	22(1)	23(1)	19(1)	2(1)	4(1)	2(1)
C(1)	26(1)	26(1)	16(1)	4(1)	5(1)	4(1)
C(2)	32(1)	27(1)	18(1)	7(1)	7(1)	2(1)
C(3)	41(1)	26(1)	25(1)	8(1)	6(1)	7(1)
C(31)	28(1)	24(1)	25(1)	5(1)	10(1)	3(1)

C(35)	37(1)	24(1)	32(1)	5(1)	13(1)	5(1)
C(33)	28(1)	25(1)	20(1)	2(1)	8(1)	-3(1)

4 Crystallographic data for *fac*-[Mn(Acac)(CO)₃(OHCH₃)]

Table 10: Atomic coordinates (x 10^4) and equivalent isotropic displacement parameters (Å^{2}x 10^3) for *fac*-[Mn(Acac)(CO)₃(OHCH₃)]

Mn(1)	1714(2)	831(2)	2817(1)	29(1)
O(2)	-6(9)	2306(8)	1450(7)	38(2)
O(1)	72(8)	2217(7)	4353(6)	30(1)
O(02)	4408(10)	-1474(9)	4687(8)	52(2)
O(03)	4340(10)	2746(8)	2230(7)	48(2)
O(04)	-322(8)	-365(8)	3266(6)	38(2)
C(3)	-1960(14)	4352(13)	2945(10)	42(2)
C(01)	3131(12)	-492(11)	1490(10)	33(2)
C(4)	-1342(13)	3658(11)	1648(10)	35(2)
C(02)	3281(13)	-559(12)	3994(10)	36(2)
O(01)	4102(11)	-1385(10)	717(9)	65(2)
C(2)	-1304(13)	3611(11)	4187(9)	34(2)
C(1)	-2194(14)	4402(13)	5545(11)	44(2)
C(5)	-2344(16)	4554(15)	379(12)	54(3)
C(03)	3314(12)	2023(11)	2465(9)	29(2)
C(04)	-1270(17)	-787(14)	2233(12)	56(3

Table 11. Bond lengths [Å] and angles [°] for *fac*-[Mn(Acac)(CO)$_3$(OHCH$_3$)]

Mn(1)-C(02)	1.793(10)	C(02)-Mn(1)-C(03)	88.4(4)
Mn(1)-C(03)	1.801(8)	C(02)-Mn(1)-C(01)	86.3(4)
Mn(1)-C(01)	1.802(9)	C(03)-Mn(1)-C(01)	89.8(4)
Mn(1)-O(2)	2.003(7)	C(02)-Mn(1)-O(2)	177.6(3)
Mn(1)-O(1)	2.022(5)	C(03)-Mn(1)-O(2)	92.5(3)
Mn(1)-O(04)	2.085(6)	C(01)-Mn(1)-O(2)	91.4(3)
O(2)-C(4)	1.263(11)	C(02)-Mn(1)-O(1)	92.6(3)
O(1)-C(2)	1.296(11)	C(03)-Mn(1)-O(1)	93.0(3)
O(02)-C(02)	1.171(12)	C(01)-Mn(1)-O(1)	176.9(3)
O(03)-C(03)	1.128(10)	O(2)-Mn(1)-O(1)	89.6(3)
O(04)-C(04)	1.474(12)	C(02)-Mn(1)-O(04)	94.4(3)
C(3)-C(2)	1.372(13)	C(03)-Mn(1)-O(04)	175.2(3)
C(3)-C(4)	1.417(13)	C(01)-Mn(1)-O(04)	94.3(3)
C(01)-O(01)	1.137(11)	O(2)-Mn(1)-O(04)	84.8(2)
C(4)-C(5)	1.527(14)	O(1)-Mn(1)-O(04)	83.0(2)
C(2)-C(1)	1.524(12)	C(4)-O(2)-Mn(1)	127.7(6)
		C(2)-O(1)-Mn(1)	125.9(6)
		C(04)-O(04)-Mn(1)	125.7(6)
		C(2)-C(3)-C(4)	125.5(10)
		O(01)-C(01)-Mn(1)	175.5(9)
		O(2)-C(4)-C(3)	124.7(10)
		O(2)-C(4)-C(5)	115.8(8)
		C(3)-C(4)-C(5)	119.5(9)
		O(02)-C(02)-Mn(1)	175.3(8)
		O(1)-C(2)-C(3)	125.6(8)
		O(1)-C(2)-C(1)	113.2(8)
		C(3)-C(2)-C(1)	121.1(9)
		O(03)-C(03)-Mn(1)	178.7(7)

4 Crystallographic data for *fac*-[Mn(TfAcac)(CO)₃(OHCH₃)]

Table 12: Atomic coordinates (x 104) and equivalent isotropic displacement parameters (Å2x 103) for *fac*-[Mn(TfAcac)(CO)₃(OHCH₃)]

	x	y	z	U(eq)
C(5)	10991(8)	1474(3)	8045(8)	50(1)
C(1)	10939(11)	2653(3)	2947(10)	72(2)
F(2)	11899(6)	912(2)	8580(6)	76(1)
F(1)	9654(8)	1452(2)	8698(6)	96(2)
F(3)	11982(7)	2000(3)	8702(6)	97(2)
O(02)	6022(6)	-387(2)	3866(5)	59(1)
O(03)	6139(8)	652(3)	-191(6)	85(2)
C(02)	6807(7)	85(3)	3685(6)	43(1)
C(03)	6838(8)	728(3)	1167(8)	52(1)
O(01)	4840(7)	1627(3)	3572(8)	90(2)
C(01)	6035(9)	1333(3)	3469(8)	58(2)
O(04)	10230(5)	328(2)	3253(5)	47(1)
C(04)	11240(10)	436(4)	2181(9)	67(2)
Mn(1)	7924(1)	849(1)	3288(1)	39(1)
O(2)	9291(5)	974(2)	5635(4)	44(1)
O(1)	9161(5)	1674(2)	2761(4)	48(1)
C(4)	10296(7)	1496(2)	6223(7)	43(1)
C(3)	10740(9)	2020(3)	5414(7)	53(1)
C(2)	10214(7)	2078(2)	3709(7)	48(1)

Table 13: Bond lengths [Å] and angles [°] for *fac*-[Mn(Tfacac)(CO)₃(OHCH₃)]

C(5)-F(3)	1.315(7)	F(3)-C(5)-F(2)	108.0(5)
C(5)-F(2)	1.318(7)	F(3)-C(5)-F(1)	106.5(5)
C(5)-F(1)	1.335(8)	F(2)-C(5)-F(1)	103.8(5)
C(5)-C(4)	1.512(8)	F(3)-C(5)-C(4)	114.6(5)
C(1)-C(2)	1.499(8)	F(2)-C(5)-C(4)	112.5(5)
O(02)-C(02)	1.148(6)	F(1)-C(5)-C(4)	110.8(5)
O(03)-C(03)	1.153(8)	O(02)-C(02)-Mn(1)	176.2(5)
C(02)-Mn(1)	1.817(5)	O(03)-C(03)-Mn(1)	179.8(7)
C(03)-Mn(1)	1.800(7)	O(01)-C(01)-Mn(1)	179.0(6)
O(01)-C(01)	1.130(8)	C(04)-O(04)-Mn(1)	126.8(4)
C(01)-Mn(1)	1.808(7)	C(03)-Mn(1)-C(01)	90.1(3)
O(04)-C(04)	1.406(7)	C(03)-Mn(1)-C(02)	88.5(2)
O(04)-Mn(1)	2.092(4)	C(01)-Mn(1)-C(02)	87.5(2)
Mn(1)-O(1)	2.005(4)	C(03)-Mn(1)-O(1)	89.4(2)
Mn(1)-O(2)	2.016(4)	C(01)-Mn(1)-O(1)	93.8(2)
O(2)-C(4)	1.300(6)	C(02)-Mn(1)-O(1)	177.5(2)
O(1)-C(2)	1.259(7)	C(03)-Mn(1)-O(2)	176.3(2)
C(4)-C(3)	1.346(8)	C(01)-Mn(1)-O(2)	93.4(2)
C(3)-C(2)	1.417(8	C(02)-Mn(1)-O(2)	93.04(19)
		O(1)-Mn(1)-O(2)	88.97(14)
		C(03)-Mn(1)-O(04)	94.3(2)
		C(01)-Mn(1)-O(04)	175.4(2)
		C(02)-Mn(1)-O(04)	94.20(19)
		O(1)-Mn(1)-O(04)	84.60(14)
		O(2)-Mn(1)-O(04)	82.26(16)
		C(4)-O(2)-Mn(1)	124.9(3)
		C(2)-O(1)-Mn(1)	128.9(4)
		O(2)-C(4)-C(3)	128.1(5)
		O(2)-C(4)-C(5)	112.2(5)
		C(3)-C(4)-C(5)	119.7(5)
		C(4)-C(3)-C(2)	124.2(5)
		O(1)-C(2)-C(3)	124.3(5)
		O(1)-C(2)-C(1)	116.5(6)
		C(3)-C(2)-C(1)	119.1(5)

\

_____